5-2008

GEOTECHNICAL INVESTIGATIONS AT THREE SITES IN THE SOUTH CAROLINA COASTAL PLAIN THAT DID NOT LIQUEFY DURING THE 1886 CHARLESTON EARTHQUAKE

Ronald Boller
Clemson University, rcboller1@yahoo.com

GEOTECHNICAL INVESTIGATIONS AT THREE SITES IN THE SOUTH CAROLINA COASTAL PLAIN THAT DID NOT LIQUEFY DURING THE 1886 CHARLESTON EARTHQUAKE

A Thesis
Presented to
the Graduate School of
Clemson University

In Partial Fulfillment
of the Requirements for the Degree
Master of Science

---

by
Ronald C. Boller Jr.
May 2008

Accepted by:
Dr. Ronald D. Andrus, Committee Chair
Dr. C. Hsein Juang
Dr. Ronald W. Falta

This research was supported by the National Science Foundation, under NSF grant number CMS-0556006. Any opinions, findings, and conclusions or recommendations expressed in this material are those of the author and do not necessarily reflect the views of the National Science Foundation.

ABSTRACT

Geotechnical investigations were performed at three sites in the South Carolina Coastal Plain where liquefaction is believed to not have occurred in 1886 or during other Holocene earthquakes. The three sites are the Coastal Research and Education Center (CREC) located near Charleston, and the Borrow Pit and Marsh Road sites at Hobcaw Barony near Georgetown. The investigations consisted of nine seismic cone penetration test (SCPT) soundings, three non-seismic cone penetration test (CPT) soundings, one standard penetration test (SPT) boring, and two dilatometer test (DMT) soundings. Shear wave velocities (V_s) were calculated from the SCPTs using pseudo interval measurements at the CREC site and true interval measurements at the two Hobcaw Barony sites. The SPTs were performed with hammer energy measurements so the most accurate corrected blowcounts $(N_1)_{60}$ could be obtained. The at rest lateral earth pressure coefficients (K_o) were estimated from the DMT measurements.

It was determined that thick medium dense surficial sand deposits exist at each site. These near-surface deposits (below the ground water table) have average normalized cone tip resistance (q_{t1N}) values ranging from 95 to 139 and stress-corrected shear wave velocity (V_{s1}) values between 230 and 296 m/s. Values of K_o for the near-surface sand deposits at the CREC site and the Borrow Pit site average 0.9 and 0.7, respectively.

Measured values of V_S from the SCPTs were compared with predicted values of V_S based on the empirical relationships by Andrus et al. (2007). At the three sites the measured to predicted V_S ratios (MPV_SR) are 1.38, 1.47 and 1.45, respectively. For the CREC site the value of 1.38 is practically the same as the MPV_SR determined by Hayati and Andrus (2008) for the 100,000 year old Wando Formation in Charleston, which did not liquefy during the 1886 earthquake. The Borrow Pit site and the Marsh Road site have similar MPV_SR values, indicating the thick sand layer at these sites are similar in age (about 200,000 years old). These MPV_SR values support the belief that liquefaction did not occur at the three sites during the recent past.

ACKNOWLEDGMENTS

First, I would like to acknowledge the Clemson University Graduate School and Civil Engineering Department for giving me the opportunity to further my education.

I give very special thanks to my advisor Dr. Ronald Andrus for his leadership, support and strong positive attitude throughout my graduate studies. I would also like to thank my committee members Dr. C. Hsein Juang and Dr. Ronald Falta for devoting their time and efforts for my studies. I also acknowledge Billy Camp of S&ME for his efforts in advancing my studies. I appreciate my fellow graduate students at Clemson University for their thoughtful discussions and recommendations given during my research.

I am grateful to the National Science Foundation for funding my research and understanding its importance. I am thankful to Dr. James Rushing (Director of the Coastal Research and Education Center) and Dr. George Askew (Director of the Baruch Institute for Coastal Ecology and Forest Science) for accepting the project proposal and making available land from their respective facilities for field testing.

Finally, I would like to thank my Lord and Savior Jesus Christ for giving me the spirit and health to accomplish all things that I desire, and all my love ones for their encouragement in all of my endeavors.

TABLE OF CONTENTS

Page

Table of Contents (Continued)

Page

Table of Contents (Continued)

Page

LIST OF TABLES

List of Tables (Continued)

Table Page

LIST OF FIGURES

List of Figures (Continued)

List of Figures (Continued)

Figure Page

List of Figures (Continued)

Figure Page

List of Figures (Continued)

Figure Page

CHAPTER ONE

INTRODUCTION

1.1 Liquefaction Resistance of Aged Soils

A review of the literature suggests that the liquefaction resistance of saturated sands increases with age (e.g., Youd and Perkins, 1978; Seed, 1979; Troncoso et al., 1988; Lewis et al., 1999; Arango et al., 2000; Leon et al., 2006; Hayati et al., 2008). Youd and Perkins (1978) suggested that the liquefaction susceptibility of soil decreases with geologic age, where Pleistocene-age (10,000 to 1.8 million years) deposits generally have very low susceptibility and Holocene-age (less than 10,000 years) deposits have moderate to high susceptibility to liquefaction. It is believed that mechanical and/or chemical bonds that occur during aging provide greater strength and stiffness to older soils, thus increasing the resistance of the deposit to liquefaction (Leon et al., 2006).

Lewis et al. (1999) studied the effect age had on the liquefaction resistance of sands in the Charleston, South Carolina area using field data and liquefaction reports from the 1886 Charleston earthquake. From their study it was determined that sands older than Holocene have a greater cyclic strength than what is predicted by the empirical liquefaction resistance chart developed by Seed et al. (1984) based on standard penetration test blowcounts in Holocene-age deposits. Their study also found deposits that should have liquefied during the 1886 earthquake based on the empirical chart did not. Lewis et al. (1999)

attributed these findings to the strength gains incurred during the aging process. However, it should be noted that there were cases of liquefaction in Pleistocene-age deposits.

The South Carolina Coastal Plain (SCCP) provides favorable geology for researching the relationship between age and liquefaction resistance. The near surface geology of the SCCP consists of beach sand deposits of different ages with relatively high ground water tables. Shown in Figure 1.1 is the geologic map by McCartan et al. (1984) that gives the depositional trends for the beach sands of the SCCP. The depositional trend indicated by the map is that beach deposits increase in age the farther inland they are located.

1.2 Purpose

The purpose of this research, which was sponsored by the National Science Foundation (NSF), is to performed geotechnical investigations at three sites where liquefaction did not occur during the 1886 Charleston earthquake or other Holocene events. The three sites are located near Charleston and Georgetown, as illustrated in Figure 1.1. The Coastal Research and Education Center (CREC) site is located in Charleston County on a beach sand deposit that is 100,000 years old. The Borrow Pit site and the Marsh Road site are located within Hobcaw Barony of Georgetown County. The Borrow Pit site is located on 200,000 year old beach sand deposit, while the Marsh Road site is located on a Holocene beach sand, according to McCartan et al. (1984).

Field investigations performed at the three sites include seismic cone penetration testing (SCPT), non-seismic cone penetration testing (CPT), dilatometer testing (DMT), standard penetration testing (SPT) with standard split-spoon sampling, and fixed piston sampling. The objectives of these field investigations are to characterize the in-situ properties of beach deposits at the three sites and to develop the sites for future geotechnical investigations.

1.3 Organization

Following this introduction, the test methods and procedures used to gather and reduce field data are discussed in Chapter 2. Chapter 3 presents the results of investigations performed at the CREC site. Chapters 4 and 5 present the results of the investigations performed at the Borrow Pit site and the Marsh Road site, respectively. The conclusions made from the results are summarized in Chapter 6.

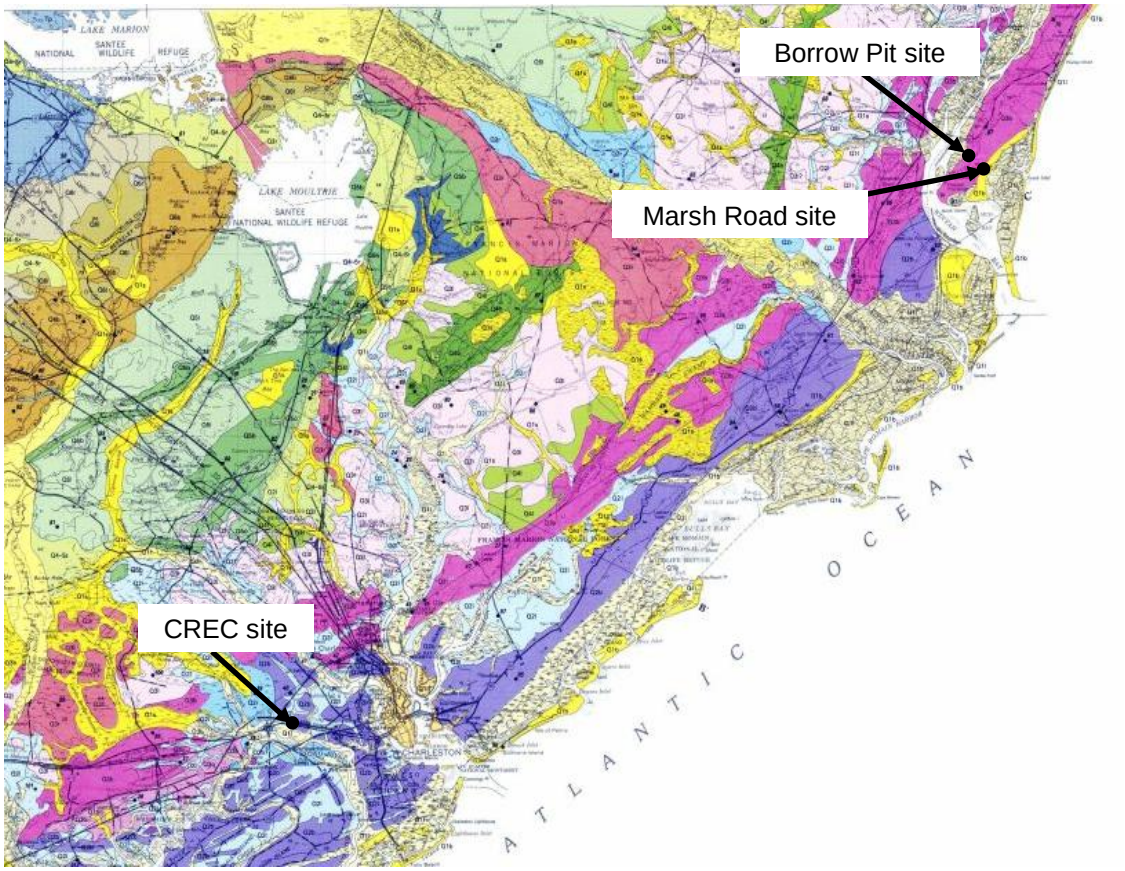

Figure 1.1 Geologic Map of the South Carolina Coastal Plain (McCartan et al., 1984) showing the locations of the three geotechnical experimentation sites.

CHAPTER TWO

TEST METHODS

Presented in this chapter is information about the testing methods employed at the three geotechnical investigation sites (see Figure 1.1). The procedures and assumptions used to reduce the data are also discussed in this chapter.

2.1 Seismic and Non-Seismic Cone Penetration Tests

The seismic cone penetration tests with pore pressure measurements (SCPTu) and non-seismic cone penetration tests with pore pressure measurements (CPTu) were conducted according to ASTM D 5778. The tests involve hydraulically pushing a 15 cm^2 electric piezocone pentrometer through the earth's subsurface at rate of 2 cm/s. At this rate, recordings of cone tip resistance (q_t), sleeve friction (f_s), and pore water pressure (u_2), were taken at a fairly continuous rate (27 samples per meter). Load cells behind the cone tip and embedded near the sleeve recorded the q_t and the f_s that the soil applies during the hydraulic push.

Pore water pressures recorded behind the cone tip (u_2 position) were determined by a saturated pore pressure transducer. The pore pressure transducer uses a saturated filter to provide a coupling between the pore water pressure and the transducer. The filters used in all soundings were saturated in a vacuum with silicon oil. The filters were saturated for several days, and

according to the technician on site, the filters did not leave the silicon oil container until the filters needed to be installed.

In order to capture seismic wave energy, the cone rods contained a geophone(s) or receiver(s) that was oriented in the direction of shear wave particle motion. Pseudo interval velocity measurements were made using rods with only one geophone, while true or direct interval velocity measurements were made using two geophones.

2.1.2 Test Setup

Figure 2.1 shows the tire-mounted truck rig (Freight Liner 112) used to conduct cone soundings at the CREC site. The truck rig weighed approximately 25 tons and gave the reaction needed to push the cone into the ground. The cones used were manufactured by Vertek and had a projected area of 15 cm^2 with rod lengths of 1 m. Figure 2.2 shows the cone being lowered through the floor of the truck rig. The inside of the truck rig housed the data acquisition software and the hydraulic components for gripping and pushing the rods.

The seismic wave energy produced for the SCPTu's at the CREC site came from an automatic solenoid hammer source that doubled as the truck's front hydraulic leveling jacks. The solenoid hammer was controlled by the operator inside of the truck. At 1 m depth intervals, the operator stopped the push of the rods and activated the hammer. The solenoid hammer made one horizontal strike from the left (forward hit) and then one horizontal strike from the right (reverse hit). The horizontal strikes were parallel to the ground surface and

shear waves were captured by one geophone. A combined time history plot of voltage versus time was produced from the left and right strikes. Figure 2.3 shows the time history record for SC 1 at a depth of 16.6 m. The combined plots have a butterfly pattern, meaning the strikes are 180º out of phase with each other.

At the CREC site the shear wave velocities (V_s) were determined using the pseudo interval method. The pseudo interval method is illustrated in Figure 2.4 and involves striking the plank source at one depth, pushing the cone to the next depth and then striking the plank source again. Values of V_s are calculated by the following equation:

$$V_s = \frac{d_2 - d_1}{t_2 - t_1} \qquad 2.1$$

where d_2 and d_1 are the shear wave's travel distances at consecutive depths and t_2 and t_1 are the average first arrival times of the shear waves for both strikes at consecutive depths.

Figure 2.1 Photograph of the 25 ton CPT truck rig used at the CREC site.

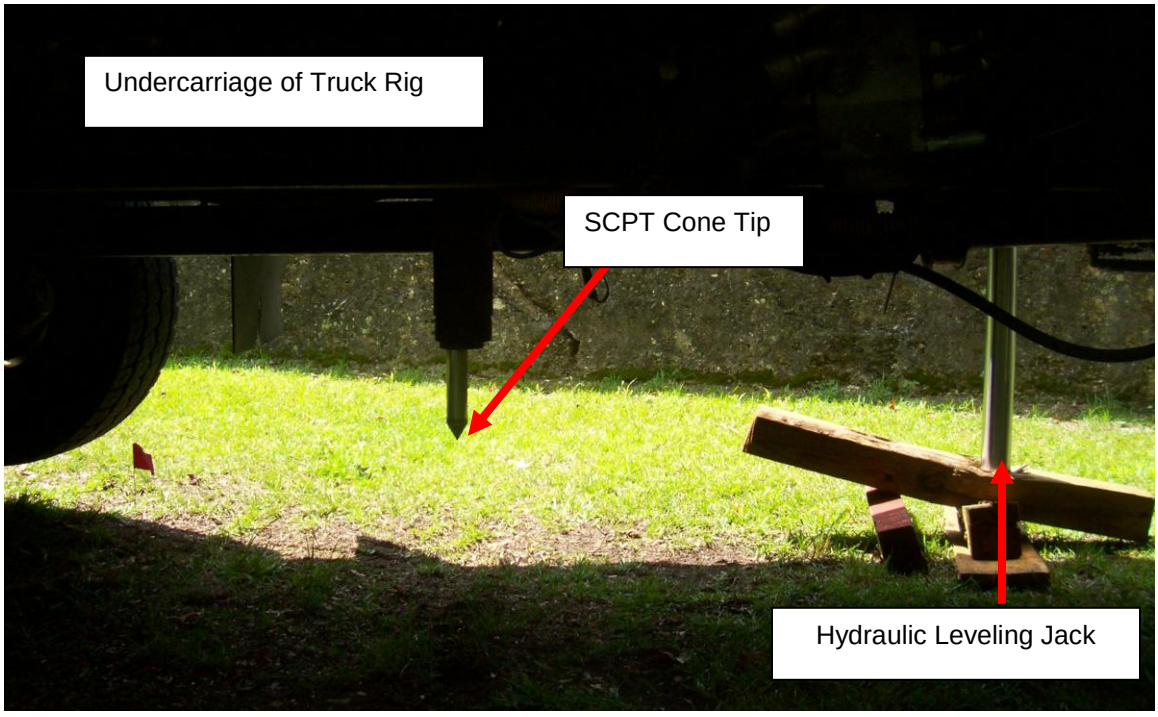

Figure 2.2 Photograph of the cone being lowered through the floor of the truck rig.

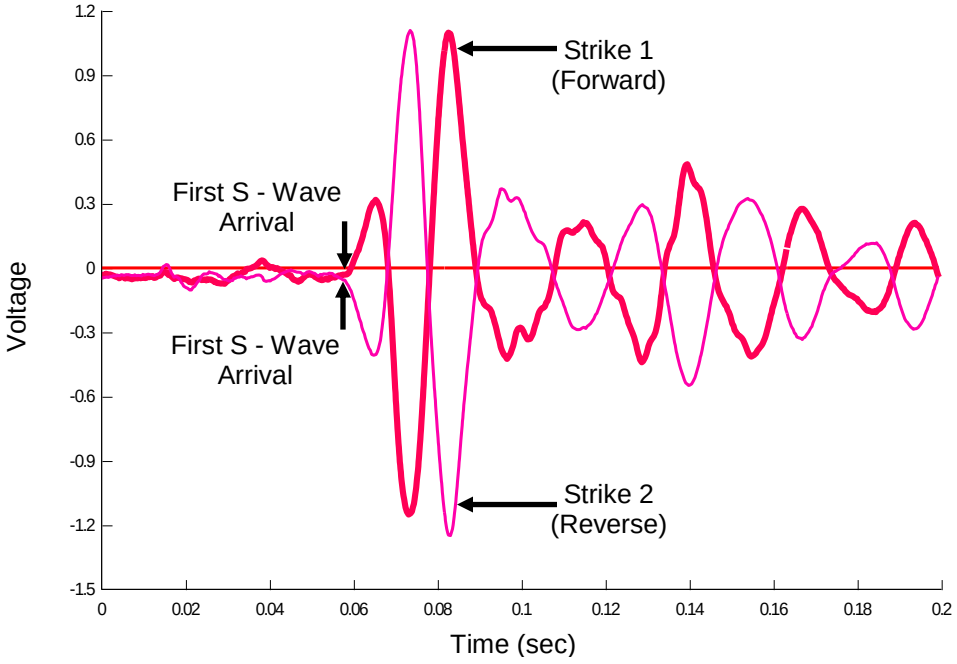

Figure 2.3 Stress – wave time history from SC 1 for a depth of 16.6 m at the CREC site.

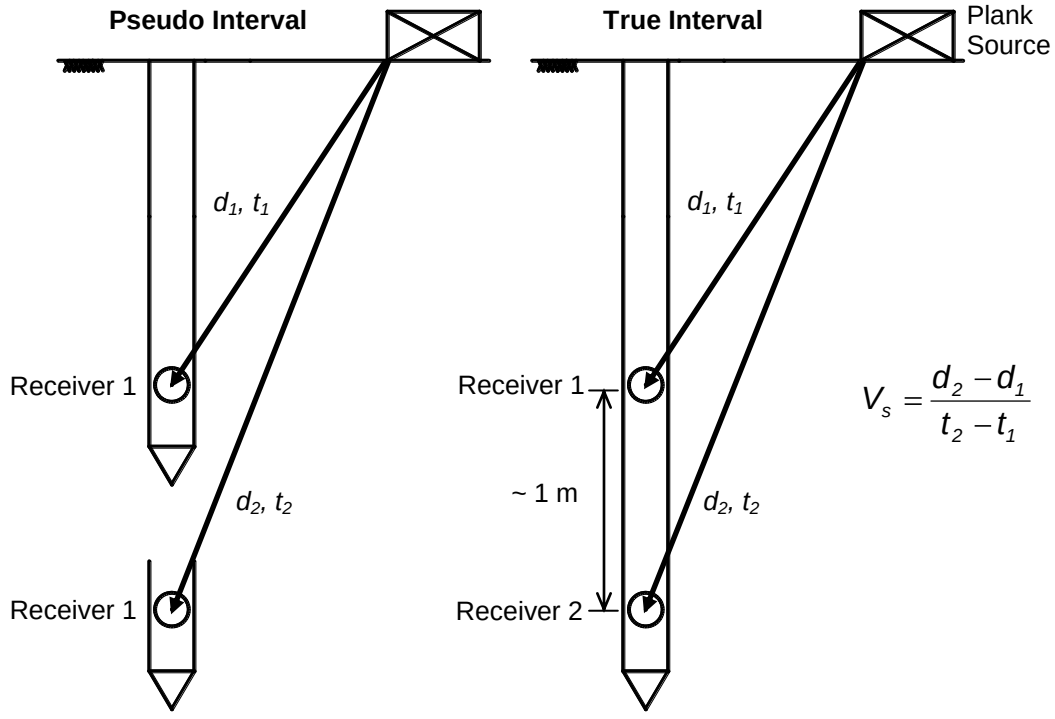

Figure 2.4 Diagram of the pseudo and true interval measurement methods used to find shear wave velocity from SCPT.

Shown in Figure 2.5 is the track-mounted rig used for the cone testing performed at Hobcaw Barony. The track-mounted rig has better off road mobility than the truck rig. The track-mounted rig has a similar setup to the truck rig, but provided no housing for the data acquisition software and hydraulics.

The track rig's seismic source came from a manual sledge hammer strike to the side of a wooden plank. The track rig's back-right hydraulic leveling jack pushed the wooden source plank firmly into the ground surface. The wooden plank was positioned diagonally so that both ends were equally spaced from the cone rod. Horizontal strikes were made on the head (forward hit) and toe (reverse hit) of the plank. The horizontal strikes were parallel to the ground surface and shear waves were captured by two geophones during each strike. Figure 2.6 shows this two geophone setup used at Hobcaw Barony. This setup allowed for true interval measurements (see Figure 2.4). The operator saved the four time histories during the first and second strikes that came from the two geophones. Shown in Figure 2.7 are the time history records of SCPT HB 1 at a depth of 10.7 m.

Values V_s were also calculated using Equation 2.1, where d_2 and d_1 are the shear wave's travel distances to the bottom and top geophones during each strike and t_2 and t_1 is the arrival of the shear wave for the bottom and top geophones for each strike. Arrival times of the shear wave are based on first arrival, first peak, and first crossover (see Figure 2.7). This led to six V_s calculations that were averaged together.

The basic difference between the two methods is that the pseudo interval calculates V_s based on one hit and one time history whereas in the true interval method there is one hit and two time histories from the top and bottom geophones. Therefore, the true interval method provides a more accurate velocity measurement because V_s is calculated from a single seismic wave. Also, any problems associated with trigger times is eliminated with true interval measurements

Figure 2.5 Photograph of the CPT track-mounted rig used at Hobcaw Barony.

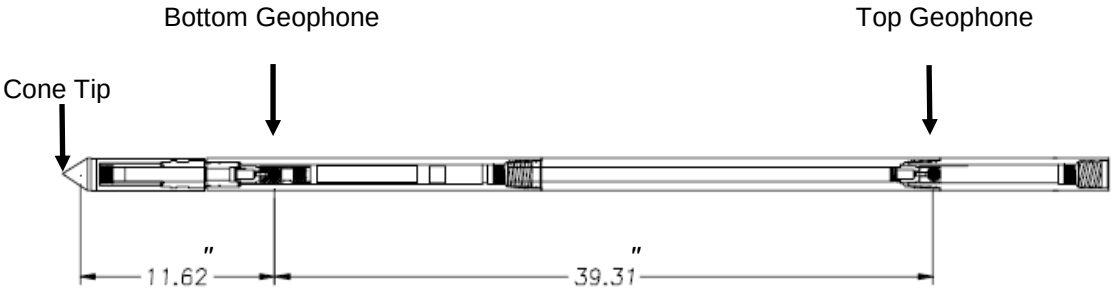

Figure 2.6 Seismic piezocone penetrometer showing the positions of the geophones used in true interval shear wave velocity measurements.

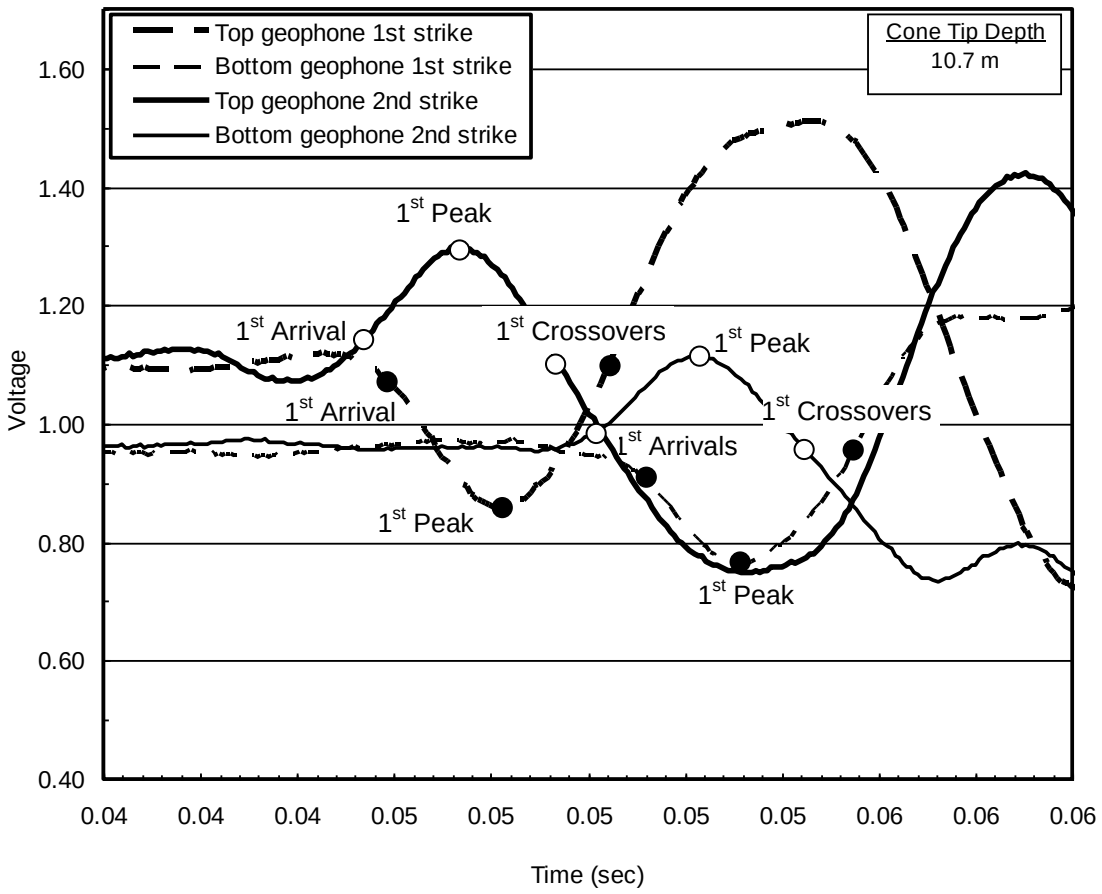

Figure 2.7 Typical true interval time history records from SCPT HB 1 at the Borrow Pit site. Shear wave travel times were calculated by averaging the offset of key points in the first wavelet as illustrated in the figure.

2.2 Standard Penetration Test

Standard penetration tests (SPT) were performed following ASTM D 1586. The SPT is a dynamic soil penetration test that provides information on soil density and consistency. Penetration into the soil layer is commonly provided by a 140 lb hammer falling a distance of 30 inches. To quantify penetration, the number of blows needed to penetrate the soil layer every six inches for a total distance of 18 inches is counted. The number of blows counted for the last 12 inches is reported as the blowcount or *N* value. The SPT rods were advanced by drilling to a desired test depth. The drilling produced cuttings and unwanted soil disturbance when approaching the test depth and this is reason why the first six inch blowcounts is not used in the *N* value. As the SPT advances from the hammer blows soil is forced into a split-barrel or split-spoon sampler that is attached to the SPT rods. The split barrel sampling followed ASTM D 1586 - 99.

2.2.1 Test Setup

The CREC site was the only site where SPTs were performed. A fast mixing high viscosity bentonite drilling mud was used to help with the removal of drill cuttings and to provide some protection from cave-ins. The cuttings were forced out of the borehole by pumping the drilling mud through the drill rods and bit. The cuttings fell into a drilling mud box, which was periodically emptied and filled with fresh drilling mud. The most time consuming aspect of the SPT testing was the removal of drill rods to replace the SPT rods and split-spoon sampler. A

standard split-spoon sampler was used. The samples recovered were stored and labeled for laboratory testing.

A CME 550X automatic trip hammer was used to drive the split-spoon sampler into the ground. To determine the hammer energy or efficiency, which is the ratio of the hammer's kinetic to potential energy, a section of SPT rod was instrumented with a pair of accelerometers and strain gages and then added to the rod string. Shown in Figure 2.8 is the automatic trip hammer and the instrumented SPT rod. Figure 2.9 shows a typical energy efficiency plot. The average energy efficiency of hammer for SPTs conducted at the CREC site ranged from 35 - 88 %.

The SPT *N* values were corrected for hammer efficiency, borehole diameter, and a sampler correction. A rod length correction was not needed because the effect of rod lengths is included in the energy measurement. Short rod lengths may cause a reduction in hammer energy. These correction yield a *N* value corrected for field conditions (N_{60}) that is given by the following equation:

$$N_{60} = N * C_E * C_B * C_S \qquad 2.2$$

where C_E is the hammer efficiency, C_B is the borehole diameter correction and C_S is the sampler correction. The values of C_S for all tests were 1.0 because a standard split-spoon sampler was used. The N_{60} value is multiplied by an overburden stress correction factor (C_N) to obtain the stress-corrected *N* value ($(N_1)_{60}$) that is given by the following equation:

$$(N_1)_{60} = N_{60} * C_N \qquad 2.3$$

Table A.2 gives the correction factors, N_{60} and $(N_1)_{60}$ values for the SPT performed at the CREC site.

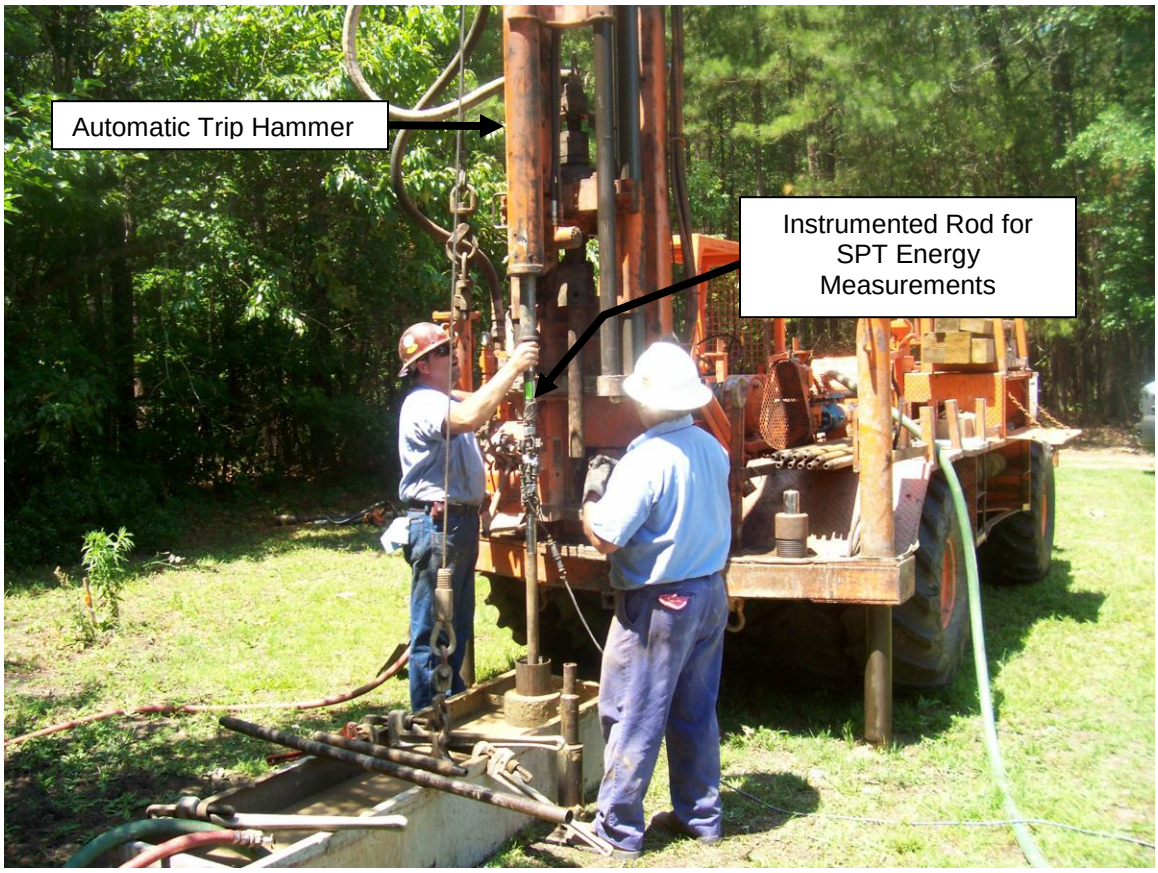

Figure 2.8 Photograph of the setup for SPT with energy measurements at the CREC site.

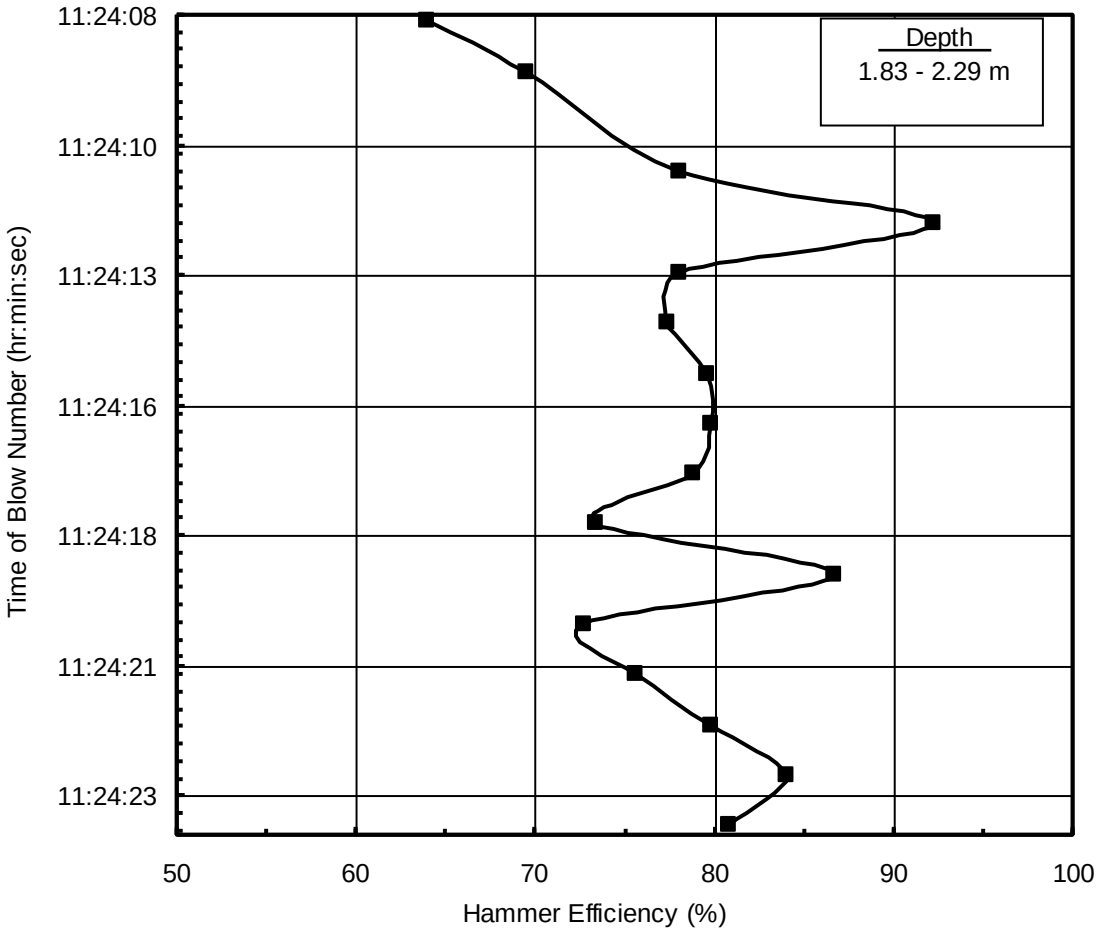

Figure 2.9 Typical energy measurement plot for SPT boring B 3 performed at the CREC site.

2.3 Dilatometer Test

The flat plate dilatometer test (DMT) was performed according to ASTM D 6635 01. The DMT involved hydraulically pushing a tapered steel blade (240 mm X 95 mm) a rate of 20 mm/sec, stopping only at testing depths. At each testing depth, a calibrated steel membrane was expanded under nitrogen gas pressure and pressures at deformations of 0.05 mm and 1.1 mm were recorded. The expansion pressures were noted as the lift off pressure (P_0) and the expansive pressure (P_1) for deformations of 0.05 mm and 1.1 mm, respectively. The membrane was depressurized and the pressure reading to return to zero deformation was taken. This pressure is referred to as the closing pressure (P_2). Pressure readings are all taken within a 15 to 30 second time interval.

2.3.1 Test Setup

Shown in Figure 2.10 is a photograph of the DMT setup. At the start of the DMT membrane stiffness correction factors ΔA and ΔB were determined. ΔA was found by applying a vacuum pressure to the membrane using a syringe. A buzzer alerted the operator that the pressured needed to collapse the membrane was reached and ΔA was recorded. The membrane was then expanded from the collapsed position to a deformation of 1.1 mm. At this deformation, the buzzer sounded and ΔB was recorded. The same procedures were followed to calculate ΔA and ΔB at the conclusion of the DMT. The CREC site had initial ΔA and ΔB values of 0.2 and 0.7, respectively, and final ΔA and ΔB values of 0.2 and 0.5, respectively. The Hobcaw Borrow Pit site had initial ΔA and ΔB values

of 0.13 and 0.65, respectively, and final ΔA and ΔB values of 0.15 and 0.50, respectively. The two ΔA and ΔB values were averaged together and the correction was applied to the values of P_o and P_1.

The values of P_o, P_1 and P_2 were calculated by finding pressure readings A, B and C which relate to the lift off, expansive, and closing pressures, respectively. To find these values the operator was signaled by a buzzer when to take the appropriate pressure reading. The operator opened a vent value and a buzzer beeped when the membrane had reached 0.05 mm, and the lift off pressure "A" is recorded. The membrane continued to expand until a deformation of 1.1 mm was reached and expansive pressure "B" is recorded. The membrane was slowly depressurized until the membrane was flush with the DMT blade. This pressure is the closing pressure "C". Values of P_o and P_1 were calculated by the following equations (Marchetti, 1980):

$$P_0 = 1.05(A + \Delta A - Z_m) - 0.05(B - \Delta B - Z_m) \quad 2.4$$

$$P_1 = B - \Delta B - Z_m \quad 2.5$$

were Z_m is the reading of the gauge for zero pressure.

2.3.2 DMT Data Reduction

The different pressure readings, with respect to membrane deformation, aid in providing a DMT material index (I_D), horizontal stress index (K_D), at rest earth pressure coefficient (K_o), and DMT constrained modulus (E_D).

These indexes are calculated by the following equations (Marchetti, 1980):

$$I_D = \left(\frac{P_1 - P_o}{P_o - u_o} \right) \qquad 2.6$$

$$K_D = \frac{P_1 - u_o}{\sigma'_{vo}} \qquad 2.7$$

$$E_D = 34.7(P_1 - P_0) \qquad 2.8$$

where u_o is hydrostatic pore pressure and σ_{vo}' is the effective overburden-stress.

For I_D < 1.2, K_o was calculated by the following equation (Marchetti, 1980):

$$K_0 = \left(\frac{K_D}{1.5} \right)^{0.47} - 0.6 \qquad 2.9$$

For $I_D \geq 1.2$, Schmertmann's correlation between K_D and K_o with respect to the effective friction angle (ϕ') as cited by Baldi et al. (1986) was used. Values of ϕ' were estimated using the following equation (Kulhawy and Mayne, 1990):

$$\phi' = \tan^{-1}\left[0.1 + 0.3\log\left(\frac{q_t}{\sigma_{vo}'} \right) \right] \qquad 2.10$$

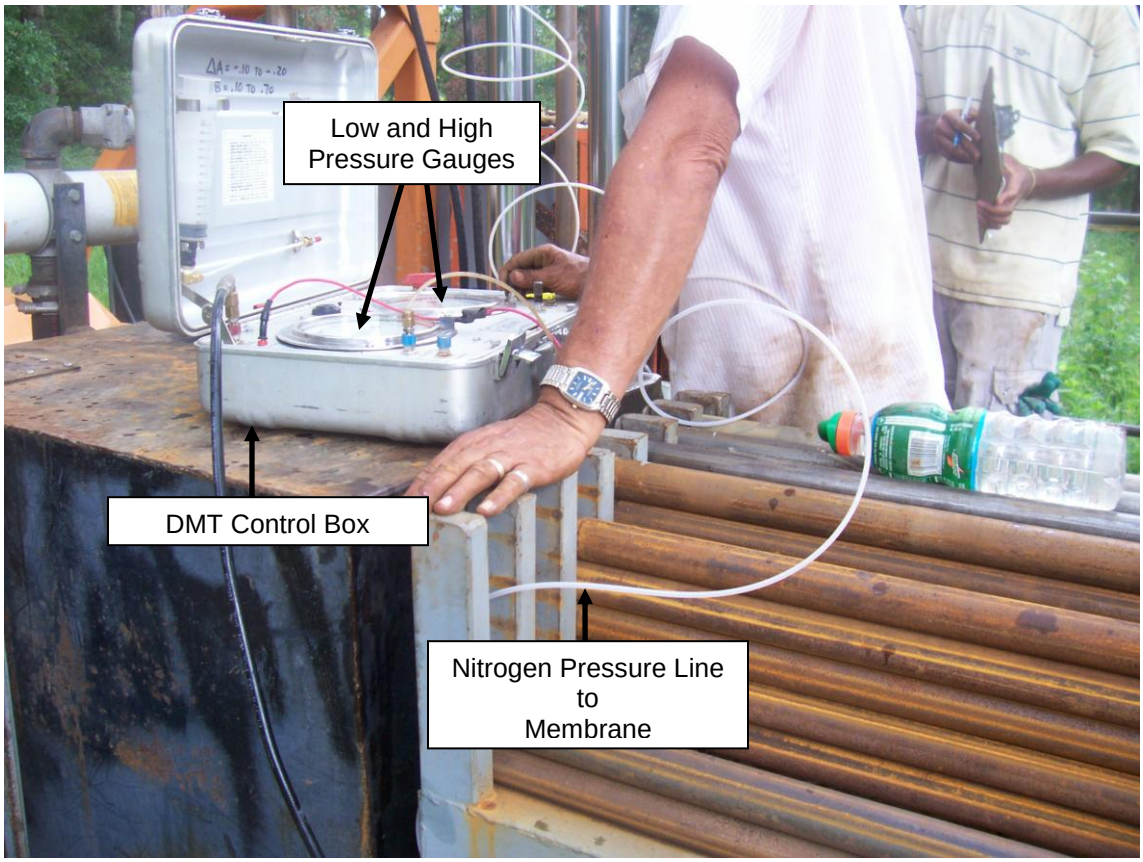

Figure 2.10 Photograph of DMT setup at the Borrow Pit site.

2.4 Laboratory Index Testing

Laboratory index testing was performed on the split-spoon samples from boring B 3 and one fixed piston sample from boring B 1 at the CREC site. The samples were first visually inspected to determine if Atterberg Limits (liquid limit (LL) and plastic limit (PL)) could be conducted. This estimation was based on the plastic nature of the sample at the in-situ moisture content. The LL and PL tests were performed following the general procedures outlined in ASTM D 4318.

The LL test used a manual Casagrande liquid limit device for determining the blow number at certain moisture contents. The ranges of blow numbers were 35 to 25, 25 to 20, and 20 to 15. The moisture content versus blow number was plotted and a logarithmic linear regression line was determined. Using the equation of the regression line, the moisture content corresponding to 25 blows was considered to be the LL.

The determination of the PL was difficult because the majority of the samples had low clay content. In the PL test, samples were rolled on a plastic plate into 3.18 mm diameter threads, where 3.18 mm was the smallest diameter the samples could be rolled before breaking. The majority of the samples could not be formed into the threads because the samples contained too much sand. The threads were formed by carefully hand-rolling the samples until the desired diameter was reached. Three separate moisture contents of the threads were averaged together to find the PL.

Samples not initially considered for LL and PL testing were dried and moisture contents were determined. This procedure for determined moisture content is outlined by ASTM D 2216. The dried samples were washed over the #200 sieve to remove fine grained or silt and clay particles. The fine grained soil was saved and eventually used in a hydrometer analysis.

The soil that was retained on the #200 sieve was oven dried and a sieve analysis following ASTM D 421 was performed. The sieve analysis used sieves #4, #10, #20, #40, #60, #100, and #200. This sieve arrangement best captured the grain size distribution of the samples. The samples were sieved in a mechanical shaker for 15 minutes. A second sieve analysis was performed on samples containing a high percent of gravel size particles. These samples were soaked in distilled water and lightly tamped to break down any cemented particles. The results of the two sieve analysis were then combined to provide one grain size distribution.

The hydrometer analysis was performed for samples with fines contents greater than 10%. The hydrometer analysis was conducted using an ASTM 152 H hydrometer and followed ASTM D 422. The hydrometer had a test duration of 48 hours. It is important to note that the last two hydrometer readings had a 24 hour time interval. The average change between these two readings was not greater than 1 increment on the hydrometer.

The silt and clay particle size boundaries is based on AASHTO classification, where silt ranges from 0.075 to 0.002 mm and clay particles have

grain sizes less than 0.002 mm. The LL, PL, grain size distribution, and hydrometer allowed for classification of soil samples. The soil classifications were based on the Unified Soil Classification System, given in ASTM D 2487.

2.5 Summary

The geotechnical field tests performed for this study included SCPTu, CPTu, SPT and DMTs that followed ASTM procedures. These penetration tests allowed for the determination of common soil index properties. The SCPTu's allows for pseudo and true interval V_S measurements to be determined. The SPT performed at the CREC site allowed for in-situ split-spoon samples to be recovered. These samples were used in soil classification and laboratory index testing.

CHAPTER THREE

INVESTIGATIONS AT THE COASTAL RESEARCH AND EDUCATION CENTER

3.1 Introduction

The Coastal Research and Education Center (CREC) is primarily a vegetable research facility that is directed by Clemson University. CREC is located near Charleston, South Carolina just off of Highway U.S. 17 (Savannah Highway) and approximately 3 km west of Interstate Highway 526. The main administrative building and indoor research laboratories of CREC are located north of Savannah Highway, while the Clemson owned outdoor experimental farmland is south of the highway. Presented in Figure 3.1 is a map showing the location of the experimental farmland of CREC with respect to the Savannah Highway.

Clemson University's main activities at CREC include research for increasing vegetable production in South Carolina and enhancing the efficiency of the vegetable industry. CREC contains multiple fields of level farmland and has made available a 0.4 acre field for geotechnical testing for this study (see Figure 3.1). This geotechnical investigation site is herein called the CREC site. Presented in this chapter are the results of the investigations conducted at the CREC site as part of this study.

3.2 Geology

The geologic map by McCartan et al. (1984) identifies the surficial deposits at the CREC site as 100,000 year old beach sands (see Figure 1.1). These beach sands are in a similar geomorphic position as the Wando Formation mapped by Weems and Lemon (1993) in Charleston. Weems and Lemon (1993) estimated the age of the Wando Formation to be 70,000 to 130,000 years old. Thus, the surficial sands at the CREC site are likely between 70,000 to 130,000 years old.

Below the Wando Formation is the Cooper Group or Marl that is believed to be around 30 million years old. The Cooper Marl is a calcareous marine deposit consisting of silty clay to clayey silt (Weems and Lemon, 1993).

Martin and Clough (1990) reviewed several earthquake reports and found no evidence of liquefaction in the area where the CREC site is located. Also, the director of the CREC site stated that no sand boil deposits were observed in the research fields (oral communication, March 2007). Currently no evidence has been found in this area indicating liquefaction during earlier earthquakes.

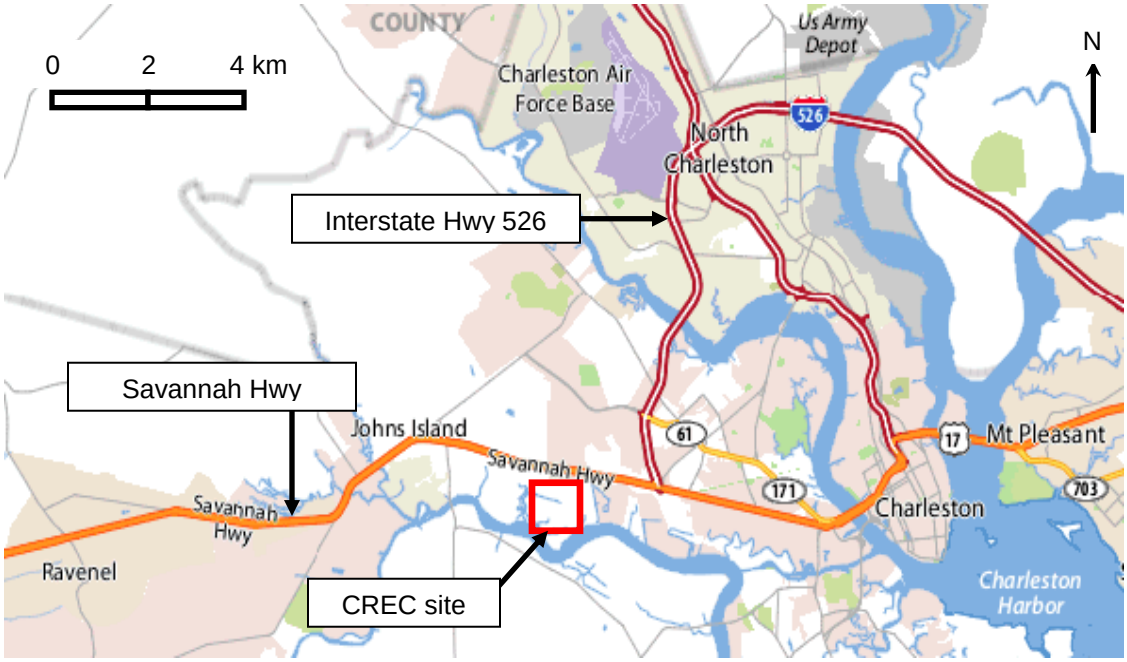

Figure 3.1 Map showing the location of the CREC geotechnical experimentation site with respect to Savannah Hwy (U.S. Highway 17) and Interstate Highway 526.

3.3 Investigations

Figure 3.2 provides an aerial view of the CREC site and surrounding areas. The CREC site is located south of the Field E-7, and is bordered to south and east by a line of trees and to west by an unnamed dirt access road. The site slopes gently to the south and is covered with low-level grass vegetation. A map showing the locations of the geotechnical tests performed at the CREC site is presented in Figure 3.3. The map shows the locations of the three CPTs, three SCPTs, three boreholes, one DMT, and three reference points used to construct the map. The three reference points are located next to two oaks and a pear tree.

A photograph of the CREC site is shown in Figure 3.4. The photograph provides a north to south view of the site showing the locations of CPT C 4, the pear tree containing a reference point, the dirt road, and the ditch that separates Field E-7 from the CREC site. A photograph of boreholes B 3 and B 2 is shown in Figure 3.5.

Cone penetration and dilatometer testing began the morning of March 17, 2007. Three SCPTs (SC 1, SC 3 and SC 6) and three CPTs (C 2, C 3 and C 5) were performed at the site. It should be noted that C 2 was originally a SCPT but the time histories records were very poor. The soundings were pushed on the perimeter of the CREC site. The one dilatometer (D 1) was performed 4 m north of SC 6. SCPT SC 6 and DMT D 1 were pushed until refusal, which occurred at

depths of 27.8 m and 10.0 m, respectively. The other cone soundings were terminated at a depth of about 11.2 m.

Standard penetration tests and fixed piston sampling began the morning of June 5, 2007. The SPT was performed at boring B 3. The fixed piston sampling was performed at boring B 1. Four of the five fixed piston samples recovered were transported to the University of South Carolina for future cyclic triaxial testing. An attempt was made to conduct a consolidation test on the fifth fixed piston sample. However, non-uniform cementation made it impossible to carve a consolidation specimen. No sampling or penetration tests were performed at boring B 2. All borings were concluded at a depth of 11.3 m. Inclination casings were installed in the three boreholes (see Figure 3.5) for future seismic cross hole testing.

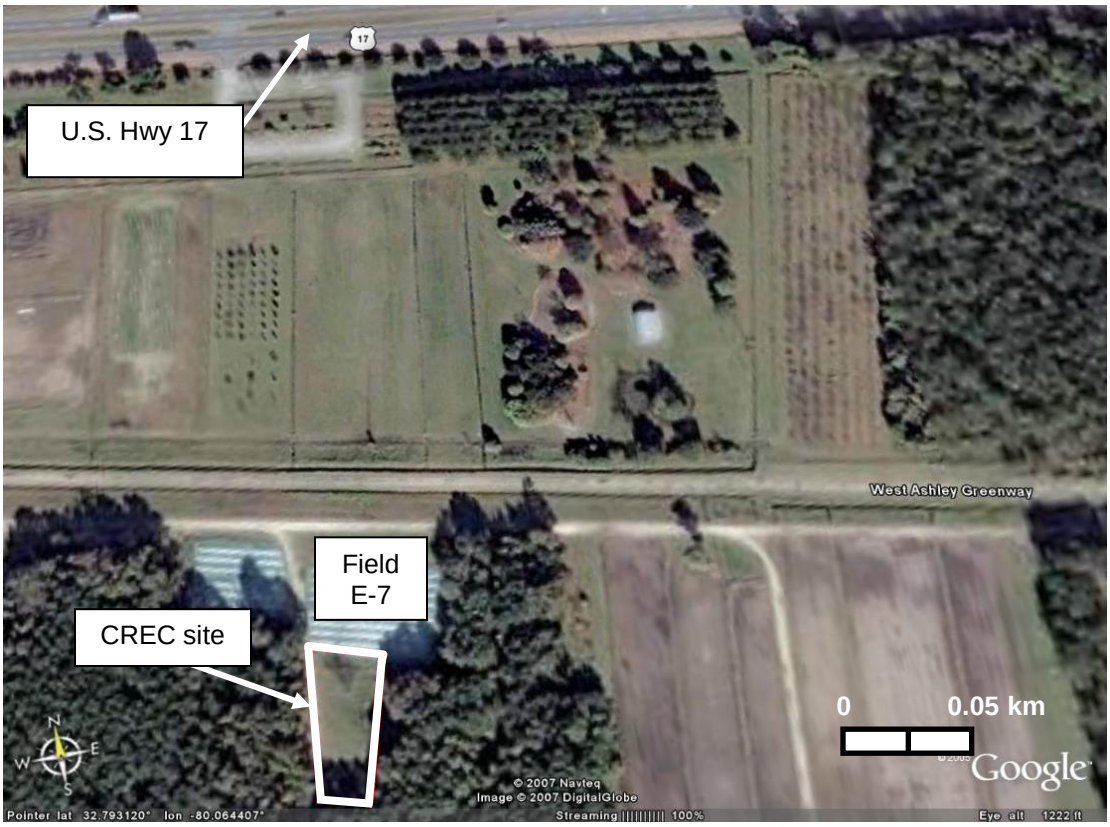

Figure 3.2 Aerial photograph of the CREC site with respect to U.S. Highway 17.

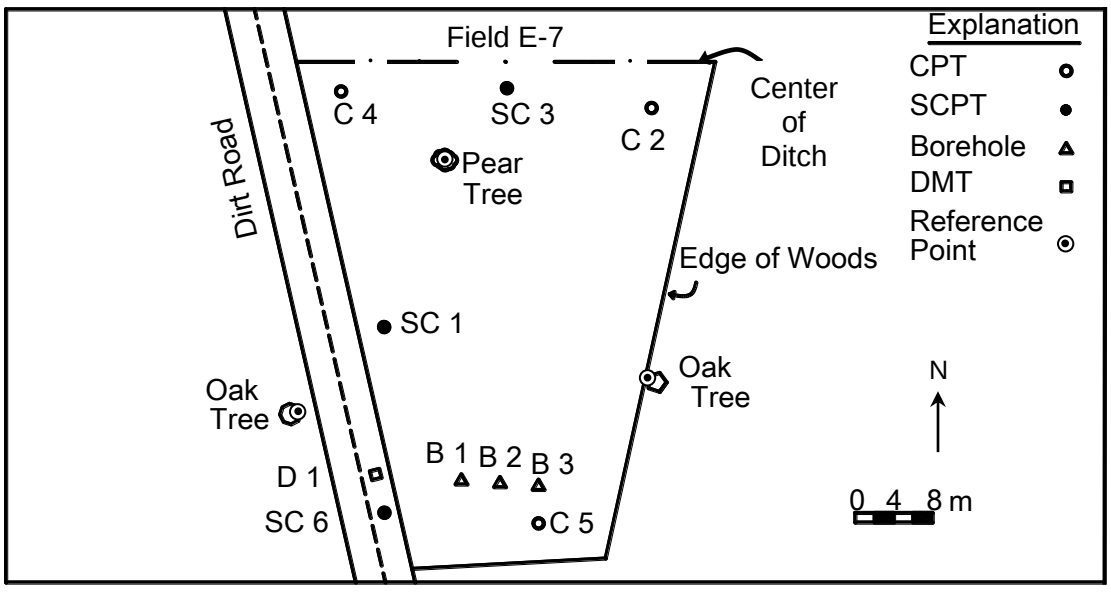

Figure 3.3 Map showing test locations at the CREC site.

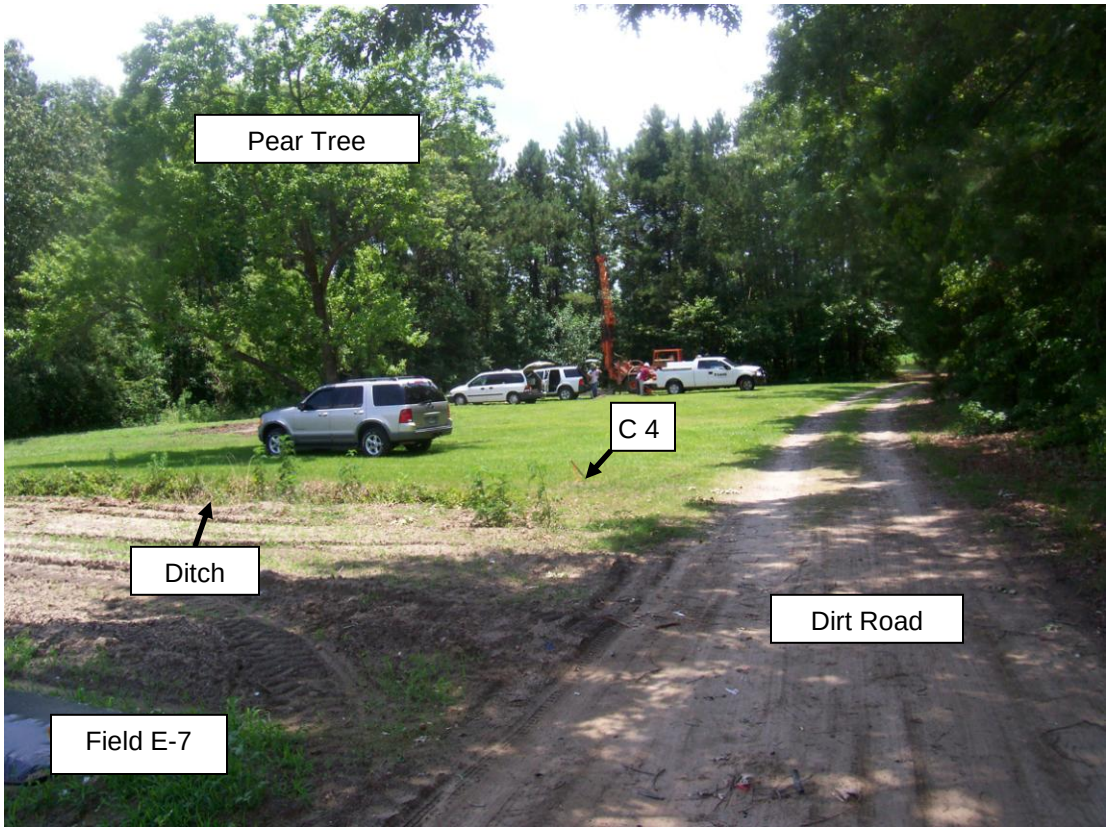

Figure 3.4 Photograph of the CREC site showing the location of CPT sounding C 4.

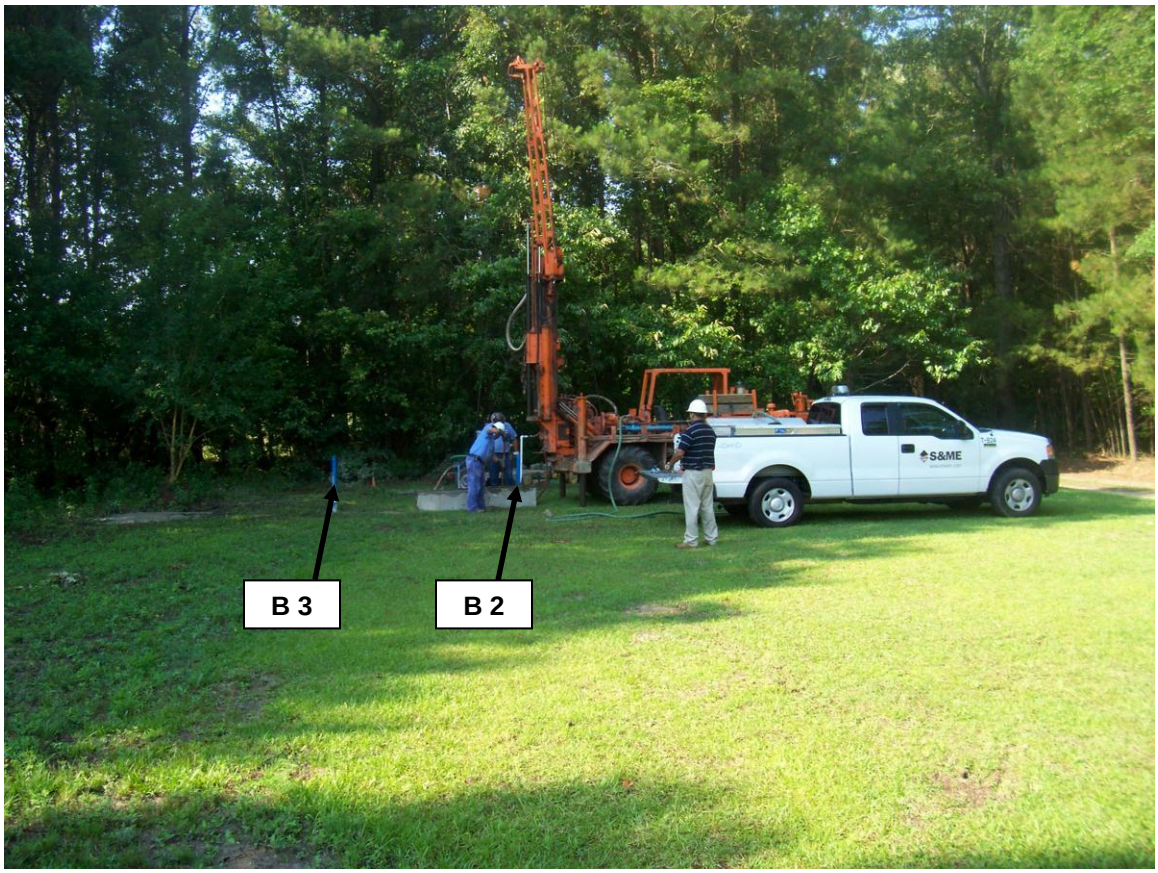

Figure 3.5 Photograph of southern corner of the CREC site showing the drill rig at boring B 2.

3.4 Results

The SCPT, SPT, and DMT test results for the CREC site are tabulated in Appendix A. The results are discussed in the following paragraphs to characterize stratigraphy, soil classification, soil type, lateral earth pressure, liquefaction susceptibility, and shear wave velocity.

3.4.1 Stratigraphy

Figure 3.6 provides a composite profile of CPT C 5 and SPT boring B 3. The figure consists of corrected tip resistance (q_t), friction ratio (FR), pore water pressures measured behind the cone tip (u_2), corrected SPT Blowcount $(N_1)_{60}$, and layer designation with USCS soil classifications. The soil layer designations are A, B, C and D. Layer A is completely above the ground water table, which lies at a depth of about 0.9 m. Layer A extends to a depth of 0.6 m and has an average q_t of 2.7 MPa and $(N_1)_{60}$ of 5. The layer also exhibits average FR of 1.4 % and u_2 of 0.01 MPa. These values suggest Layer A is sandy with some fine grained material.

Layer B extends from a depth of 0.6 m to a depth of 4.4 m. The layer exhibits uniform values of q_t with an average of 7.3 MPa and $(N_1)_{60}$ values as high as 22. Values of FR are less than 1 % and u_2 are close to u_o, suggesting layer B to be a sand deposit.

Layer C lies between depths of 4.4 and 6.6 m. The layer is characterized by low values of q_t averaging 1.4 MPa with $(N_1)_{60}$ values of 2 and 1. Values of FR are as high as to 9.4 % in this layer. There is a slight increase in the u_2

profile with an average of 0.2 MPa. These results indicate that Layer C has significant fines content (silt and clay).

Layer D begins at a depth of 6.1 m and is characterized by average q_t of 3.4 MPa, $(N_1)_{60}$ of 5, *FR* of 0.8 %, and u_2 of 1.9 MPa. These values indicate that the soils of Layer D are medium dense silty sands. It is believed that Layer D is the Cooper Marl.

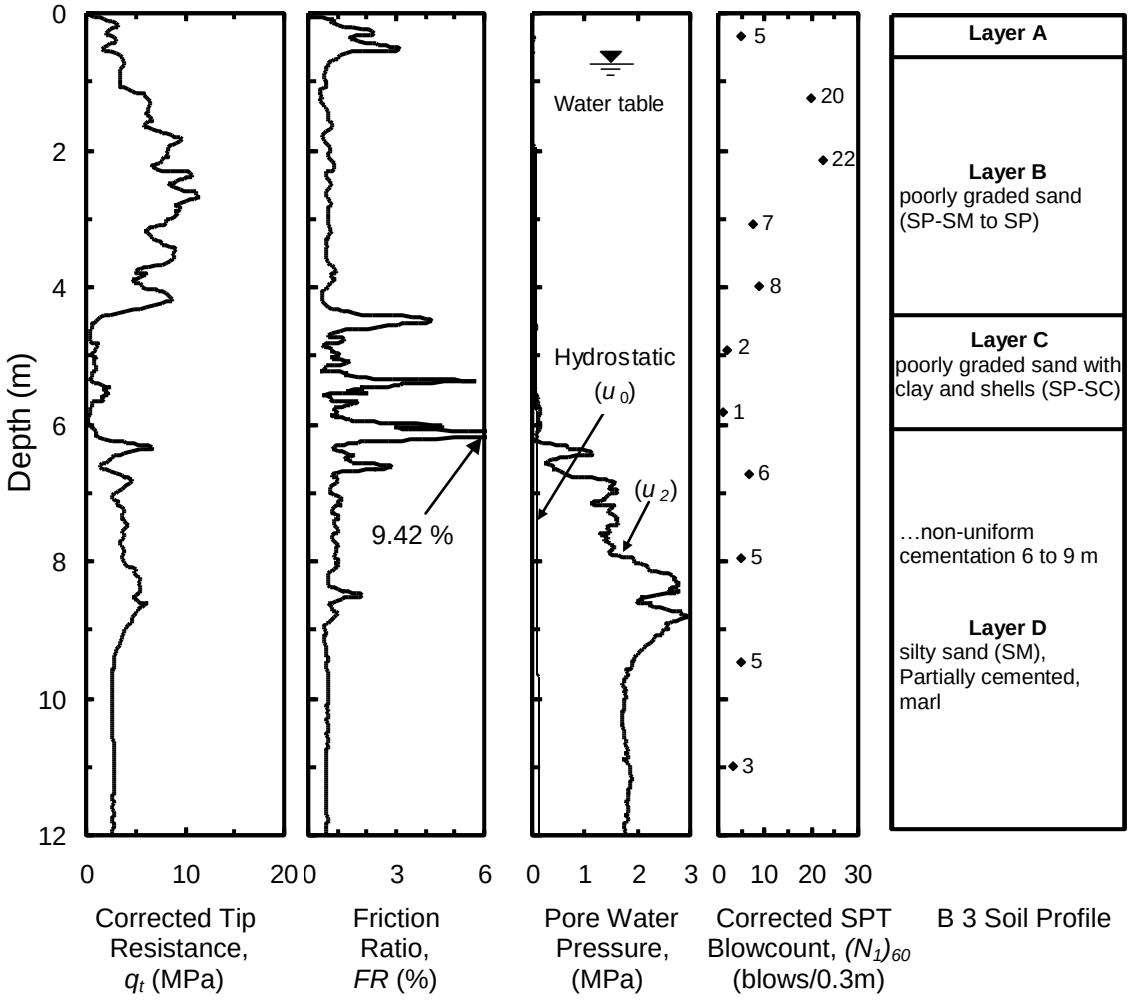

Figure 3.6 Composite profiles for cone sounding C 5 and SPT boring B 3 at the CREC site.

Figures 3.7 and 3.8 provide cross-sections of the CREC site to a depth of 11 m based on q_t and *FR* of the cone soundings. Layers A, B, C and D are present in the top 11 m at all test locations. Layer depth intervals and tabulated averages of q_t and *FR* for the SCPTs can be found in Table 3.1. Appendix A contains the complete profiles for all cone soundings.

In Figure 3.7, Layer A ranges in thickness from 0.7 to 1.0 m. The base of Layer A is fairly close to the depth of the ground water table that lies at a depth of about 0.9 m. Layer B has non-uniform profiles of q_t averaging 6.0 MPa and *FR* averaging less than 1 %. The layer extends to an average depth of 4.6 m. Layer C is less than 1.0 m thick at C 4 and SC 1, and is nearly 1.7 m thick at SC 6. Layer D begins at an average depth of 5.7 m at C 4 and SC 1 and 6.3 m at SC 6. Although there is some lateral variation within the layers, the cross-section suggests the major layers are continuous across the site.

In Figure 3.8, Layer A is less than 1.0 m thick at C 2 and C 5, and the ground water table lies at a depth of about 1.0 m. Layer B has non-uniform profiles of q_t averaging 6.5 MPa and *FR* averaging less than 1 %. The layer extends to depths of 4.3 to 4.4 m at C 2 and C 5. Layer C is approximately 2 m thick at both CPT locations. Layer D begins at an average depth of 6.1 m. This cross-section also indicates that the layers are continuous across the site.

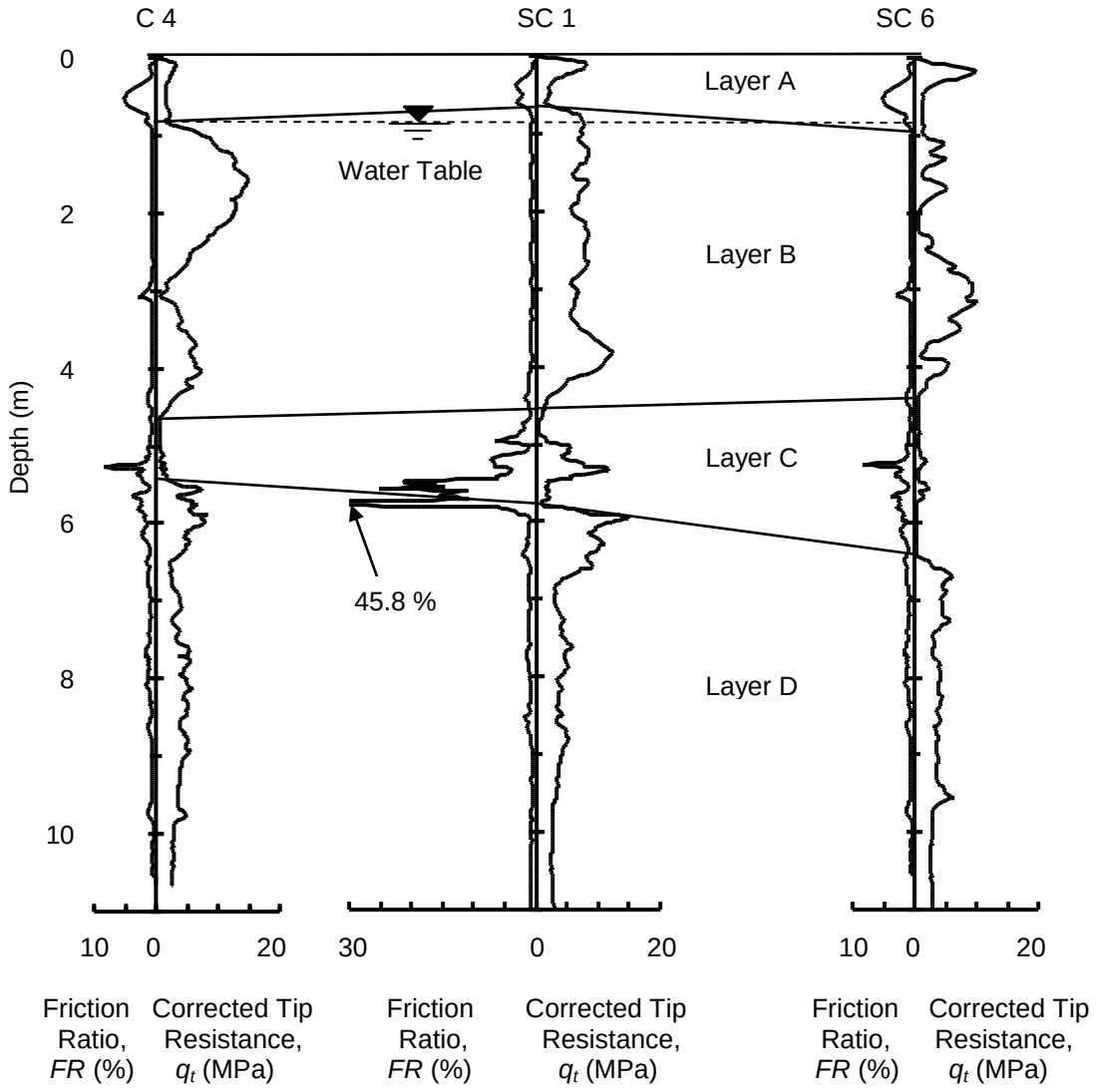

Figure 3.7 CPT cross-section for cone soundings C 4, SC 1, and SC 6 at the CREC site.

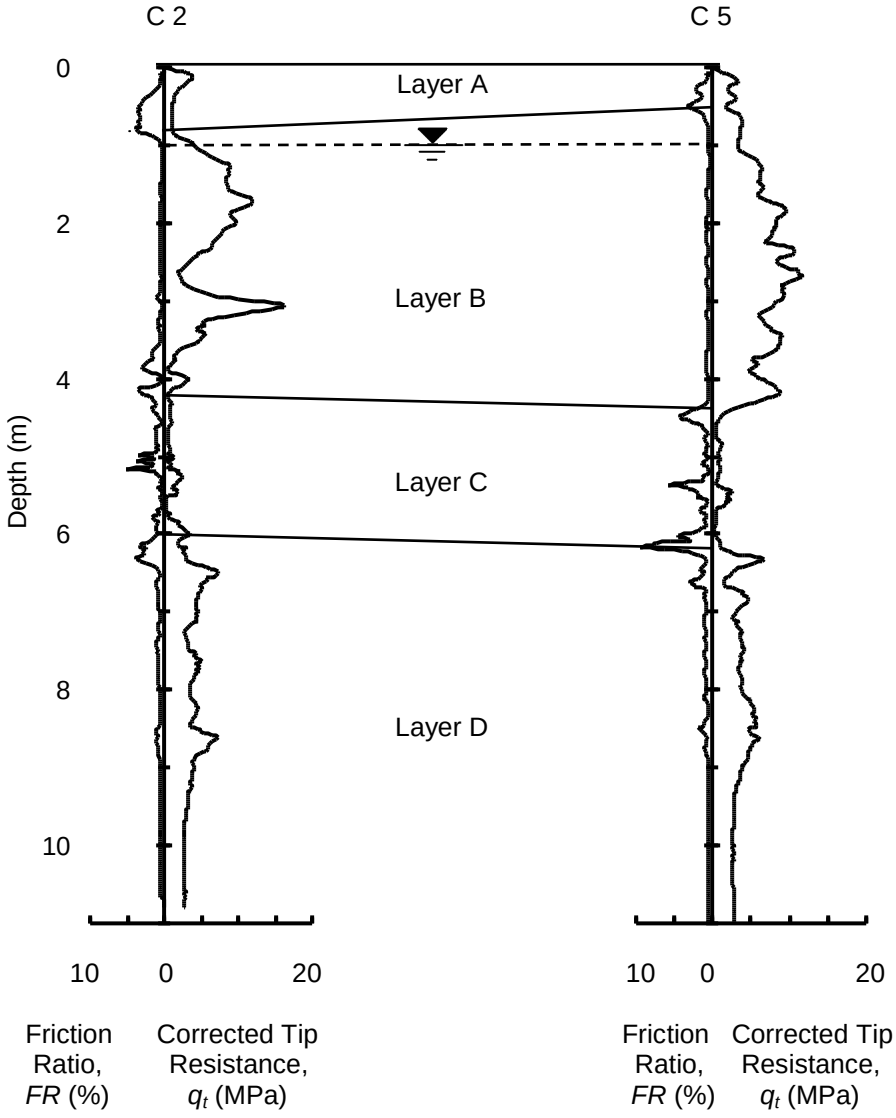

Figure 3.8 CPT cross-section for cone soundings C 2 and C 5 at the CREC site.

Table 3.1 Average measured properties of the near surface soil layers at the CREC site.

Layer Interval (m)		V_s [a] (m/s)	V_{s1} [b] (m/s)	G_{max} [c] (MPa)	q_t (MPa)	q_{t1N} [d]	$(q_{t1N})_{cs}$ [e]	I_c [f]	FR (%)	F_N [g]	Q_t [h]	B_q [i]	u_2/u_o	I_D [j]	K_D [k]	K_o [l]	E_D [m] (MPa)
SC 1																	
B	0.8 - 4.7	190	258	63.5	6.8	144	147	1.6	0.82	0.83	309.6	0.005	0.56	-	-	-	-
C	4.7 - 5.8	-	-	-	3.6	55	168	2.7	9.28	9.93	82.8	0.076	1.90	-	-	-	-
D	5.8 - 27.8	363	353	231.9	3.8	38	76	2.4	0.95	1.04	36.8	0.616	15.99	-	-	-	-
SC 3																	
B	1.0 - 4.6	177	235	55.1	7.2	141	144	1.5	0.66	0.67	279.2	-0.002	0.65	-	-	-	-
C	4.6 - 6.4	141	169	35.0	1.5	21	61	2.8	2.55	3.73	28.6	-0.172	2.27	-	-	-	-
D	6.4 - 10.7	520	565	475.9	4.2	52	70	2.0	0.80	0.83	63.3	-0.493	22.96	-	-	-	-
SC 6															DMT D 1		
B	1.0 - 4.5	170	233	50.9	3.9	74.6	83	2.0	1.57	1.61	143.9	-0.002	0.95	3.5	8.3	0.88	28
C	4.5 - 6.5	178	214	55.8	0.7	10	45	2.9	1.73	2.32	14	0.076	1.26	0.6	3.2	0.74	3
D	6.5 - 11.8	571	620	573.8	3.6	43	62.6	2.1	0.78	0.78	51.53	0.547	21.81	1.8	12.2	1.80	36

[a] Pseudo interval measured shear wave velocity.
[b] $V_{s1} = V_s (P_a / \sigma_v')^{0.25}$, stress corrected shear wave velocity (Andrus et al., 2007).
[c] $G_{max} = \rho V_s^2$, where ρ = total unit weight / acceleration of gravity, assumed to be 0.00176 MPa – s^2/m^2.
[d] $q_{t1N} = (q_t / P_a)(P_a / \sigma')^n$, were P_a = 100 kPa (Robertson and Wride, 1998).
[e] $(q_{t1N})_{cs} = q_{t1N} * K_c$, equivalent clean sand value of q_{t1N}.
[f] $I_c = [(3.47 - \log Q_t)^2 + (\log F_N + 1.22)^2]^{0.5}$ (Robertson and Wride, 1998).
[g] $F_N = f_s / (q_t - \sigma_v)*100\%$, normalized cone friction ratio (Robertson, 1990).
[h] $Q_t = (q_t - \sigma_v) / \sigma_v'$, normalized cone tip resistance (Robertson, 1990).
[i] $B_q = (u_2 - u_o)/(q_t - \sigma_v)$, normalized cone pore pressure ratio (Robertson, 1990).
[j] $I_D = (P_1 - P_o) / (P_o - u_o)$, dilatometer material index (Marchetti, 1980).
[k] $K_D = (P_o - u_o) / \sigma_v'$, dilatometer horizontal stress index (Marchetti, 1980).
[l] $K_o = (K_D / 1.5)^{0.47} - 0.6$, For $I_D \geq 1.2$; Schmertmann curves used to estimate at rest earth pressure coefficient (Marchetti, 1980).
[m] $E_D = 34.7(P_1 - P_o)$, DMT constrained modulus (Marchetti, 1980).

3.4.2 Soil Classification

Standard split-spoon sampling allowed for grain size analysis of materials in boring B 3. The boring log for borings B 3 and B 1 can be found in Figure A.7. The grain size distribution curves for boring B 3 are presented in Figure 3.9 and the tabulated grain size analysis data can be found in Table A.3. Only Layers B, C and D are shown in the figure. Layer B classifies as a poorly graded sand with silt (SP-SM) with fines content less than or equal to 7 %. It is interesting to note that grain size distribution curves for all four Layers B samples are practically the same indicating consistent depositional processes.

Layer C classifies as a poorly graded sand with silty clay (SP-SC), with average fines content of 13 % and plasticity index (PI) of 17. This layer contains shells, molluscan fauna and black phosphate pebbles which account for the gravel content listed as 20 %.

Layer D classifies as a silty sand (SM) with a fines content ranging from 28 to 43 % and an average PI less than 2. This layer has weak to moderate non-uniform cementation with mollusk fossils and black phosphate nodules. It is interesting to note that the grain size distribution curves for all four Layer D samples are similar, except the two from shallow depths containing more fines, indicating that soil forming processes may have occurred at the top of Layer D.

3.4.3 Soil Behavior Type

Because samples were only collected at borings B 3 and B 1, the soil behavior type classification charts by Robertson (1990) displayed in Figure 3.10

are used to classify the soils in each layer at the CREC site. The charts are based on normalized cone tip resistance (Q_t), normalized cone sleeve friction ratio (F_N), and normalized cone pore pressure ratio (B_q). The Q_t -F_N chart classifies Layer B as clean sand to silty sand (Zone 6), while the Q_t - B_q chart classifies the layer as gravelly sand to sand (Zone 7). Lunne et al. (1997) suggests that the actual soil type would be somewhere between the two predictions. The Q_t - F_N chart considers Layer C to be clayey silt to silty clay (Zone 4). The Q_t - B_q chart considers Layer C to be clayey silt to silty clay (Zone 4) or silty sand to sandy silt (Zone 5). The Q_t - F_N chart determines Layer D to be silty sand to sandy silt (Zone 5), while the Q_t - B_q chart determines the layer to be clayey silt to silty clay (Zone 4) or clay to silty clay (Zone 5).

These CPT-based soil behavior type classifications generally agree with the soil type classification made from the standard split-spoon samples.

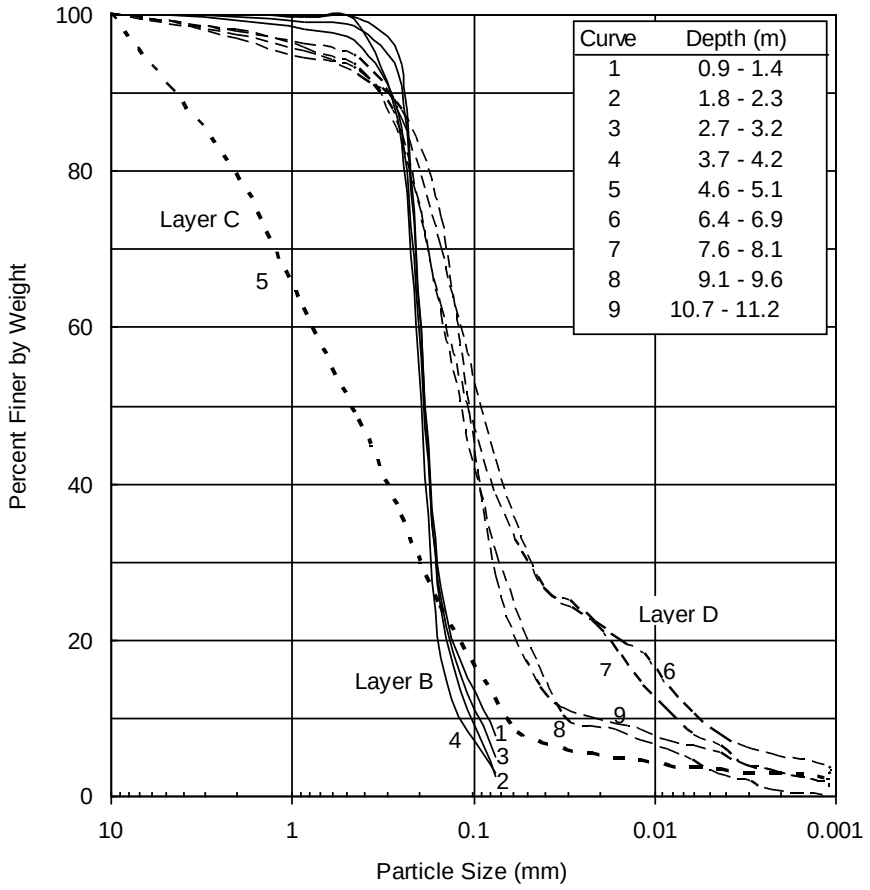

Figure 3.9 Grain size distribution curves for samples taken from boring B 3 at the CREC site.

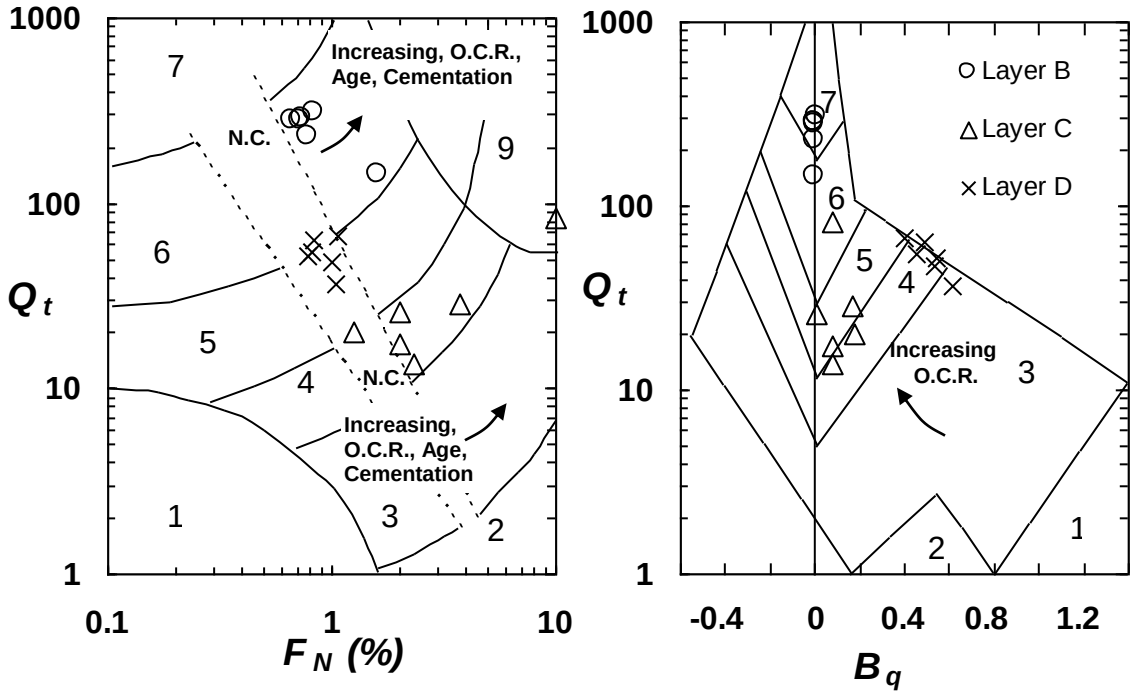

Zone	Soil behavior type	Zone	Soil behavior type
1.	Sensitive, fine grained;	6.	Sands: clean sands to silty sands;
2.	Organic soils, peats;	7.	Gravelly sand to sand;
3.	Clays: clay to silty clay;	8.	Very stiff sand to clayey sand;
4.	Silt mixtures: clayey silt to silty clay;	9.	Very stiff fine grained
5.	Sand mixtures: silty sand to sandy silt;		

N.C. = Normally Consolidated
O.C.R. = Overconsolidation Ratio

Figure 3.10 Soil behavior type classification charts by Robertson (1990) with data from the CREC site.

3.4.4 Results of the Dilatometer Test

Figures 3.11 and 3.12 give the results of DMT D 1 performed at the CREC site. Figure 3.11 is comprised of profiles of the material index (I_D), the horizontal stress index (K_D), the estimated at-rest earth pressure coefficient (K_o), and the dilatometer constrained modulus (E_D). Plotted in Figure 3.12 are the I_D and E_D values for Layers A, B, C and D. Soil type and stiffness can be estimated from Figure 3.12. Layer A has an average I_D and E_D of 1.78 and 17 MPa, respectively. These values indicate the layer to be a low to medium dense silty sand. Layer B has an average I_D of 3.48 and E_D ranges from 18 to 44 MPa. Layer B classifies as medium dense to dense silty sand to sand. Layer C has an average I_D and E_D of 0.60 and 3 MPa, respectively. Based on these values, Layer C is a very soft to soft clay to silty clay. Layer D has an average I_D of 1.78 and E_D ranges from 10 to 113 MPa. This layer classifies as a medium to dense clayey silt to silty clay. These classifications generally agree with the CPT–based classifications discussed in the previous section.

Values of K_D (see Figure 3.11b) were used to estimate the K_o values plotted in Figure 3.11c. The procedure used to estimate these K_o values is described in Section 2.3.2. The estimated K_D and K_o values for Layer A are much greater than 1, which may be due to the formulation of K_D. Near the ground surface and above the water table depth u_o and σ'_v decrease significantly and affect liftoff pressures (P_o) less, leading to high K_D values. The high K_D values may also stem from overconsolidation, which may have resulted from

repeated wetting and drying of soil deposits near the ground surface during the 100,000 years after the initial deposition of the deposit. In Layer B below the water table, K_o varies from 1.40 to 0.45, with an average value of 0.88. Layer C has an average K_o of 0.74. Layer D has an average K_o of 1.80. This high K_o value may be a result of the materials of Layer D being heavily overconsolidated.

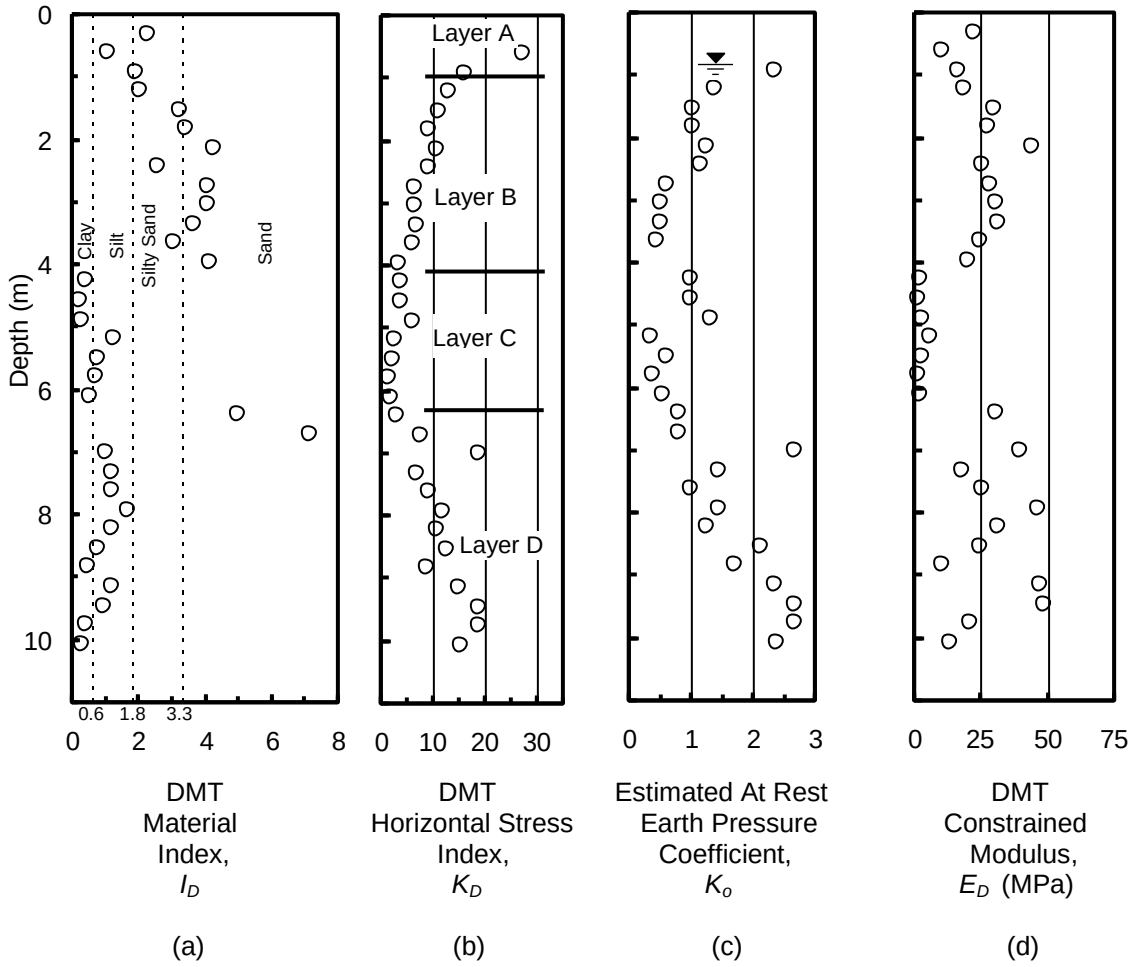

Figure 3.11 Results of DMT D 1 performed at the CREC site.

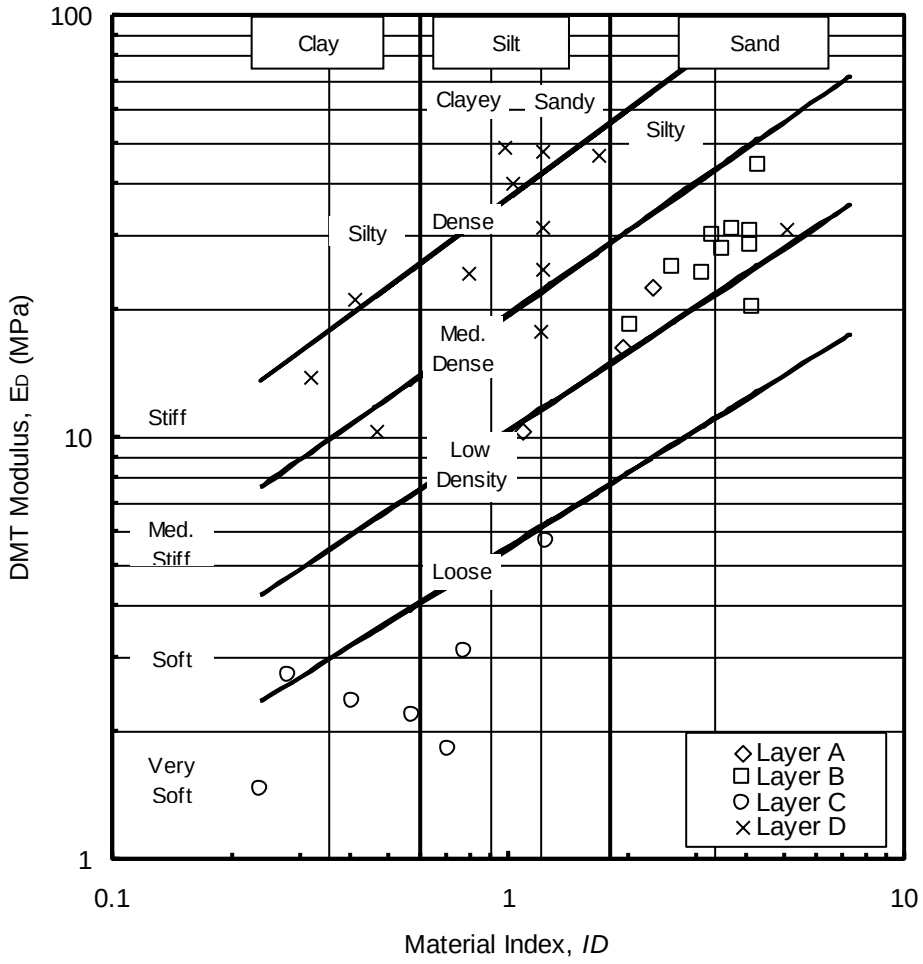

Figure 3.12 DMT modulus and material index chart (ASTM D 6635) with data from the CREC site.

3.4.5 Liquefaction Susceptibility

Figure 3.13 presents the CPT-based liquefaction susceptibility chart by Hayati and Andrus (2008). Plotted on the chart are the data from the CREC site. Data points with negative B_q values are plotted as having a value of zero. According to the chart, only Layer B has a consistency that is susceptible to liquefaction. Layers C and D are not susceptible to liquefaction or need additional testing to determine the susceptibility because of high I_c or plastic fines content. It can be concluded that only B at the CREC site is susceptible to liquefaction, at least according to composition.

Liquefaction susceptibility according to density for the CREC site is determined by using average values of $(q_{t1N})_{cs}$ and $(N_1)_{60cs}$. Materials with $(q_{t1N})_{cs}$ values greater than 160 to 190 are considered to be not susceptible to liquefaction (Robertson and Wride, 1998; Idriss and Boulanger, 2004; Moss et al., 2006). With average values of $(q_{t1N})_{cs}$ ranging from 83 to 147, Layer B is susceptible to liquefaction based on the density criteria. Materials with $(N_1)_{60cs}$ values greater than 30 to 36 are considered to be not susceptibility to liquefaction (Seed et al., 1984; Idriss and Boulanger, 2003; and Cetin et. al., 2004). Layer B has $(N_1)_{60cs}$ values that range from 8 to 20, indicating the layer is susceptible to liquefaction.

These results indicated that Layer B is susceptible to liquefaction. A liquefaction potential evaluation considering the seismic loading (magnitude and

acceleration) of the 1886 earthquake is planned. This analysis will be done as part of the next phase of this NSF supported project.

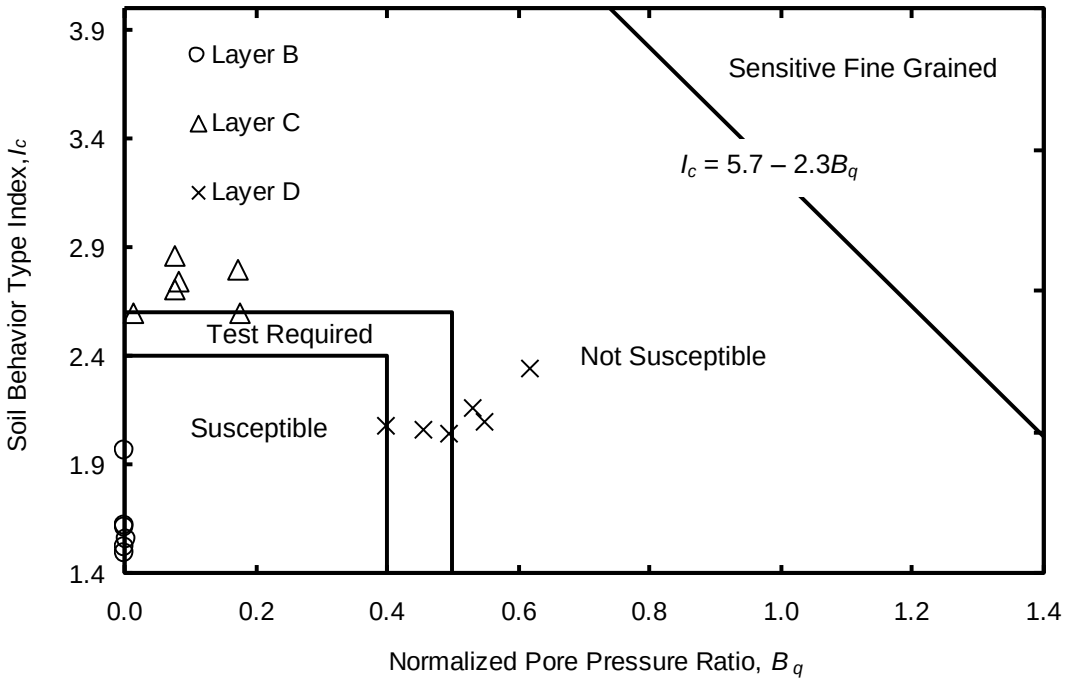

Figure 3.13 CPT–based liquefaction susceptibility chart by Hayati and Andrus (2008) with data from the CREC site.

3.4.6 Shear Wave Velocity

Profiles of shear wave velocity (V_s) based on pseudo interval measurements for SCPTs SC 1, SC 3 and SC 6 are presented in Figure 3.14. Within the profiles, values of V_s range from 141 to 732 m/s. The average values of V_s for Layers B and C are 179 and 160 m/s, respectively. Layer D for SC 3 and SC 6 have an average V_s of 545 m/s. The profile for SC 6 extends to a depth of 27.8 m and has an average V_s of 329 m/s in the lower 13 m.

Table 3.1 contains the average values of measured V_s and overburden-stress corrected shear wave (V_{s1}) for each layer at the CREC site. The assumptions and equations used to calculate V_{s1}, and other in-situ properties, are given in the footnotes of the table. Average V_s and V_{s1} values for Layer C of SC 1 are not given in the table because a measurement interval is not completely within the layer.

Table 3.2 presents the measured to predicted shear velocity ratios (MPV_sR) and the measured to predicted shear modulus to tip resistance ratios (MPG_{max}/q_tR) for the CREC site. Layer B has an average MPV_sR and MPG_{max}/q_tR of 1.38 and 1.48, respectively. Layer C has an average MPV_sR and MPG_{max}/q_tR of 1.55 and 1.66, respectively, suggesting the deposits of this layer are somewhat older than Layer B. Layer D has average MPV_sR and MPG_{max}/q_tR values of 3.23 and 8.70, respectively. The higher MPV_sR values for Layer D, indicates the layer is significantly older and/or more cemented than the overlying layers.

Shown in Figure 3.15 is the measured to predicted V_{s1} chart for Holocene deposits by Andrus et al. (2007). Layers B, C and D for the CREC site plot below the trend line representing a MPV_sR value equal to 1.0, indicating Holocene-age deposits. The position of the CREC site's data points is due to the site containing Pleistocene and Tertiary-age deposits.

The average MPV_sR of 1.38 determined for Layer B is very similar to the average MPV_sR of 1.39 that Hayati and Andrus (2008) determined for the 100,000 year old Wando Formation in Charleston that did not liquefy during the 1886 Charleston Earthquake. Thus, it is believed that the CREC site was not disturbed by liquefaction during the 1886 earthquake or other Holocene events. Supporting this conclusion is the fact that significant sand boil deposits or significant changes in soil type have not been observed in the fields of CREC.

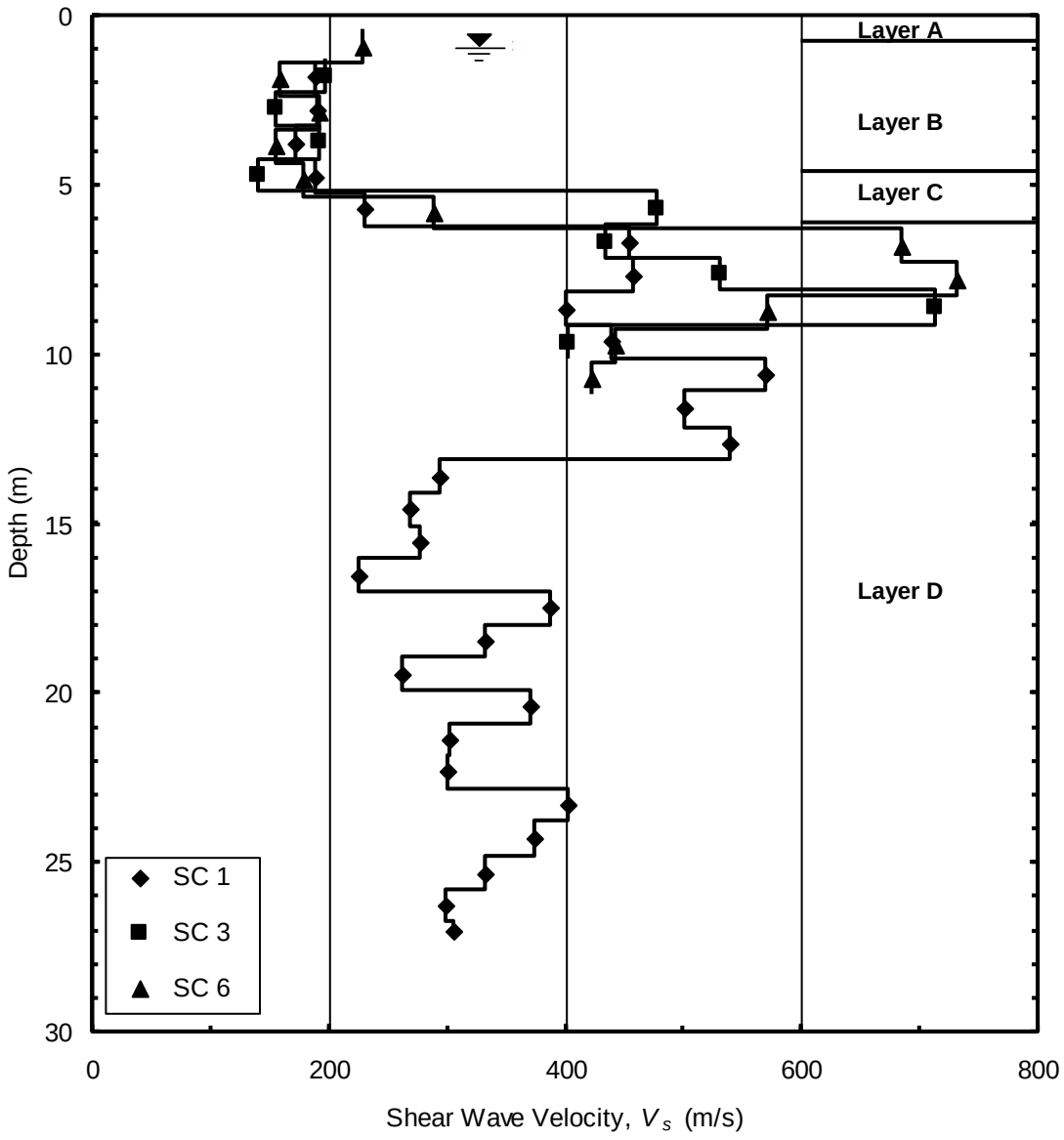

Figure 3.14 Shear wave velocity profiles for SCPT SC 1, SC 3 and SC 6 at the CREC site.

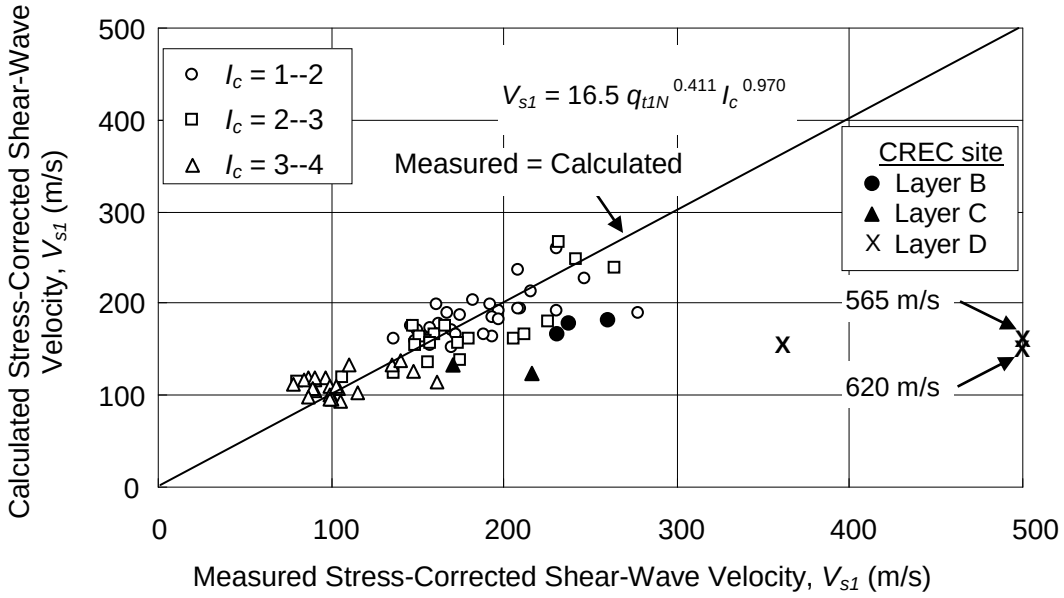

Figure 3.15 Comparison of measured to predicted V_{s1} for Holocene deposits by Andrus et al. (2007) with data from the CREC site.

Table 3.2 Average predicted properties of the near surface soil layers at the CREC site.

Layer	Interval (m)	V_s [a]	V_{s1} [b]	G_{max} / q_t [c]	Measured / Predicted	Measured / Predicted
		(m/s)		(MPa)	V_{s1}	G_{max} / q_t
SC 1						
B	0.8 – 4.7	136	186	5.72	1.38	1.63
C	4.7- 5.8	-	-	-	-	-
D	5.8 - 27.8	168	160	14.61	2.21	4.12
SC 3						
B	1.0 - 4.6	132	173	5.79	1.36	1.32
C	4.6 - 6.4	108	128	21.68	1.32	1.08
D	6.4 - 10.7	149	162	11.57	3.49	9.76
SC 6						
B	1.0 – 4.5	121	168	9.04	1.39	1.45
C	4.5 - 6.5	101	120	35.71	1.78	2.23
D	6.5 - 11.8	145	156	13.15	3.98	12.21

[a] $V_s = 2.27\ q_t^{0.412} I_c^{0.989} D^{0.033}$, where D = Depth (Andrus et. al., 2007).
[b] $V_{s1} = 16.5\ q_{t1N}^{0.411} I_c^{0.970}$ (Andrus et. al., 2007).
[c] G_{max} / q_t (predicted) = 185 $(q_{t1N})^{-0.7}$ for freshly deposited silica sand (Baldi et al., 1986).

3.5 Summary

The investigations conducted at the CREC site show there is a fairly uniform medium dense sand layer (Layer B) that extends from 0.7 m to a depth of 4.5 m. Layer B has an average q_t of 6.3 MPa, FR of 0.87 %, and B_q of -0.001. According to grain size analysis, the materials of Layer B classifies as clean sand to silty sand. Based on the DMT, the average K_o in Layer B is estimated to be around 0.88. The ground water table depth at the CREC site lies at about 0.80 m.

The average measured and predicted V_s values are 177 m/s and 130 m/s, respectively. These values provide a MPV_sR of 1.38 for Layer B. This value is very similar to the MPV_sR of 1.39 that Hayati and Andrus (2008) determined for the Wando Formation. McCartan et al. (1984) mapped the surficial deposits at the CREC site as 100,000 beach sands, which are considered equivalent to the Wando Formation in Charleston mapped by Weems and Lemon (1993). Had the MPV_sR been closer to 1.0, a Holocene age would be more likely.

These findings agree with the observation that the area on which the CREC site is located did not liquefy in 1886 (Martin and Clough, 1990). The high MPV_sR values also support no liquefaction at the CREC site during other Holocene events.

CHAPTER FOUR

INVESTIGATIONS AT THE HOBCAW BARONY BORROW PIT SITE

4.1 Introduction

Hobcaw Barony is a 17,500 acre outdoor laboratory owned and operated by the Belle W. Baruch Foundation. Hobcaw Barony is located east of Georgetown, South Carolina off of Highway U.S. 17, which is about 100 km northwest of Charleston and the CREC site. Hobcaw, a word from the Waccamaw Indian language meaning between waters, is located between the Waccamaw River and the Atlantic Ocean. Presented in Figure 4.1 is a map of the Hobcaw Barony area.

The Belle W. Baruch Foundation's primary research and educational activities include forestry, wildlife, and marine science. To support these activities, Clemson University and the University of South Carolina have established research facilities located on the reserve. In addition, the Foundation maintains multiple historic homes and a 19th century slave village. The Foundation has made available two locations for geotechnical testing and research for this study.

Shown in Figure 4.1 are the locations of the two geotechnical investigation sites. The first site is near an active borrow pit area west of the Bellefield House and Stables. The second location is at the intersection of Marsh Road and Clambank Road. These two sites are herein called the Borrow Pit site and the

Marsh Road site, respectively. Presented in this chapter are the results of the investigations at the Borrow Pit site. Results of the investigations at the Marsh Road site are presented in Chapter 5.

Martin and Clough (1990) and Lewis et al. (1999) reviewed several earthquake reports and found no evidence that liquefaction was observed in the Hobcaw Barony area during the 1886 earthquake. Currently no paleoliquefaction studies have been conducted at the Borrow Pit site.

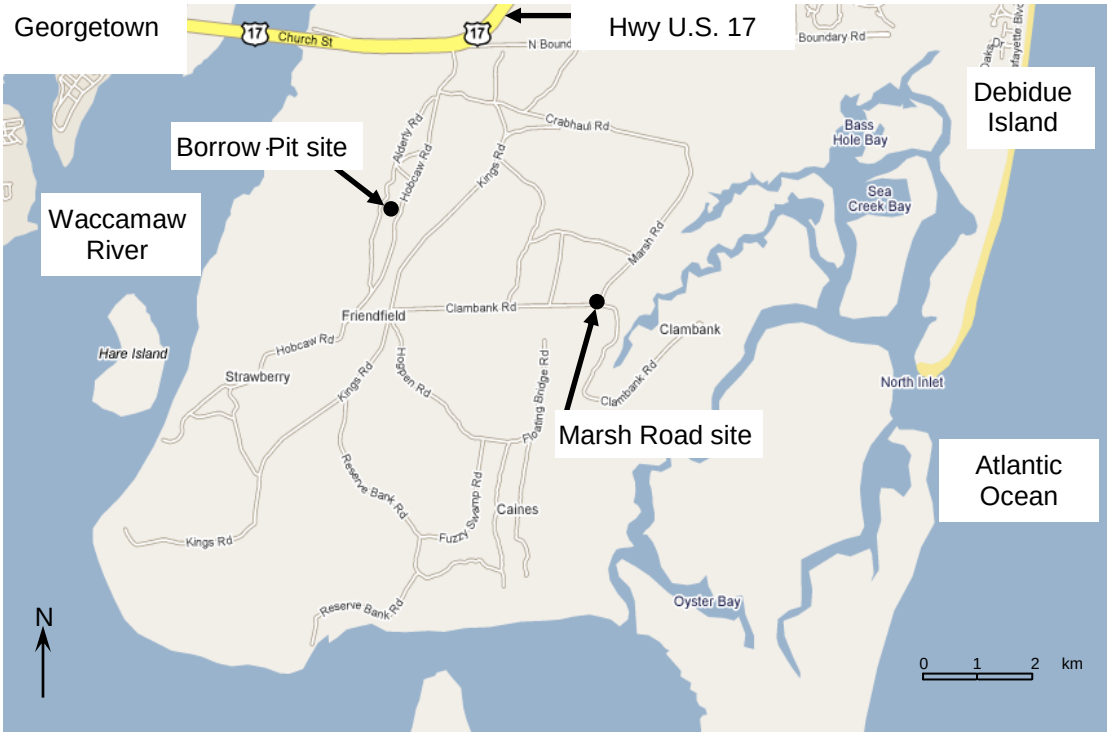

Figure 4.1 Map of Hobcaw Barony showing locations of the Borrow Pit and Marsh Road geotechnical experimentation sites.

4.2 Geology

Hobcaw Barony is formed on the east by modern beach barriers and tidal flats. Inland, the area is covered by beach ridges that were formed by the deposition of sand from waves, which resulted from regression of the ocean or a seaward growth of the coastline (May 1978, p. 29). Figure 4.2 gives the depositional trends of the beach ridges, as interpreted by May (1978), and the location of the Borrow Pit site and Marsh Road site. The beach ridges are labeled from oldest (number 1) to youngest (number 7). The Borrow Pit site is located between beach ridges 1 and 3. Beach ridges in this area are partially covered with dune deposits.

Based on borehole information, May (1978) developed one of the first general geologic cross-sections of the Hobcaw area. Figure 4.3 shows the locations of boreholes considered by May (1978) and the cross-section alignments. The cross-section for the alignment containing boreholes 3, 5, M, and D is shown in Figure 4.4. Pleistocene-age deposits range in thickness from 9 to 15 m (29 to 50 ft). Underlying the Pleistocene deposits is the Tertiary-age Black Mingo Formation. This formation is approximately 58 m (190 ft) thick. The Paleocene-age Peedee Formation concludes the layering of the cross-section, beginning at an average depth below sea level of about 66 m (217 ft). Siple (1957) characterized the Black Mingo Formation as a sand to sandstone with possible interbedded clay layers. The Peedee Formation was characterized as a black to gray sand with thick interbedded clay layers.

May (1978) concluded the beach deposits around the Borrow Pit site to be 100,000 to 200,000 years old. This conclusion agrees with the geologic map by McCartan et al. (1984) shown in Figure 1.1, which identifies the surficial deposits at the Borrow Pit site as 200,000 year old beach sands.

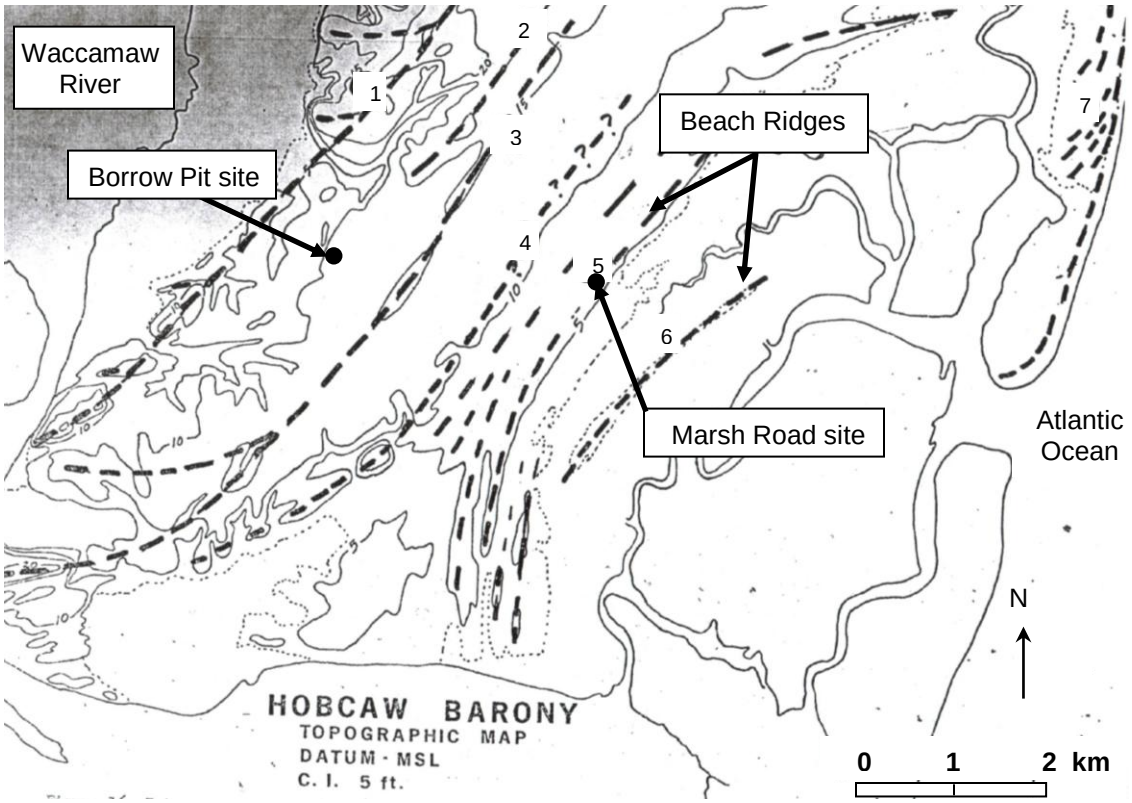

Figure 4.2 Topographic map indicating beach ridges and geotechnical investigation sites (May, 1978).

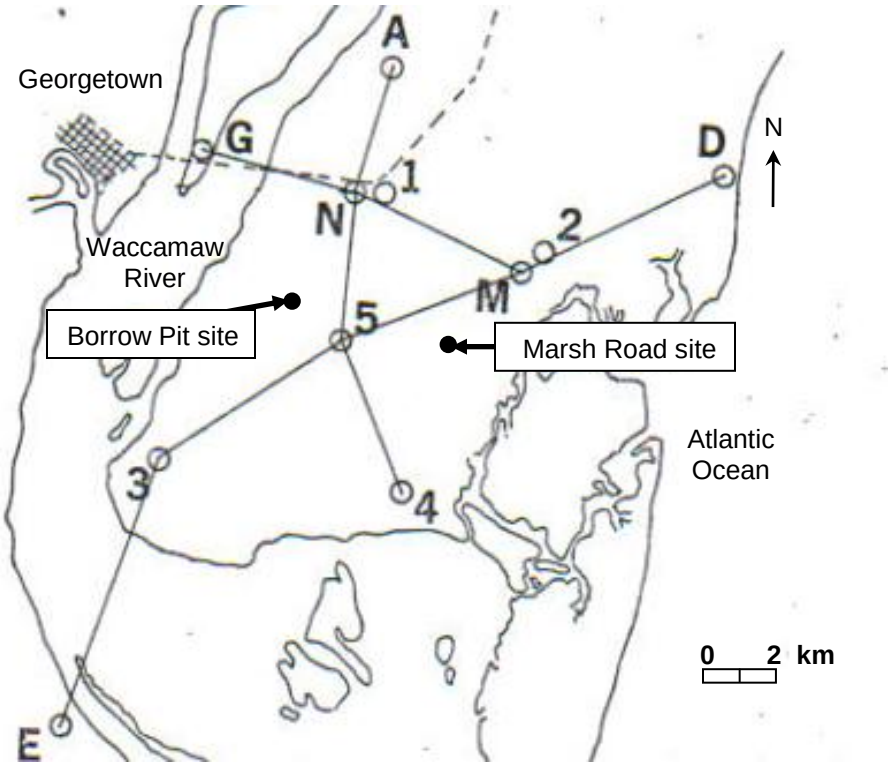

Figure 4.3 Map of Hobcaw Barony showing boreholes used by May (1978) to create geologic cross-sections.

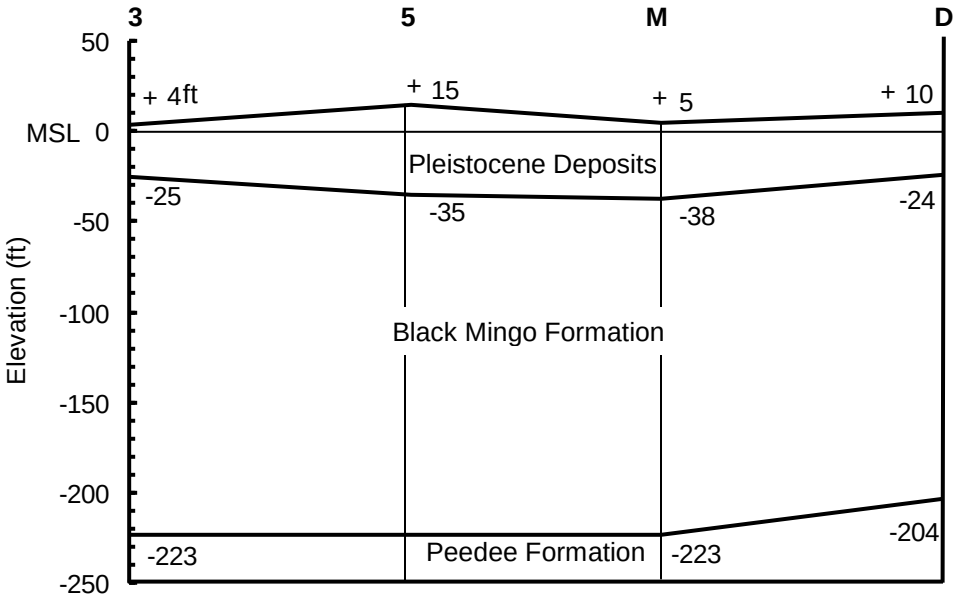

Figure 4.4 Geologic cross-section for boreholes 3, 5, M and D shown in Figure 4.3 (May, 1978).

4.3 Investigations

Figure 4.5 provides an aerial view of the Borrow Pit site and surrounding area. The Borrow Pit site is located between three roads - Airport Road to the south, Hobcaw Road to the east, and Bellefield Road to the west. The site is located about 0.1 km north of the active borrow area. The Borrow Pit site is intersected by an unnamed dirt access road and is covered with moderate grass vegetation. A photograph of the Borrow Pit site is shown in Figure 4.6. The photograph provides a south to north view of the site showing locations of SCPTs HB 2 and HB 3, reference points 2 and 3, the dirt road, and the tree line that surrounds the site. The two reference points plus a third were used to construct the sitemap in Figure 4.7 that illustrates the test locations and layout.

Testing began the morning of July 25, 2007. Three SCPTs (HB 1, HB 2 and HB 3) were first performed at the site. SCPTs HB 1 and HB 3 were located in the center of the dirt road (see Figure 4.7). HB 2 was located approximately 20 m west of HB 3 and 4 m east of the oak tree at reference point 3. A dilatometer test, D 1 was then performed 2 m away from HB 1. Table B.1 gives the local coordinates for the test locations. All SCPTs were pushed until refusal. The total depths of the SCPTs were 15.7 m, 12.2 m and 13.1 m for SCPT HB 1, HB 2 and HB 3, respectively. The DMT extended to a depth of 10.4 m.

Figure 4.5 Aerial photograph of the Borrow Pit site and surrounding areas.

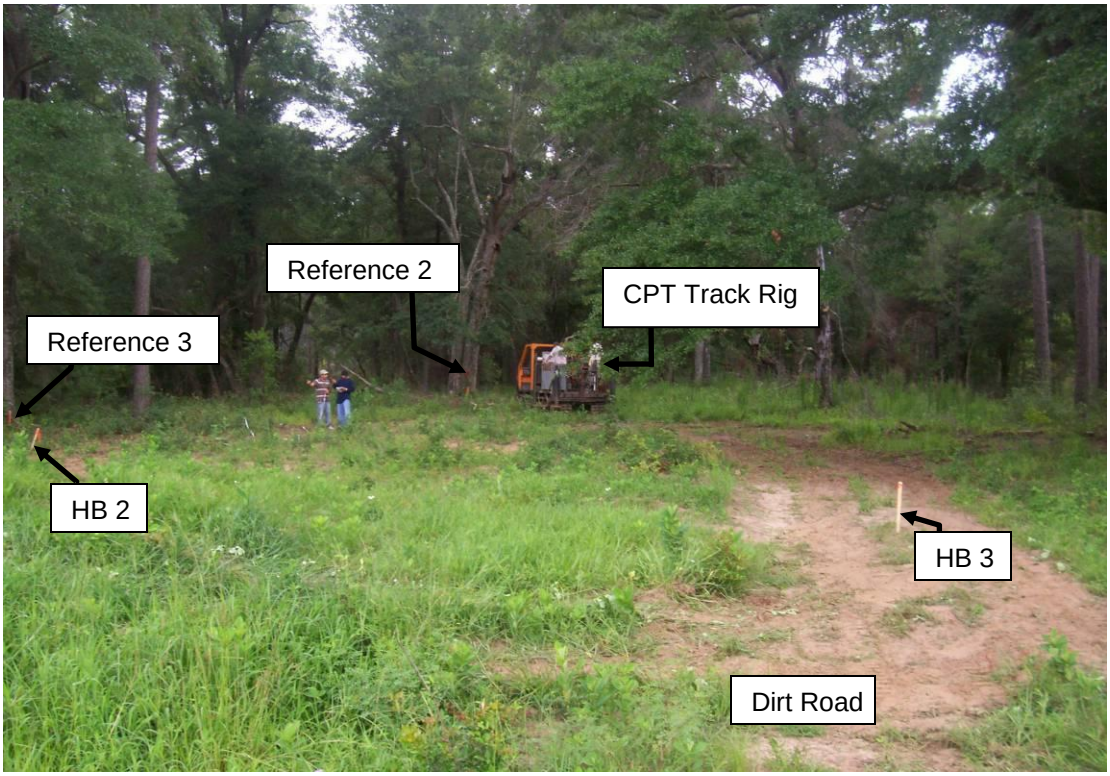

Figure 4.6 Photograph of the Borrow Pit site showing the location of cone soundings HB 2 and HB 3. The CPT track rig is on DMT D1.

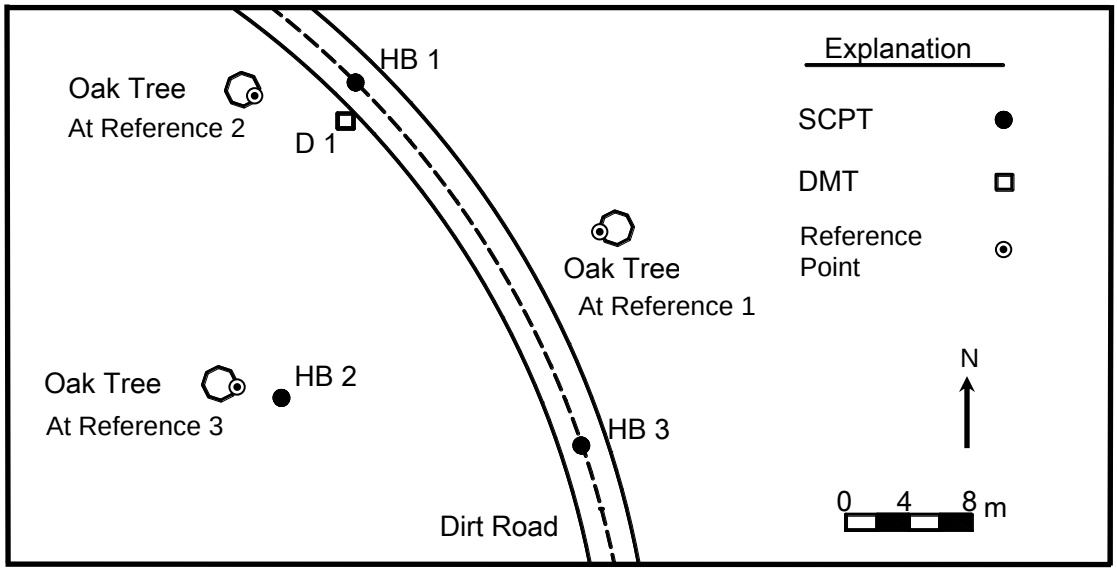

Figure 4.7 Map showing test locations at the Borrow Pit site.

4.4 Results

The SCPT and DMT test results are tabulated in Appendix B. The results are discussed in the following paragraphs to characterize stratigraphy, soil type, lateral earth pressure, liquefaction susceptibility, and shear wave velocity.

4.4.1 Stratigraphy

Figure 4.8 provides a composite profile of SCPT HB 1. The figure consists of corrected tip resistance (q_t), friction ratio (*FR*), pore water pressures measured behind the cone tip (u_2), shear wave velocity (V_s), and soil layer designation. The soil layer designations are A, B, C, D, and E. Layer A extends to a depth of 8.7 m and has an average tip resistance of 7.4 MPa. The layer also has low values of *FR* and u_2 averaging 0.1 % and 0.03 MPa, respectively, suggesting the deposits to be predominately sand.

Layers B and D at HB 1 lie between depths of 8.9 to 9.8 m and 13.0 to 13.8 m, respectively. The layers are characterized by low averages of q_t (less than 3 MPa) and *FR* (approximately 1 %). Within the layers, there is a noticeable increase in the u_2 profile with average values of 0.3 MPa. These results indicate that Layers B and D have significant fines content (silt and clay).

Layer C extends from a depth of 9.8 m to a depth of 13.0 m. The layer exhibits non-uniform values of q_t with an average of 7.4 MPa. Values of *FR* are less than 1 % and u_2 values are close to u_o, suggesting Layer C to be a sand deposit.

Layer E begins at a depth of 13.8 m and is characterized by average q_t of 12.5 MPa, *FR* of 2.2 %, and u_2 of 3.4 MPa. These values imply that the soil of Layer E is a stiff clayey sand or silty sand. It is possible that Layer E represents a transition into the Black Mingo Formation. This finding agrees with the geologic profile by May (1978) shown in Figure 4.4, where the Black Mingo Formation begins around depths of 14 to 16 m in the borrow area.

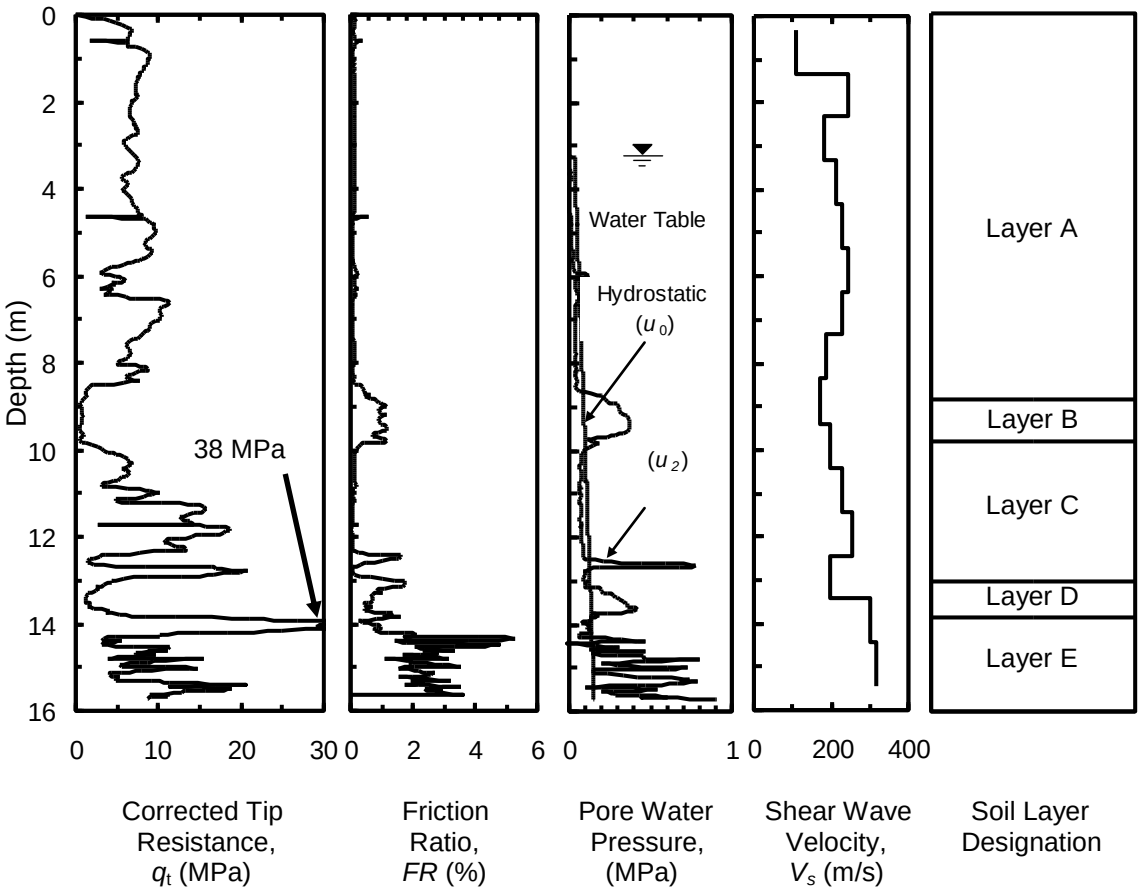

Figure 4.8 Composite profiles for SCPT HB 1 at the Borrow Pit site.

Figure 4.9 provides a cross-section of the Borrow Pit site to a depth of 13 m based on q_t and *FR* of the three SCPTs. Only Layers A, B and C are present in the top 13 m at the three test locations. Layer depth intervals and tabulated averages of q_t and *FR* can be found in Table 4.1. Layer A exhibits fairly consistent profiles with an average q_t of 7.7 MPa and *FR* less than 1 %, and a lower boundary at 8.9 m. Layer B is about 1 m thick at HB 1 and HB 3, and thins to a thickness of 0.4 m at HB 2. The thickness of Layer C ranges from 3 m to over 4 m. The ground water table depth at the site lies at a depth of about 2.7 m.

4.4.2 Soil Behavior Type

Because no samples were collected at the Borrow Pit site, as part of these investigations, the soil behavior type classification charts by Robertson (1990) displayed in Figure 4.10 are used to classify the soils in each layer. The charts are based on normalized cone tip resistance (Q_t), normalized cone sleeve friction ratio (F_N), and normalized cone pore pressure ratio (B_q). Based on the Q_t - F_N and Q_t - B_q charts, Layers A and C classify as clean sand to silty sand (Zone 6). Layer B is considered to be clay to silty sand (Zones 3 to 5) according to both charts. Layer D classifies as silty sand to sandy silt (Zone 5) according to both of the charts. Layer E classifies as a silty sand to sandy silt (Zone 5) based on the Q_t - F_N chart and a clean sand to silty sand (Zone 6) according to the Q_t - B_q chart. The actual soil type is likely between the predictions of the two charts (Lunne et al., 1997).

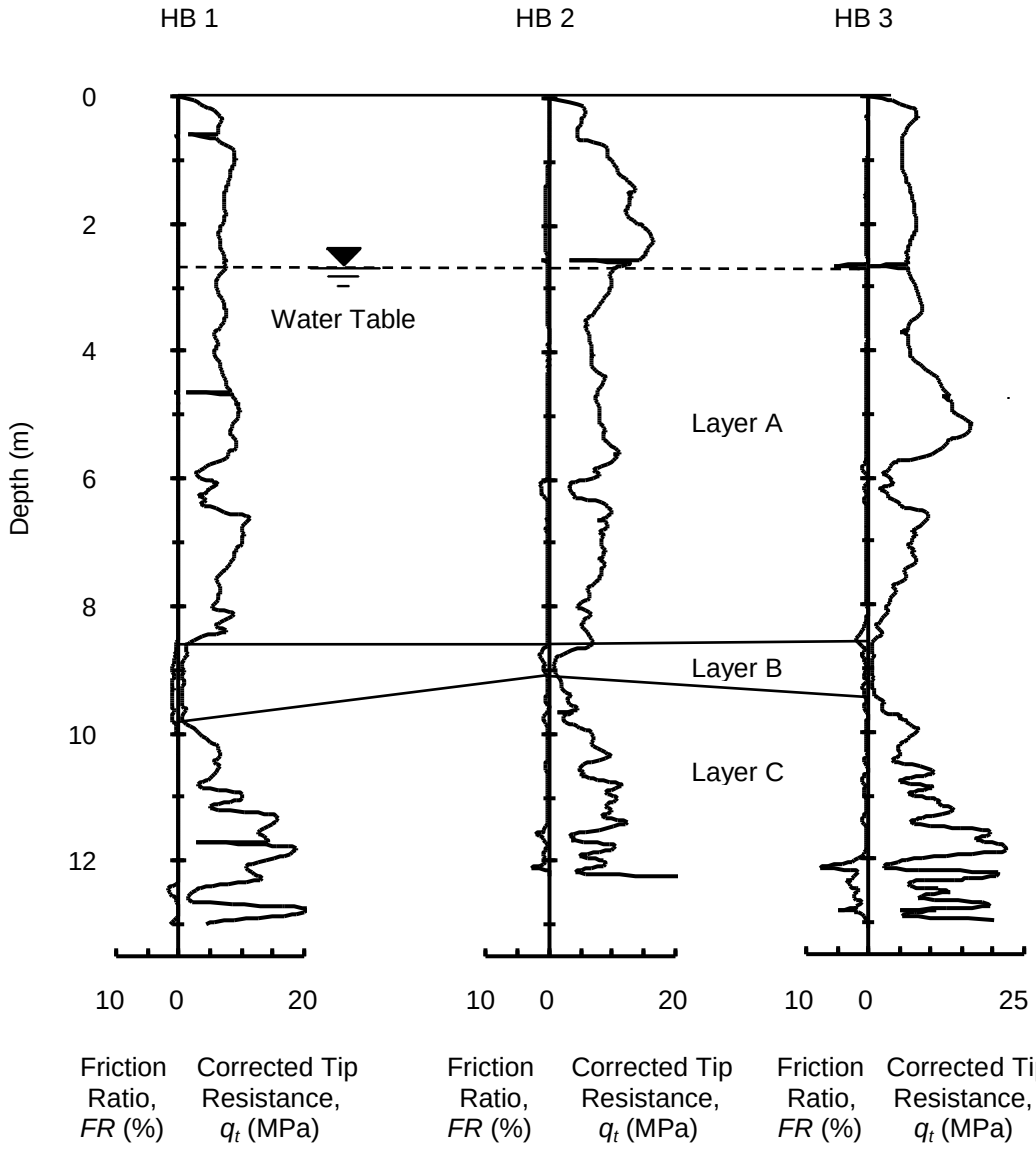

Figure 4.9 CPT cross-section for soundings HB 1, HB 2, and HB 3 at the Borrow Pit site.

Table 4.1 Average measured properties of the near surface soil layers at the Borrow Pit site.

Layer Interval (m)		V_s[a] (m/s)	V_{s1}[b] (m/s)	G_{max}[c] (MPa)	q_t (MPa)	q_{t1N}[d]	$(q_{t1N})_{cs}$[e]	I_c[f]	FR (%)	F_N[g]	Q_t[h]	B_q[i]	u_2/u_o	I_D[j]	K_D[k]	K_o[l]	E_D[m] (MPa)
HB 1															DMT D 1		
A	3.2 - 8.9	222	241	86.7	7.4	88	89	1.5	0.11	0.11	105	-0.004	0.49	4.3	4.18	0.69	38
B	8.9 - 9.8	-	-	-	0.8	8	49	3.0	0.94	1.22	6.33	0.400	3.02	0.3	4.00	0.98	4
C	9.8 - 13.0	224	217	88.3	11.7	111	118	1.6	0.21	0.23	103.4	0.010	0.88	2.3	1.96	0.61	13
D	13.0 – 13.8	-	-	-	2.6	24	66	2.6	0.94	1.05	19.6	0.092	1.93	-	-	-	-
E	13.8 – 15.0	316	295	175.7	13.8	111	166	2.2	2.24	2.34	96.9	0.021	1.75	-	-	-	-
HB 2																	
A	2.7 – 8.9	210	232	77.6	7.5	94	97	1.6	0.26	0.26	118.1	-0.007	0.17	-	-	-	-
B	8.9 – 9.3	-	-	-	1.5	16	39	2.5	0.44	0.45	15.5	-0.014	0.75	-	-	-	-
C	9.3 – 12.2	247	246	107.4	8.4	84	88	1.7	0.28	0.28	83.2	-0.006	0.56	-	-	-	-
HB 3																	
A	2.4 – 8.7	207	230	75.4	8.2	104	107	1.6	0.36	0.36	130.5	-0.006	0.20	-	-	-	-
B	8.7 – 9.6	-	-	-	0.9	10	42	2.8	0.57	0.70	38.7	0.029	1.07	-	-	-	-
C	9.6 – 12.0	236	233	98.0	10.5	103	111	1.8	0.47	0.48	99.7	-0.006	0.53	-	-	-	-
D	-	-	-	-	-	-	-	-	-	-	-	-	-	-	-	-	-
E	12.0 – 12. 3	-	-	-	15.8	150	213	2.1	3.20	3.36	141.0	-0.0001	0.97	-	-	-	-

[a] True interval measured shear wave velocity.

[b] $V_{s1} = V_s (P_a / \sigma_v')^{0.25}$, stress corrected shear wave velocity (Andrus et al., 2007).

[c] $G_{max} = \rho V_s^2$, where ρ = total unit weight / acceleration of gravity, assumed to be 0.00176 MPa – s^2/m^2.

[d] $q_{t1N} = (q_t / P_a)(P_a / \sigma')^n$, were P_a = 100 kPa (Robertson and Wride, 1998).

[e] $(q_{t1N})_{cs} = q_{t1N} * K_c$, equivalent clean sand value of q_{t1N}.

[f] $I_c = [(3.47 - \log Q_t)^2 + (\log F_N + 1.22)^2]^{0.5}$ (Robertson and Wride, 1998).

[g] $F_N = f_s / (q_t - \sigma_v)*100\%$, normalized cone friction ratio (Robertson, 1990).

[h] $Q_t = (q_t - \sigma_v) / \sigma_v'$, normalized cone tip resistance (Robertson, 1990).

[i] $B_q = (u_2 - u_o)/(q_t - \sigma_v)$, normalized cone pore pressure ratio (Robertson, 1990).

[j] $I_D = (P_1 - P_o) / (P_o - u_o)$, dilatometer material index (Marchetti, 1980).

[k] $K_D = (P_o - u_o) / \sigma_v'$, dilatometer horizontal stress index (Marchetti, 1980).

[l] $K_o = (K_D / 1.5)^{0.47} - 0.6$, For $I_D \geq 1.2$;Schmertmann curves used, estimated at rest earth pressure coefficient (Marchetti,1980).

[m] $E_D = 34.7(P_1 - P_o)$, DMT constrained modulus (Marchetti, 1980).

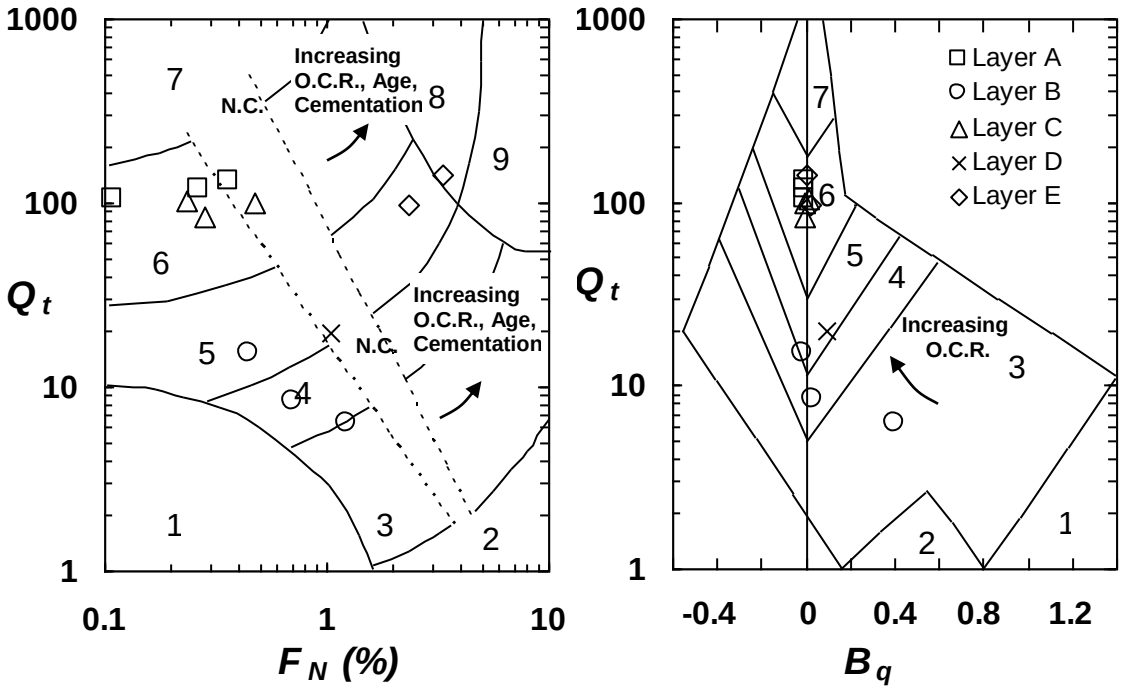

Zone	Soil behavior type	Zone	Soil behavior type
1.	Sensitive, fine grained;	6.	Sands: clean sands to silty sands;
2.	Organic soils, peats;	7.	Gravelly sand to sand;
3.	Clays: clay to silty clay;	8.	Very stiff sand to clayey sand;
4.	Silt mixtures: clayey silt to silty clay;	9.	Very stiff fine grained
5.	Sand mixtures: silty sand to sandy silt;		

N.C. = Normally Consolidated
O.C.R. = Overconsolidation Ratio

Figure 4.10 Soil behavior type classification charts by Robertson (1990) with data from the Borrow Pit site.

4.4.3 Result of Dilatometer Test

Figures 4.11 and 4.12 give the results of DMT D 1 performed at the Borrow Pit site. Figure 4.11 is comprised of profiles of the material index (I_D), the horizontal stress index (K_D), the estimated at-rest earth pressure coefficient (K_o), and the dilatometer constrained modulus (E_D). Plotted in Figure 4.12 are the I_D and E_D values for Layers A, B, and C. Soil type and stiffness can be estimated from Figure 4.12. Layer A has an average I_D of 4.3 and E_D ranges from 24 MPa to 70 MPa. The layer classifies as dense to medium dense silty sand to sand. For Layer B, the three values of I_D are 0.22, 0.29 and 0.43 and E_D averages 4 MPa. Based on these values the layer is a soft clay to silty clay. Layer C has I_D values of 2.93 and 1.59 and E_D averages 13 MPa. This layer classifies as a medium to low dense sandy silt to silty sand. These classifications generally agree with the CPT–based classifications discussed in the previous section.

Values of K_D (see Figure 4.11b) were used to estimate the K_o values plotted in Figure 4.11c. The procedure used to estimate these K_o values is described in Section 2.3.2. The estimated K_D and K_o values near the ground surface are much greater than 1, which may be due to the formulation of K_D or the repeated wetting and drying of soil deposits near the ground surface during the 200,000 years after the initial deposition of the sand. Within Layer A and below the water table, K_o is fairly uniform with an average value of 0.69. In Layer B, the average value of K_o is 0.98. Layer C has an average K_o of 0.61. In Layer B the horizontal and vertical effective stresses are nearly equal. In Layer A

below the water table and in Layer C the effective horizontal stresses are about 0.69 and 0.61 times the vertical stress.

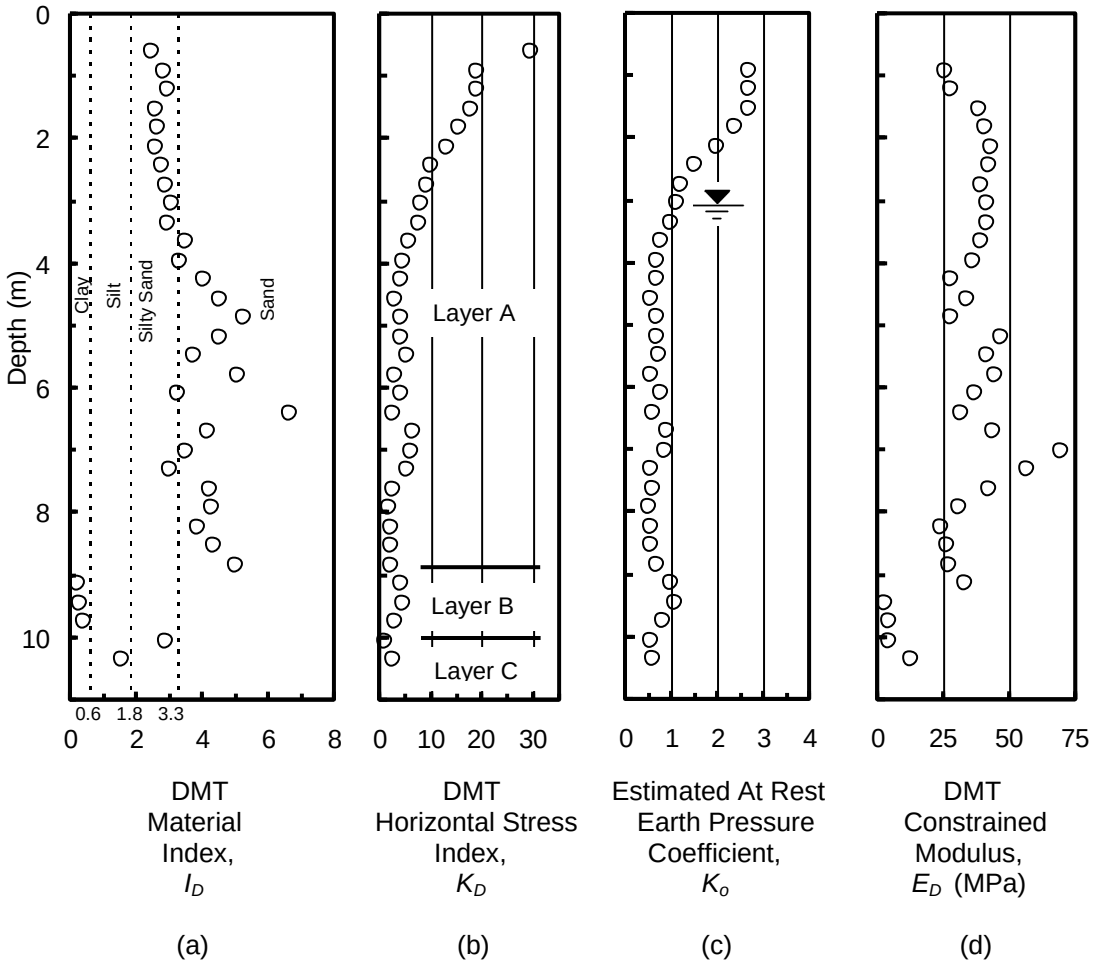

Figure 4.11 Results of DMT D 1 performed at the Borrow Pit site.

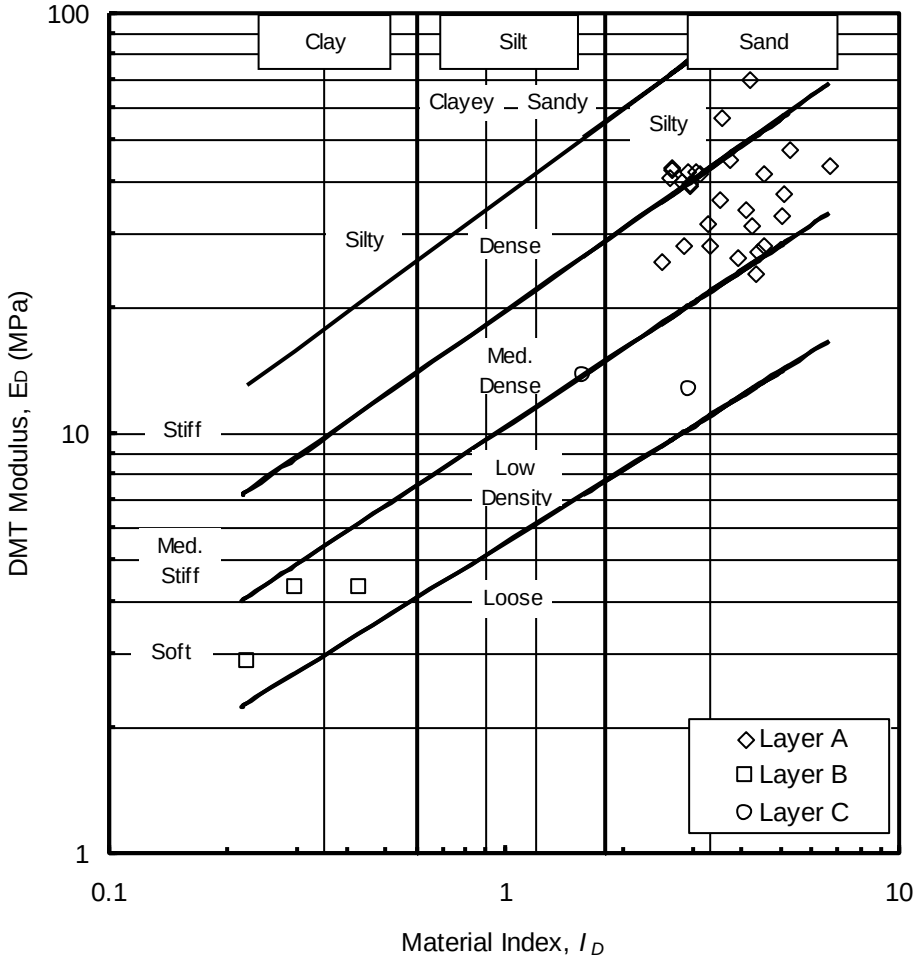

Figure 4.12 DMT modulus and material index chart (ASTM D 6635) with data from the Borrow Pit site.

4.4.4 Liquefaction Susceptibility

Figure 4.13 presents the CPT-based liquefaction susceptibility chart by Hayati and Andrus (2008). Plotted in the chart are the data from the Borrow Pit site. It should be noted that data points with negative B_q values are plotted as having a value of zero. According to the chart, Layers A, C, and E are susceptible to liquefaction. Layers B and D are not susceptible to liquefaction or need additional testing to determine the susceptibility. Thus, much of the near-surface sediment beneath the Borrow Pit site has a consistency that is susceptible to liquefaction.

Liquefaction susceptibility according to density for the Borrow Pit site is evaluated using $(q_{t1N})_{cs}$. Materials with $(q_{t1N})_{cs}$ values greater than 160 to 190 are considered to be not susceptible to liquefaction (Robertson and Wride, 1998; Idriss and Boulanger, 2004; Moss et al., 2006). Layers A, B, C and D for all three SCPTs are susceptible to liquefaction with $(q_{t1N})_{cs}$ values ranging from 39 to 118. Layer E for SCPT HB 1 has an average $(q_{t1N})_{cs}$ of 166 and is considered to have marginal to low susceptibility. Layer E for HB 3 has an average $(q_{t1N})_{cs}$ of 213 and is considered to be not susceptible to liquefaction.

These results indicate that Layers A, C and possibly E are susceptible to liquefaction. A liquefaction potential evaluation considering the seismic loading (magnitude and acceleration) of the 1886 earthquake is planned. This analysis will be done as part of the next phase of this NSF supported project.

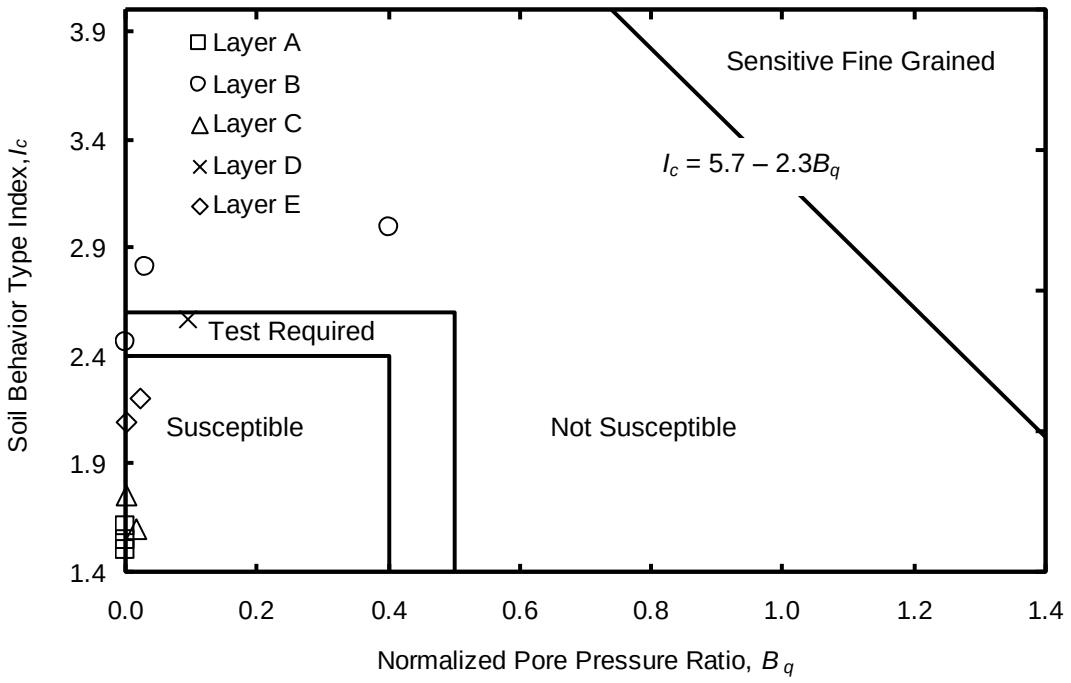

Figure 4.13 CPT–based liquefaction susceptibility chart by Hayati and Andrus (2008) with data from the Borrow Pit site.

4.4.5 Shear Wave Velocity

Profiles of V_s based on true interval measurements for SCPTs HB 1, HB 2 and HB 3 are presented in Figure 4.14. Values of V_s range from 109 to 316 m/s. The greatest variation in V_s occurs near the ground surface and above the water table, where values range from 109 to 261 m/s. The cause of this significant variation above the water table is unknown. However, it is at these shallow depths that the time history records were the poorest. The average V_s for Layer A, below the ground water table, is 213 m/s. Values of V_s decrease to about 180 m/s in Layer B. The average V_s for Layer C is 251 m/s. Near Layer D, V_s decreases to 196 m/s. In Layer E, V_s is as high as 316 m/s.

Average measured V_s and overburden-stress corrected shear wave velocities (V_{s1}) for each layer at the Borrow Pit site are presented in Table 4.1. The assumptions and equations used to calculate V_{s1}, and other in-situ properties, are given in the footnotes of the table. Only average V_s and V_{s1} values for Layers A, C and E are given because the measurement intervals were not completely within the other layers.

Table 4.2 presents the measured to predicted shear wave velocity ratios (MPV_sR) and the measured to predicted shear modulus to tip resistance ratios (MPG_{max}/q_tR) for the Borrow Pit site. Layer A has an average MPV_sR and MPG_{max}/q_tR of 1.47 and 1.43, respectively. The average MPV_sR for Layer A at the Borrow Pit is greater than the average MPV_sR of 1.38 determine for the 100,000 year old CREC site's near surface sand layer (Layer B). MPV_sR and

MPG_{max}/q_tR are not determined for Layers B and D at the Borrow Pit site because V_s measurements intervals are not completely within each layer. Layer C has an average MPV_sR and MPG_{max}/q_tR of 1.42 and 1.35, respectively, and suggests that Layer C is only somewhat older than Layer A. Layer E of SCPT HB 1 has a MPV_sR and MPG_{max}/q_tR of 1.34 and 2.05, respectively. It is unclear to why Layer E has a relatively low MPV_sR and high MPG_{max}/q_tR. The MPG_{max}/q_tR suggests the deposits of Layer E are only a little older than the overlying layers at the Borrow Pit site. Layer E contains the oldest deposits at the Borrow Pit site.

Shown in Figure 4.15 is the measured to predicted V_{s1} chart for Holocene deposits by Andrus et al. (2007). Layers A, C and E for the Borrow Pit site plot below the trend line representing a MPV_sR value equal to 1.0, indicating Holocene-age deposits. The position of the Borrow Pit site's data points is due to the Pleistocene age of the deposits.

Comparing the near surface sand layers at the Borrow Pit site and the CREC site, the Borrow Pit site has a greater MPV_sR than the MPV_sR determined at the CREC site. The MPV_sR of 1.38 for the CREC site is similar to the MPV_sR of 1.39 determined for 100,000 Wando Formation in Charleston, South Carolina that did not liquefy during the 1886 Charleston Earthquake (Hayati and Andrus, 2008). Based on Layer A's MPV_sR of 1.47, the Borrow Pit site does not appear to have been disturbed during Holocene earthquakes.

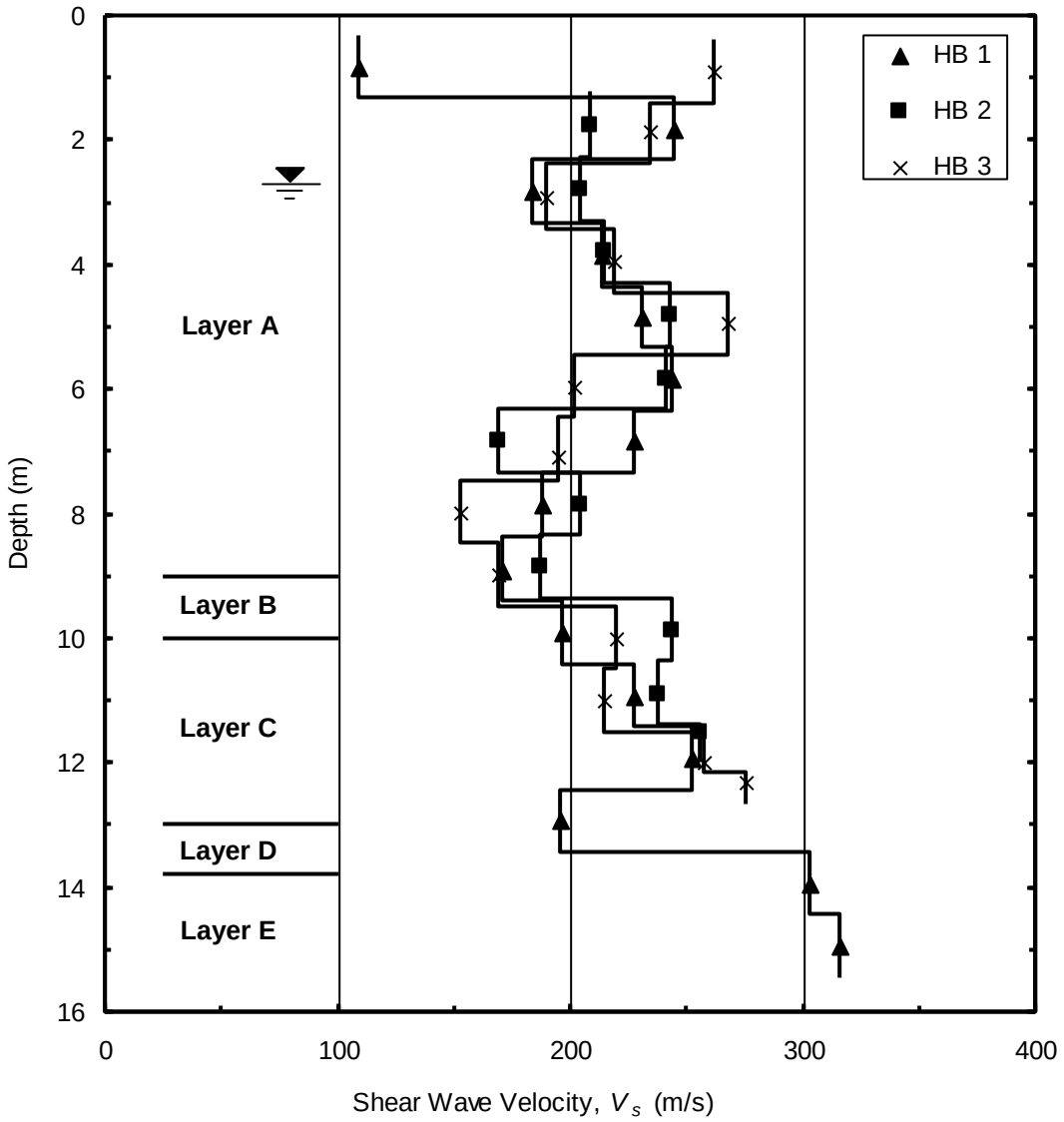

Figure 4.14 Shear wave velocity profiles for SCPT HB 1, HB 2, and HB 3 at the Borrow Pit site.

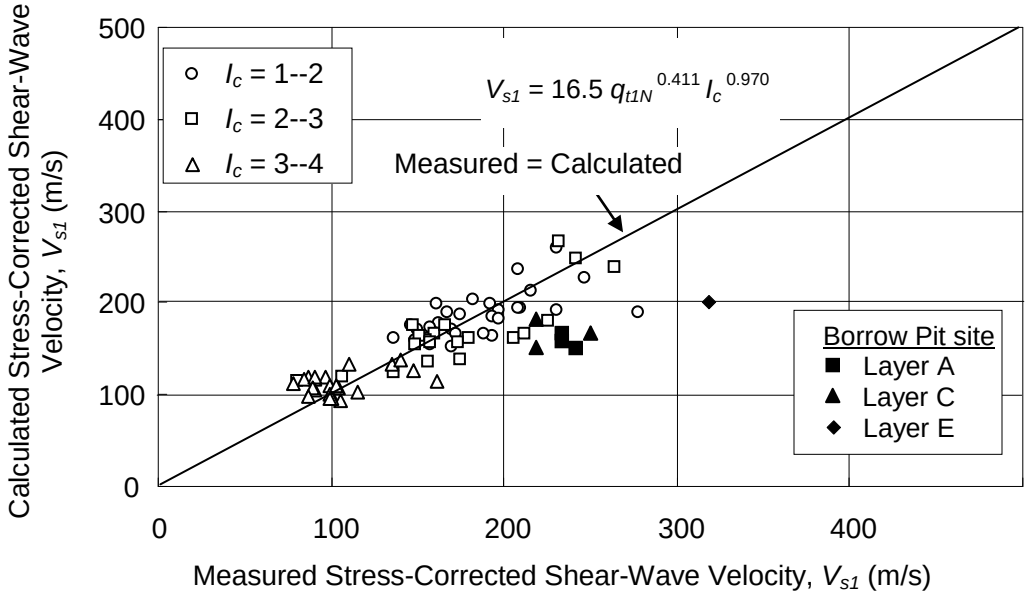

Figure 4.15 Comparison of measured to predicted V_{s1} for Holocene deposits by Andrus et al. (2007) with data from the Borrow Pit site.

Table 4.2 Average predicted properties of the near surface soil layers at the Borrow Pit site.

Layer	Interval (m)	V_s [a]	V_{s1} [b]	G_{max} / q_t [c]	Measured / Predicted	Measured / Predicted
		(m/s)		(MPa)	V_{s1}	G_{max} / q_t
HB 1						
A	3.2 - 8.9	136	150	8.03	1.61	1.47
B	8.9 - 9.8	-	-	-	-	-
C	9.8 - 13.0	159	157	6.85	1.50	1.20
D	13.0 - 13.8	-	-	-	-	-
E	13.8 - 15.0	236	220	6.83	1.34	2.05
HB 2						
A	2.7 - 8.9	143	159	7.67	1.46	1.35
B	8.9 - 9.3	-	-	-	-	-
C	9.3 - 12.2	169	165	8.29	1.49	1.54
HB 3						
A	2.4 - 8.7	149	167	7.18	1.38	1.28
B	8.7 - 9.6	-	-	-	-	-
C	9.6 - 12.0	186	183	7.21	1.27	1.30
D	-	-	-	-	-	-
E	12.0 - 12.3	-	-	-	-	-

[a] $V_s = 2.27\ q_t^{0.412} I_c^{0.989} D^{0.033}$, where D = Depth (Andrus et. al., 2007).
[b] $V_{s1} = 16.5\ q_{t1N}^{0.411} I_c^{0.970}$ (Andrus et. al., 2007).
[c] G_{max} / q_t (predicted = 185 $(q_{t1N})^{-0.7}$ for freshly deposited silica sand (Baldi et al., 1986).

4.5 Summary

The investigations conducted at the Borrow Pit site show there is a fairly uniform medium dense sand layer (Layer A) that extends from the ground surface to a depth of 8.8 m. Layer A has an average q_t of 7.4 MPa, *FR* of 0.2 %, and B_q of -0.002. According to soil behavior type classification charts by Robertson (1990) and the DMT-based chart, the sands of Layer A classify as clean sand to silty sand. Based on the DMT, the average K_o in Layer A below the water table is estimated to be around 0.69. The water table lies at a depth of 2.7 m.

The average measured and predicted V_s values are 213 m/s and 143 m/s, respectively. These values provide a MPV_sR of 1.47 for Layer A. This value is greater than the value determined for the near surface sand layer at the CREC site (Layer B), and suggests the surficial sand deposits at the Borrow Pit site are older than the comparable deposits at the CREC site. This finding is in agreement with McCartan et al. (1984), which map the surfical sand deposits at the Borrow Pits site as 200,000 years old and the surficial sand deposits at the CREC as 100,000 years old. Had the MPV_sR for the Borrow Pit site been closer to 1.0 or 1.38, an age of Holocene or similar to the CREC site would be more likely. These findings provide evidence that the Borrow Pit site did not experience liquefaction during 1886 Charleston earthquake or other Holocene events.

CHAPTER FIVE

INVESTIGATIONS AT THE HOBCAW BARONY MARSH ROAD SITE

5.1 Introduction

As discussed in the beginning of Chapter 4, the Marsh Road site is located within Hobcaw Barony, which is east of Georgetown, South Carolina and off of Highway U.S. 17. Figure 5.1 provides an aerial view of the Marsh Road site. The site is located at the intersection of two un-paved roads - Marsh Road and Clambank Road. The Marsh Road site is positioned on a low-lying beach ridge about 0.15 km west of the modern-day tidal marsh and is 3 km southeast of the Borrow Pit site.

5.2 Geology

The beach ridged, on which the Marsh Road site lies, is sharply defined (see Figure 4.2). May (1978) suggested this beach deposit to be 5,000 to 100,000 years old. On the other hand, the geologic map by McCartan et al. (1984) identifies the surficial deposits in this area as beach sands that are less than 10,000 years old (see Figure 1.1). More recent geologic mapping efforts along the South Carolina Coast have suggested ages older than 10,000 years for other beach sand deposits in similar geomorphic positions. For example, Weems and Lemon (1993) mapped the younger beach sands west of the modern tidal-marsh as sands having been deposited 33,000 to 85,000 years ago. Thus, the suggested range of ages for the surficial sand deposits at the Marsh Road site is quite large.

Martin and Clough (1990) and Lewis et al. (1999) reviewed several earthquake reports and found no evidence that liquefaction was observed in the Hobcaw Barony area during the 1886 earthquake. Currently no paleoliquefaction studies have been conducted at the Marsh Road site.

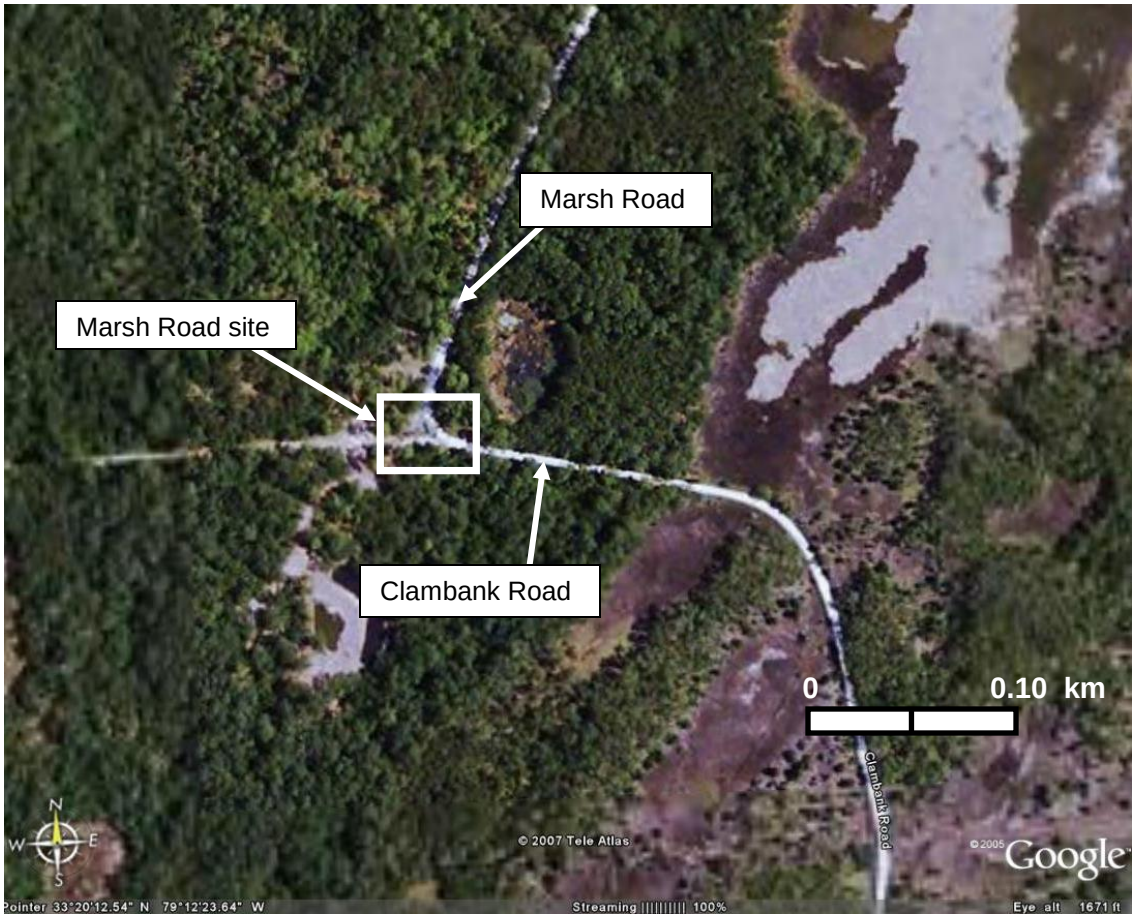

Figure 5.1 Aerial photograph of the Marsh Road site and surrounding area.

5.3 Investigations

The geotechnical investigations at the Marsh Road site consisted of three SCPTs. A photograph of testing at the Marsh Road site is presented in Figure 5.2. The photograph provides an east to west view of the site showing the locations of SCPTs HM 1, HM 2 and HM 3, and the intersection of Marsh Road and Clambank Road. The CPT track rig is located at HM 3. Presented in Figure 5.3 is the sitemap showing the three SCPT locations and reference points used to construct the sitemap. These reference points were located at two Survey Markers and a Marsh Road center point. Survey Marker 2 was labeled Baruch No. 3 1932.

Testing began on the afternoon of July 25, 2007. HM 1 was pushed in the shoulder of Clambank Road, approximately 6.4 m north of the roadway's centerline. SCPT HM 2 was also pushed in the shoulder, about 6 m west of Survey Marker 1. SCPT HM 3 was pushed in the grass median located at the intersection of Marsh Road and Clambank Road. Table C.1 gives the local site coordinates for the tests. All SCPTs were pushed until refusal, which occurred at depths ranging from 11.4 to 11.5 m. A DMT was not conducted at the site due to heavy rain in the early afternoon.

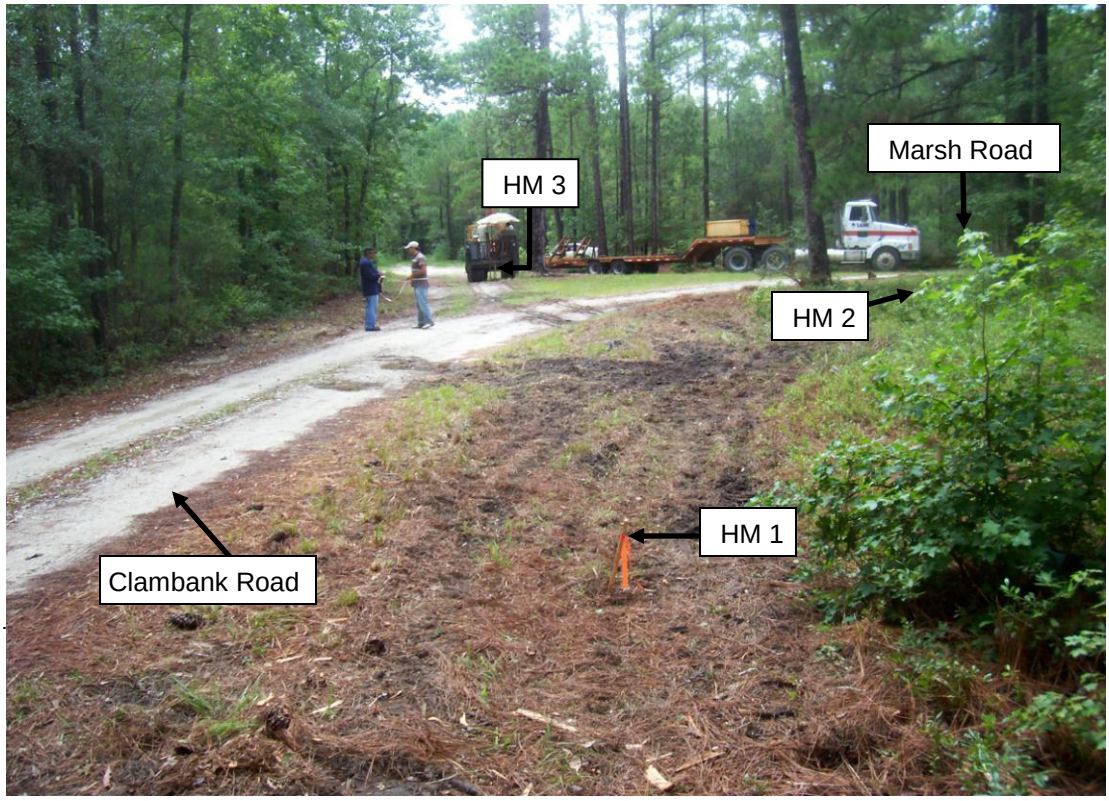

Figure 5.2 Photograph of the Marsh Road site showing locations of soundings HM 1, HM 2 and HM 3.

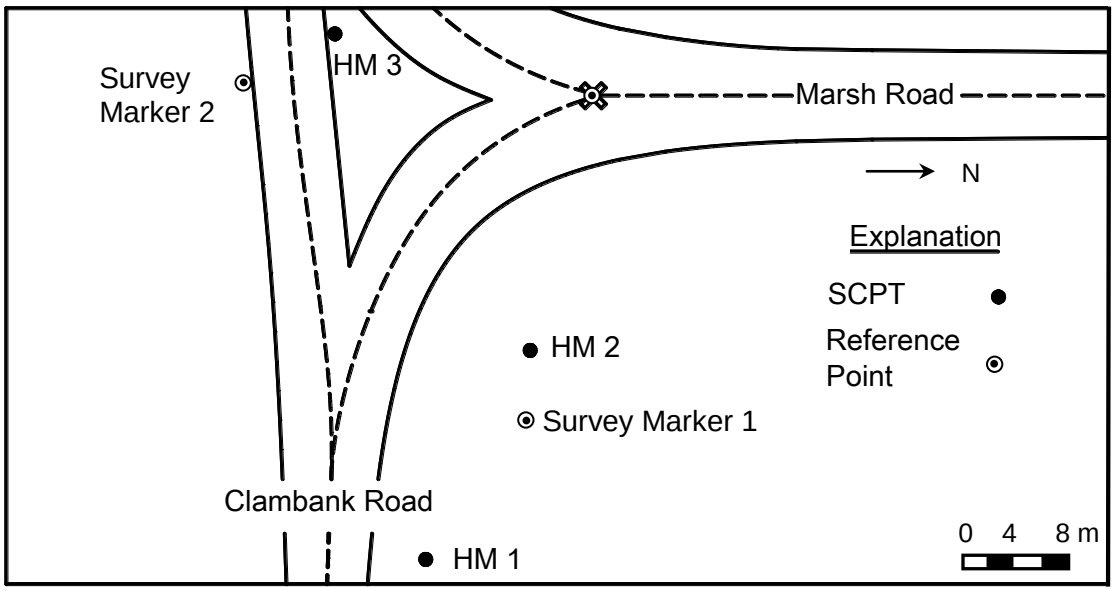

Figure 5.3 Map showing test locations at the Marsh Road site.

5.4 Results

The SCPT test results are tabulated in Appendix C. The results are discussed in the following paragraphs to characterize stratigraphy, soil type, liquefaction susceptibility, and measured to predicted shear wave velocity at the site.

5.4.1 Stratigraphy

Figure 5.4 provides a composite profile of SCPT HM 1. The figure consists of corrected tip resistance (q_t), friction ratio (*FR*), pore water pressures measured behind the cone tip (u_2), shear wave velocity (V_s), and soil layer designation. The soil layer designations are A, B, C, D, and E. Layer A extends to a depth of 5.0 m and has average q_t of 8.2 MPa. The layer also has very low values of *FR* (less than 1 %) and average u_2 of 0.01 MPa, suggesting the deposits to be predominately sand.

Layers B and D extend from depths of 5.0 to 5.7 m and 6.7 to 7.6 m, respectively. The layers are characterized by an average q_t of 1.3 MPa and *FR* peak values greater than or equal 2 %. Layer D has a noticeable increase in u_2 values, averaging 0.13 MPa. These results indicate that Layers B and D have significant fines content.

Layer C extends from a depth of 5.7 m to a depth 6.7 m. The layer has average q_t of 3.0 MPa, *FR* of 0.5 %, and u_2 of 0.06 MPa. Layer C may be a sand deposit containing some fine grained material.

Layer E begins at a depth of 7.6 m and extends to the termination of the sounding at 11.4 m. The layer is characterized by average q_t of 8.1 MPa, *FR* of 0.39 %, and u_2 of 0.07 MPa. These values suggest that Layer E consists of medium dense sand to silty sand. It is believed that the Black Mingo Formation is just below the base of the Layer E. The geologic profile by May (1978) suggests that the Black Mingo Formation begins at depths of around 13 to 15 m near the Marsh Road site (see Figure 4.4).

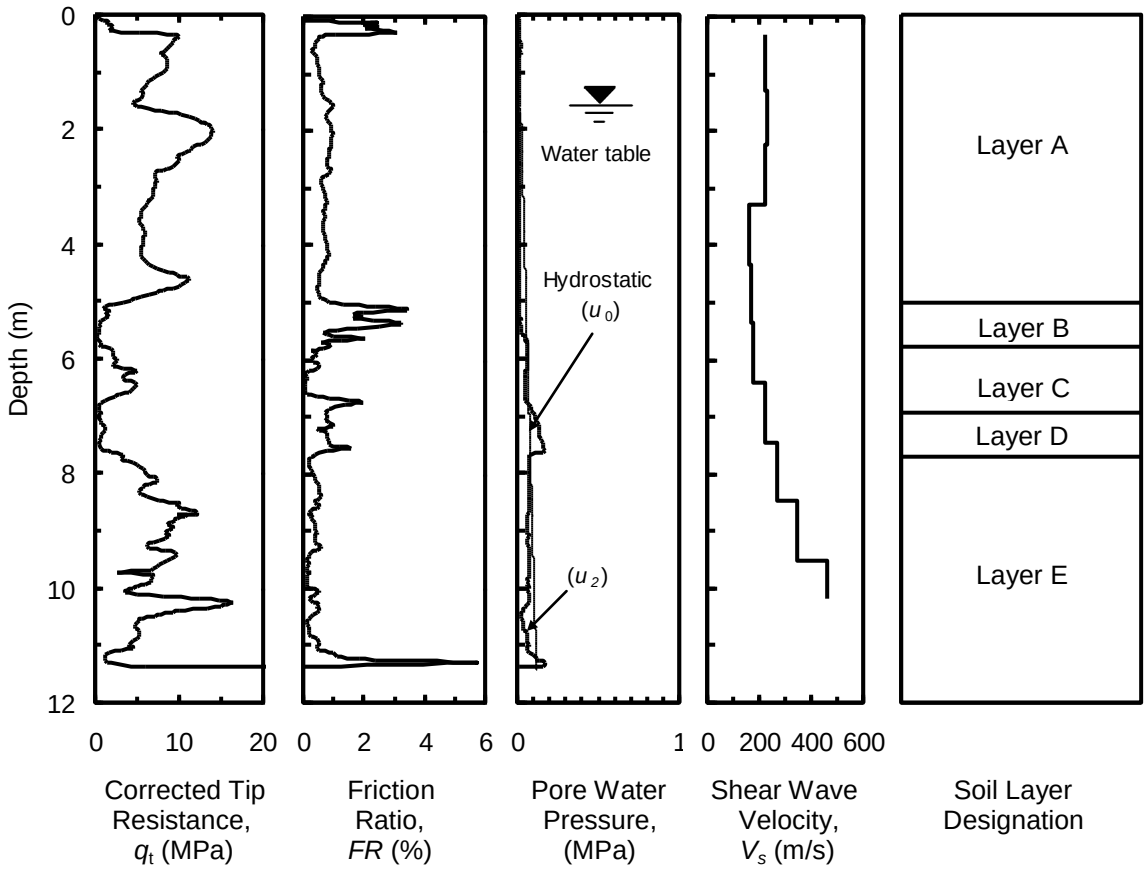

Figure 5.4 Composite profile for SCPT HM 1 at the Marsh Road site.

Figure 5.5 provides a cross-section of the Marsh Road site based on q_t and *FR* of the three SCPTs. Layers A, B, C, D, and E are present at all three test locations. Layer depth intervals and tabulated averages of q_t and *FR* can be found in Table 5.1. The base of Layer A is nearly flat and lies at a depth of 5.0 m. Layers B and C at the Marsh Road site have average thickness of about 0.7 m and 1.0 m, respectively. The top of Layer D is nearly flat and begins at a depth of 6.7 m for each SCPT and has an average thickness of 1 m. The base of Layer E is also nearly flat, at an average depth of 11.5 m. Although there is some lateral variation within the layers, the layers are continuous across the site. The ground water table at the site lies at a depth of about 1.6 m.

5.4.2 Soil Behavior Type

The soil behavior type classification charts by Robertson (1990) displayed in Figure 5.6 are used to classify the soils in each layer. The charts are based on normalized cone tip resistance (Q_t), normalized cone sleeve friction ratio (F_N), and normalized cone pore pressure ratio (B_q). The Q_t - F_N chart classifies Layer A as clean sand to silty sand (Zone 6), while the Q_t - B_q chart classifies the layer as gravelly sand to sand (Zone 7). The actual soil type is likely between these two predictions (Lunne et al., 1997). The Q_t - F_N chart considers Layer B to be clayey silt to silty clay (Zone 4) or silty sand to sandy silt (Zone 5). The Q_t - B_q chart considers Layer B to between clayey silt to silty clay (Zone 4) and clean sand to silty (Zone 6). Both the Q_t -F_N and Q_t - B_q charts determine Layers C and

E to be clean sand to silty sand (Zone 6) and Layer D to be clayey silt to silty clay (Zone 4).

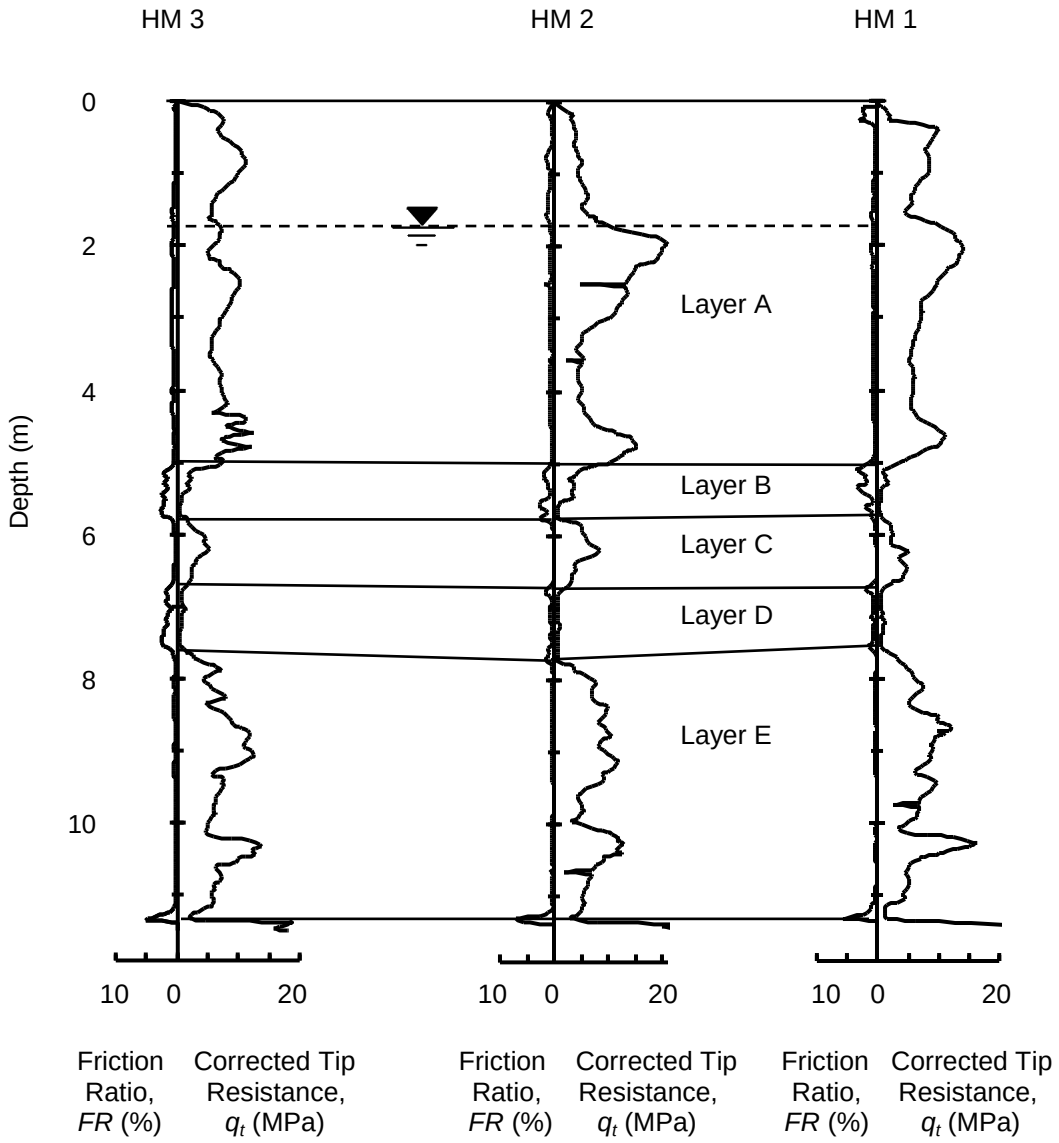

Figure 5.5 CPT cross-section for soundings HM 3, HM 2 and HM 1 at the Marsh Road site.

Table 5.1 Average measured properties of the near surface soil layers at the Marsh Road site.

Layer Interval (m)		V_s [a] (m/s)	V_{s1} [b] (m/s)	G_{max} [c] (MPa)	q_t (MPa)	q_{t1N} [d]	$(q_{t1N})_{cs}$ [e]	I_c [f]	FR	F_N [g]	Q_t [h]	B_q [i]	u_2/u_o
HM 1													
A	1.6 – 5.0	226	283	89.9	8.2	132	135	1.6	0.74	0.75	213.8	-0.003	0.38
B	5.0 – 5.7	176 [j]	199	54.5	0.9	12	53	2.9	1.83	2.14	13.7	-0.041	0.69
C	5.7 – 6.7				3.3	43	50	1.9	0.28	0.28	53.5	0.002	0.90
D	6.7 – 7.6				0.8	10	43	2.8	0.93	1.10	10.7	0.085	1.78
E	7.6 – 11.4	360	376	228.1	7.8	89	92	1.7	0.35	0.36	99.5	-0.002	0.72
HM 2													
A	1.7 – 5.0	239	296	100.5	10.2	165	168	1.6	0.70	0.70	269.7	-0.003	0.16
B	5.0 – 5.7	184	203	59.6	2.5	35	68	2.4	1.65	1.77	45.9	-0.021	0.40
C	5.7 – 6.7				4.9	65	69	1.7	0.27	0.28	81.6	-0.005	0.42
D	6.7 – 7.7				0.7	9	40	2.8	0.76	0.92	9.1	0.116	0.50
E	7.7 – 11.5	321	335	181.4	8.1	91	94	1.7	0.34	0.35	100.1	-0.004	0.34
HM 3													
A	1.7 – 5.0	204	245	73.2	7.6	119	120	1.6	0.66	0.67	184.1	-0.004	0.16
B	5.0 – 5.8	174	197	53.3	1.6	21	62	2.7	1.96	2.20	27.4	-0.040	0.40
C	5.8 – 6.7				3.3	42	52	2.0	0.41	0.43	52.5	-0.010	0.42
D	6.7 – 7.6				0.8	10	54	2.9	1.70	2.05	10.6	-0.056	0.50
E	7.6 – 11.5	327	340	188.2	7.8	87	90	1.7	0.33	0.33	94.3	-0.010	0.34

[a] True interval measured shear wave velocity.

[b] $V_{s1} = V_s (P_a / \sigma_v')^{0.25}$, overburden-stress corrected shear wave velocity (Andrus et al., 2007).

[c] $G_{max} = \rho V_s^2$, where ρ = total unit weight / acceleration of gravity (mass density), assumed to be 0.00176 MPa – s^2/m^2.

[d] $q_{t1N} = (q_t / P_a)(P_a / \sigma')^n$, where P_a = 100 kPa (Robertson and Wride, 1998).

[e] $(q_{t1N})_{cs} = q_{t1N} * K_c$, equivalent clean sand value of q_{t1N}.

$K_c = -0.403 I_c^4 + 5.581 I_c^3 - 21.63 I_c^2 + 33.75 I_c - 17.88$ for $I_c \leq 1.64$ (Robertson and Wride, 1998)

[f] $I_c = [(3.47 - \log Q_t)^2 + (\log F_N + 1.22)^2]^{0.5}$ (Robertson and Wride, 1998).

[g] $F_N = f_s / (q_t - \sigma_v)*100\%$, normalized cone friction ratio (Robertson, 1990).

[h] $Q_t = (q_t - \sigma_v) / \sigma_v'$, normalized cone tip resistance (Robertson, 1990).

[i] $B_q = (u_2 - u_o)/(q_t - \sigma_v)$, normalized cone pore pressure ratio (Robertson, 1990).

[j] V_s within Layers B, C and D.

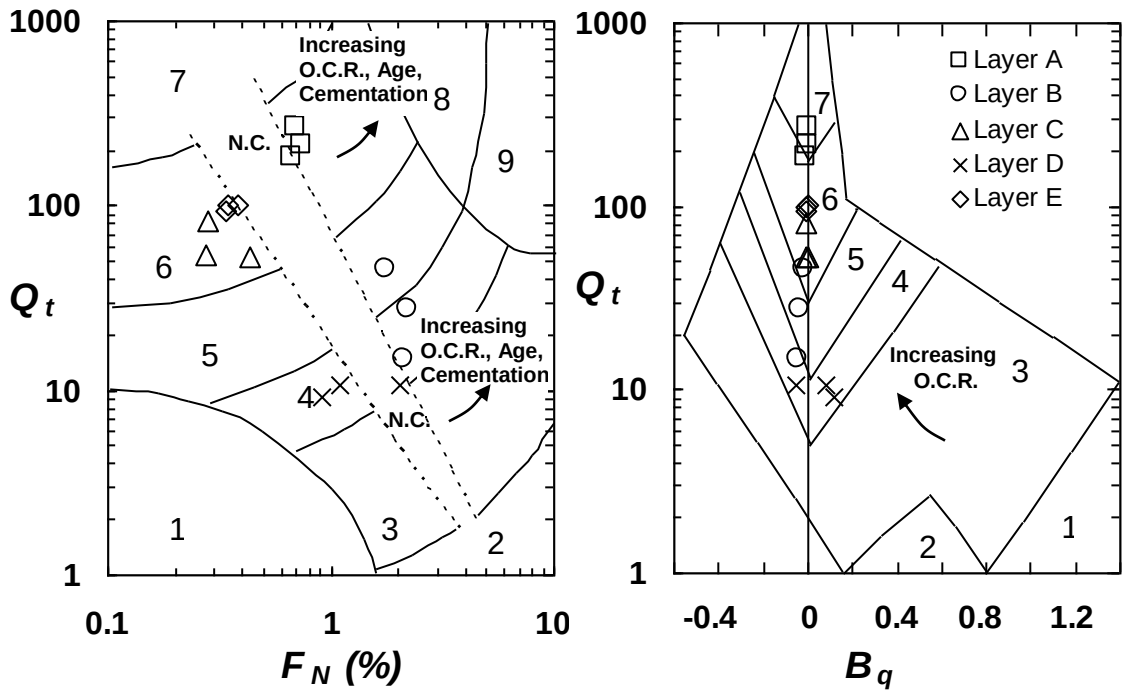

Zone	Soil behavior type
1.	Sensitive, fine grained;
2.	Organic soils, peats;
3.	Clays: clay to silty clay;
4.	Silt mixtures: clayey silt to silty clay;
5.	Sand mixtures: silty sand to sandy silt;
6.	Sands: clean sands to silty sands;
7.	Gravelly sand to sand;
8.	Very stiff sand to clayey sand;
9.	Very stiff fine grained

N.C. = Normally Consolidated
O.C.R. = Overconsolidation Ratio

Figure 5.6 Soil behavior type classification charts by Robertson (1990) with data from the Marsh Road site.

5.4.3 Liquefaction Susceptibility

Figure 5.7 presents the CPT-based liquefaction susceptibility chart by Hayati and Andrus (2008). Plotted on the chart are the data from the Marsh Road site. Data points with negative B_q values are plotted as having a value of zero. According to the chart, Layers A, C and E are susceptible to liquefaction. Layers B and D are not susceptible to liquefaction or need additional testing to determine the susceptibility because of high I_c or fines content. It can be concluded that much of the sediment beneath the Marsh Road site is susceptible to liquefaction, at least according to composition.

Liquefaction susceptibility according to density for the Marsh Road site is determined by using $(q_{t1N})_{cs}$. Materials with $(q_{t1N})_{cs}$ values greater than 160 to 190 are considered to be not susceptible to liquefaction (Robertson and Wride, 1998; Idriss and Boulanger, 2004; Moss et al., 2006). Layers B, C, D and E for all three SCPTs are susceptible to liquefaction with $(q_{t1N})_{cs}$ values ranging from 40 to 94. Layer A for SCPTs HM 1 and HM 3 have average $(q_{t1N})_{cs}$ values of 135 and 120 and are also considered to be susceptible. Layer A for HM 2 has an average $(q_{t1N})_{cs}$ of 168 and is believed to have marginal to low susceptibility to liquefaction.

These results indicated that Layers A, C and E are susceptible to liquefaction. A liquefaction potential evaluation considering the seismic loading (magnitude and acceleration) of the 1886 earthquake is planned. This analysis will be done as part of the next phase of this NSF supported project.

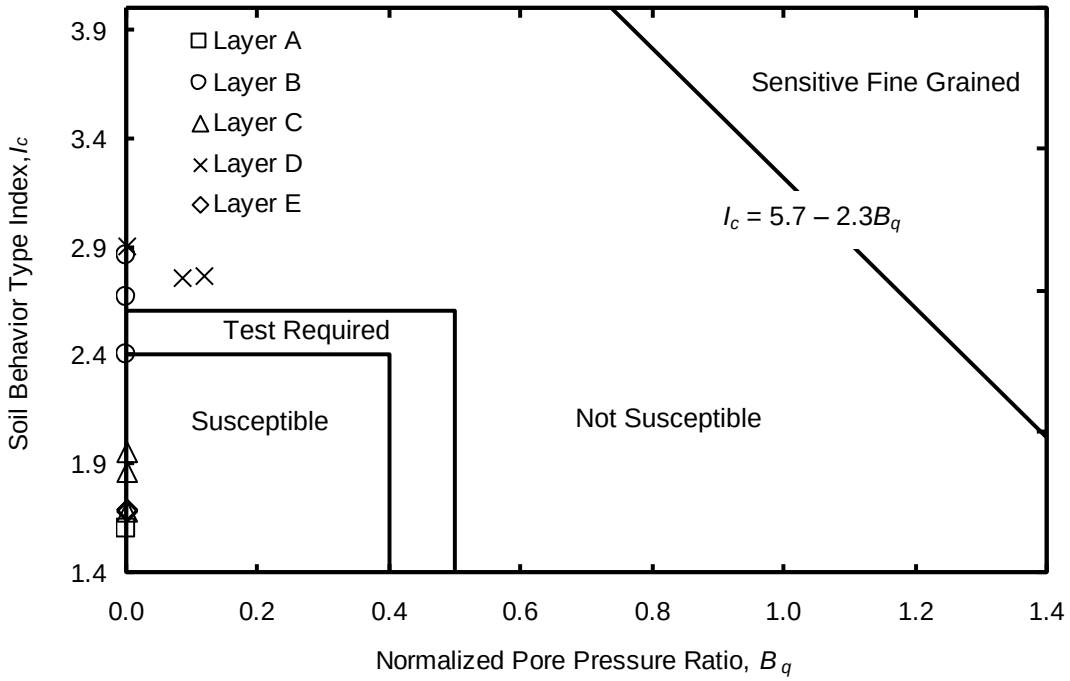

Figure 5.7 CPT–based liquefaction susceptibility chart by Hayati and Andrus (2008) with data from the Marsh Road site.

5.4.4 Shear Wave Velocity

Profiles of shear wave velocity (V_s) based on true interval measurements for SCPTs HM 1, HM 2 and HM 3 are presented in Figure 5.8. Within the profile, values of V_s range from 156 to 465 m/s. The greatest variation in V_s occurs between the ground surface and a depth of 2.8 m, where values range from 177 to 403 m/s. It should be noted that time history records from shallow depths were the most difficult to interpret. The average V_s for Layer A below the ground water table is 223 m/s. The average value of V_s is about 177 m/s in Layers B, C and D. In Layer E, V_s increases with depth and has an average value of 302 m/s.

Table 5.1 contains the average measured V_s and overburden-stress corrected shear wave (V_{s1}) for each layer at the Marsh Road site. The assumptions and equations used to calculate V_{s1}, and other in-situ properties, are given in the footnotes of the table. Only average V_s and V_{s1} values for Layers A and E are given in the table because measurement intervals are not completely within the other layers (i.e. B, C, D). However, Layers B, C and D, when combined, contain two measurement intervals of V_s and V_{s1} at each site. Average values of V_s and V_{s1} for the combine Layers B, C, and D are also given in Table 5.1.

Table 5.2 presents the measured to predicted shear velocity ratios (MPV_sR) and the measured to predicted shear modulus to tip resistance ratios (MPG_{max}/q_tR) for the Marsh Road site. Layer A has an average MPV_sR and

MPG_{max}/q_tR of 1.45 and 1.73, respectively. These values are similar to the average values of 1.47 and 1.43 determined for the Borrow Pit site, which is believed to be around 200,000 years old. Layers B, C, and D have an average MPV_sR and MPG_{max}/q_tR of 1.51 and 1.45, respectively, suggesting the deposits of these layers are not much older than Layer A. Layer E has average MPV_sR and MPG_{max}/q_tR values of 2.07 and 3.15, respectively. The higher measured to predicted ratios for Layer E, indicates a significantly greater age or cementation of the layer than in the overlying layers.

Shown in Figure 5.9 is the measured to predicted V_{s1} chart for Holocene deposits by Andrus et al. (2007). All layers for the Marsh Road site plot below the trend line representing a MPV_sR value equal to 1.0. The position of the Marsh Road site's data points is due to the site containing deposits that are greater than Holocene in age.

Based on Layer A's average MPV_sR of 1.45, the Marsh Road site does not appear to have been disturbed during recent earthquakes (e.g. the 1886 Charleston Earthquake). Had the site liquefied in 1886, MPV_sR values would have been closer to 1.0, as found by Hayati and Andrus (2008) in Charleston.

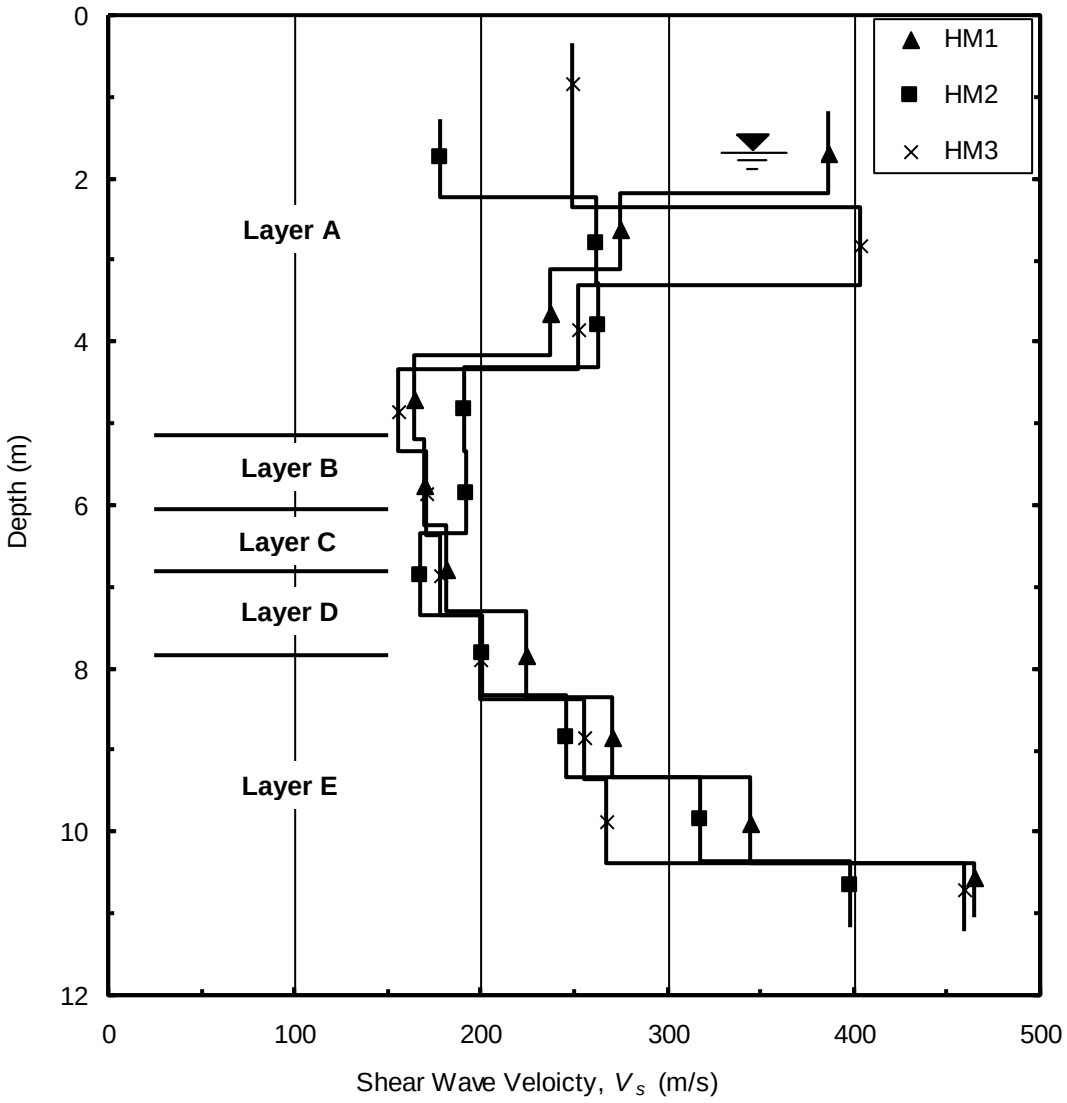

Figure 5.8 Shear wave velocity profiles for SCPT HM 1, HM 2, and HM 3 at the Marsh Road site.

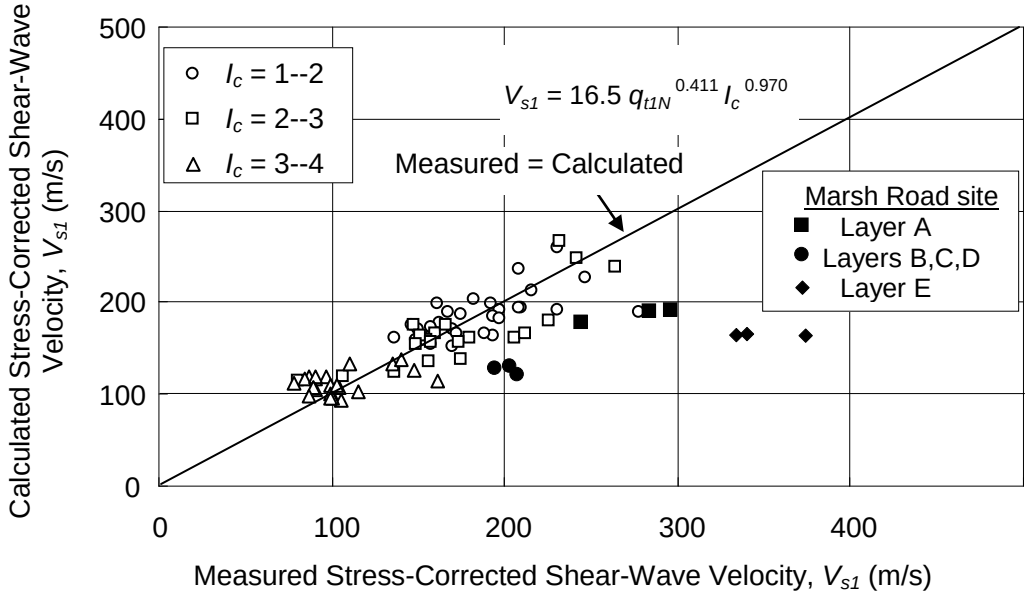

Figure 5.9 Comparison of measured to predicted V_{s1} for Holocene deposits by Andrus et al. (2007) with data from the Marsh Road site.

Table 5.2 Average predicted properties of the near surface soil layers at the Marsh Road site.

Layer	Interval (m)	V_s [a]	V_{s1} [b]	G_{max} / q_t [c]	Measured / Predicted	Measured / Predicted
		(m/s)		(MPa)	V_{s1}	G_{max} / q_t
HM 1						
A	1.6 - 5.0	152	191	6.05	1.48	1.80
B,C,D	5.3 - 7.4[d]	119	134	21.19	1.49	1.50
E	7.8 - 11.4	162	169	7.71	2.22	3.66
HM 2						
A	1.7- 5.4	152	192	5.18	1.54	1.91
B,C,D	5.3 - 7.4	114	126	14.72	1.61	1.43
E	8.0 - 11.5	163	170	7.87	1.96	2.83
HM 3						
A	1.7 - 5.0	151	182	6.54	1.34	1.47
B,C,D	5.3 - 7.4	123	138	19.32	1.42	1.42
E	7.7 - 11.5	162	169	8.15	2.02	2.97

[a] $V_s = 2.27\ q_t^{0.412}\ I_c^{0.989}\ D^{0.033}$, where D = Depth (Andrus et. al., 2007).
[b] $V_{s1} = 16.5\ q_{t1N}^{0.411}\ I_c^{0.970}$ (Andrus et. al., 2007).
[c] G_{max} / q_t (predicted) = 185 $(q_{t1N})^{-0.7}$ for freshly deposited silica sand (Baldi et al., 1986).
[d] Depth interval of two V_s tests within Layers B, C and D.

5.5 Summary

The investigations conducted at the Marsh Road site show there is a medium dense sand layer (Layer A) that extends from the ground surface to a depth of 5.0 m. Layer A has an average q_t of 8.2 MPa, *FR* of 0.7 %, and B_q of about -0.003. According to the soil behavior type classification charts by Robertson (1990), the sands of Layer A classify as clean sand to silty sand. The water table lies at a depth of 1.6 m.

The average measured and predicted V_s values for Layer A are 223 m/s and 151 m/s, respectively. These values provide a MPV_sR of 1.45 for Layer A. This MPV_sR value is nearly equal to the value determined for the Borrow Pit site, and suggests the age of the surficial sand deposits is similar at both sites. This is somewhat surprising because McCartan et al. (1984) mapped the sharply defined beach ridge sands at the Marsh Road site as less than 10,000 years old deposits and the dune-decorated beach ridge sands at the Borrow Pit site as 200,000 year old deposit. It is possible that the very young beach ridge deposits are thin (less than 1 m) at the Marsh Road site. Had the MPV_sR for the Marsh Road site been closer to 1.0, a Holocene age for the beach sands would be more likely.

These findings agree with the observation that the Marsh Road site and the Borrow Pit site did not liquefy during the 1886 Charleston earthquake (Lewis et al. 1999) or other Holocene events

.

CHAPTER 6

SUMMARY AND CONCLUSIONS

Geotechnical investigations were performed at three sites within the South Carolina Coastal Plain that did not liquefy during the 1886 Charleston earthquake. One of the three sites is located at the Coastal Research and Education Center (CREC) near Charleston, and is referred to as the CREC site. The other two sites are located within Hobcaw Barony near Georgetown, and are referred to as the Borrow Pit and Marsh Road sites. The objectives of the geotechnical investigations were to characterize the in-situ properties of near surface beach deposits at the three sites and to develop the sites for future testing. The results of the investigations were used to determine stratigraphy, soil classification, soil type, lateral at rest earth pressure, liquefaction susceptibility, and shear wave velocity at each site.

From the field investigations, it was determined that a thick medium dense surficial sand deposit is present at all three sites. Table 6.1 summarizes the average in situ properties of these surficial sand deposits below the ground water table. Table 6.2 summarizes the average estimated values of ϕ', K_o and V_{s1} of the surficial sand deposits at the three sites.

The near surface sand layer at the CREC site lies between depths of 0.8 and 4.5 m, and classifies as poorly graded sand (SP) with a fines content of approximately 4 % and I_c of 1.7 This medium dense layer has an average $(N_1)_{60}$ of 14 and q_{t1N} of 120. The K_o estimated for this layer was 0.9, suggesting near

equal horizontal and vertical effective stresses. The sand layer is characteristic of the Wando Formation that was mapped by McCartan et al. (1984) as a 100,000 year old deposit. The average MPV_sR of 1.38 determined for the CREC site is similar to the MPV_sR that Hayati and Andrus (2008) determined for the 70,000 to 120,000 year old Wando Formation in Charleston that did not liquefy during the 1886 Charleston earthquake.

The near surface sand layer at the Borrow Pit site is between depths of 2.7 and 8.8 m, and was the thickest near surface sand layer encountered during the investigations. This sand layer generally classifies as a clean sand with an average I_c of 1.6. The sand layer has the lowest average q_{t1N} of 95 and V_{s1} of 234 m/s. The average K_o is 0.7, indicating effective horizontal stress are smaller but greater than half the effective vertical stresses. McCartan et al. (1984) mapped this area as a 200,000 year old beach sand. An average MPV_sR of 1.47 was determined for the surficial beach sands, indicating that the Borrow Pit site is older than the CREC site and also has not been disturbed by recent liquefaction.

The near surface sand layer at the Marsh Road site is approximately 3.4 m thick and generally classifies as a clean sand with an average I_c of 1.6. With an average q_{t1N} of 139 and V_{s1} of 274 m/s, the Marsh Road site has the densest near surface sand layer encountered during the investigations. The average MPV_sR for these deposits is 1.45, which is similar to the Borrow Pit site and greater than the CREC site. These findings are interesting because McCartan et al. (1984) mapped the surficial deposits at the Marsh Road site as being less

than 10,000 years old. The MPV_sR indicates that the sand layer between 1.6 and 5.0 m at the Marsh Road site is similar in age to the near surface sand layer at the Borrow Pit site.

The results of this study support the use of MPV_sR as an indication of time of deposition or the time since last critical disturbance. Average values of MPV_sR were greater than 1.0 and average 1.38, 1.45 and 1.47 for the near surface sand deposits at the CREC site, Marsh Road site and Borrow Pit site, respectively. It is interesting to note that the Marsh Road site is only 3 km east of the Borrow Pit site, while the CREC site is about 100 km south of the Hobcaw Barony sites. The ages of these sites follow the increasing order the MPV_sR values.

As part of the larger NSF project, future testing consisting of SPT borings and undisturbed sampling at the Borrow Pit site and Marsh Road site, seismic cross hole testing at all sites, and test pit excavations will be performed. The results of this study provide the initial characterizations that will be used as a resource for the planned geotechnical investigations (e.g. drilling, SPT borings, seismic cross hole testing, sampling) as well as other future investigations.

Table 6.1 Average measured in situ properties of the surficial sand deposits at the three geotechnical investigation sites.

Site	Ground Water Table Depth (m)	Depth Interval (m)	$(N_1)_{60}$	q_{t1N}	I_c	Fines Content (%)	V_{s1} (m/s)
CREC	0.8	0.8 – 4.5	14	120	1.7	4	242
Borrow Pit	2.7	2.7– 8.8	-	95	1.6	-	234
Marsh Road	1.6	1.6 – 5.0	-	139	1.6	-	274

Table 6.2 Estimated properties of the surficial sand deposits at the three geotechnical investigation sites.

Site	Depth Interval (m)	CPT-based ϕ' [a] (Degrees)	DMT-based K_o [b]	V_{s1} [c] (m/s)	MPV_sR
CREC	0.8 – 4.5	43	0.88	176	1.38
Borrow Pit	2.7 – 8.8	35	0.69	159	1.47
Marsh Road	1.6 – 5.0	37	-	187	1.45

[a] $\phi' = \tan^{-1}[\,0.1 + 0.3\mathrm{Log}(q_t / \sigma'_{vo})]$, effective friction angle (Kulhawy and Mayne,1990).
[b] K_o found using Schmertmann's correlation between K_D and K_o with respect to the ϕ' as cited by Baldi et al. (1986).
[c] $V_{s1} = 16.5\, q_{t1N}^{0.411}\, I_c^{0.970}$ (Andrus et. al., 2007).

APPENDICES

APPENDIX A

SUMMARY OF DATA FOR THE CREC SITE

Table A.1 Local site coordinates for the geotechnical investigations at the CREC site.

Test Sites	X (m)	Y (m)
Western Oak Tree Reference	0	0
SC 1	7	9
C 2	35	32
SC 3	20	34
C 4	3	33
C 5	25	-11
SC 6	8	-10
B 1	15	-7
B 2	19	-7
B 3	23	-7
D 1	7	-6
Pear Tree Reference	24	27
Eastern Oak Tree Reference	36	3

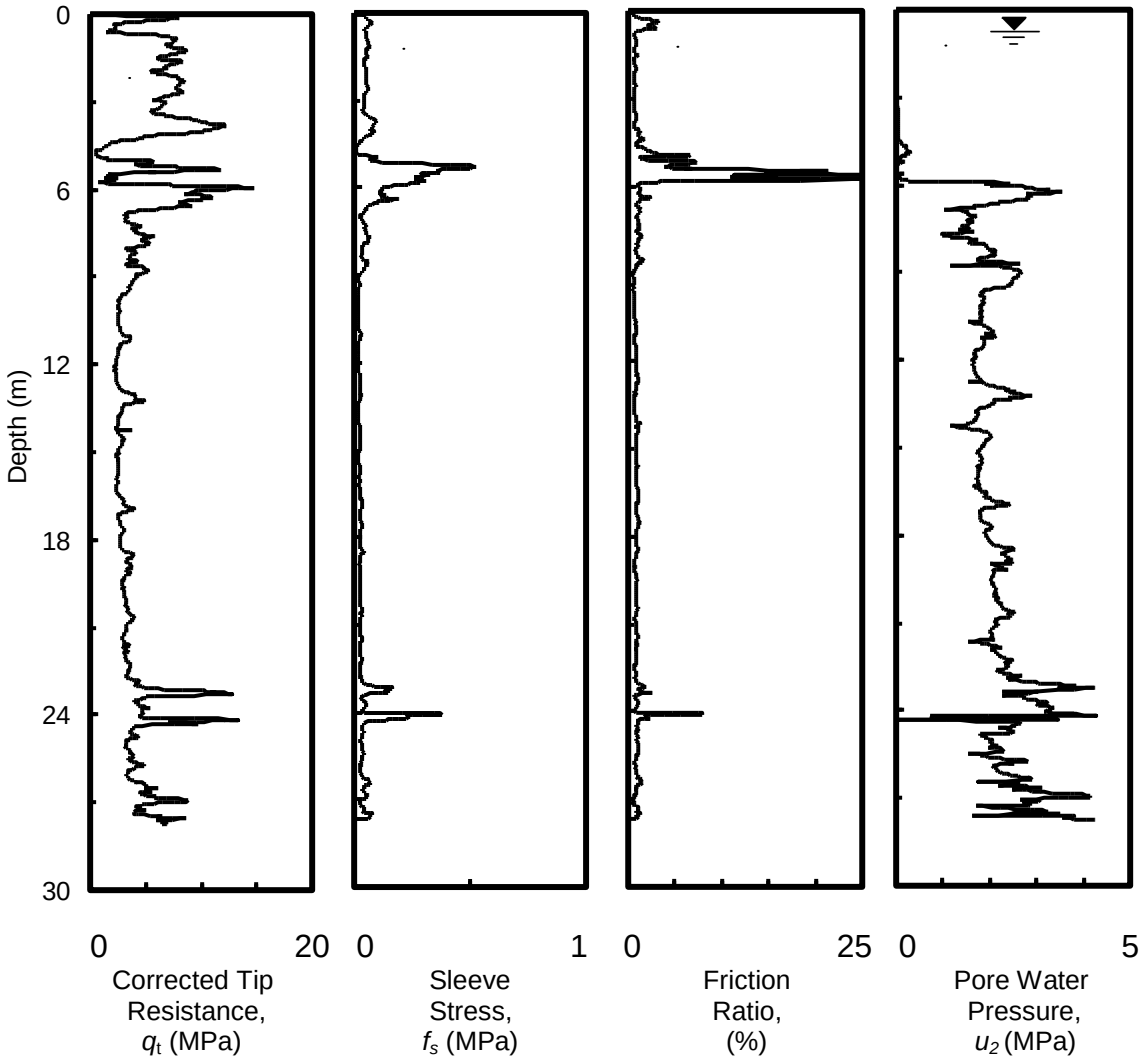

Figure A.1 Composite profile of SCPT SC 1 at the CREC site.

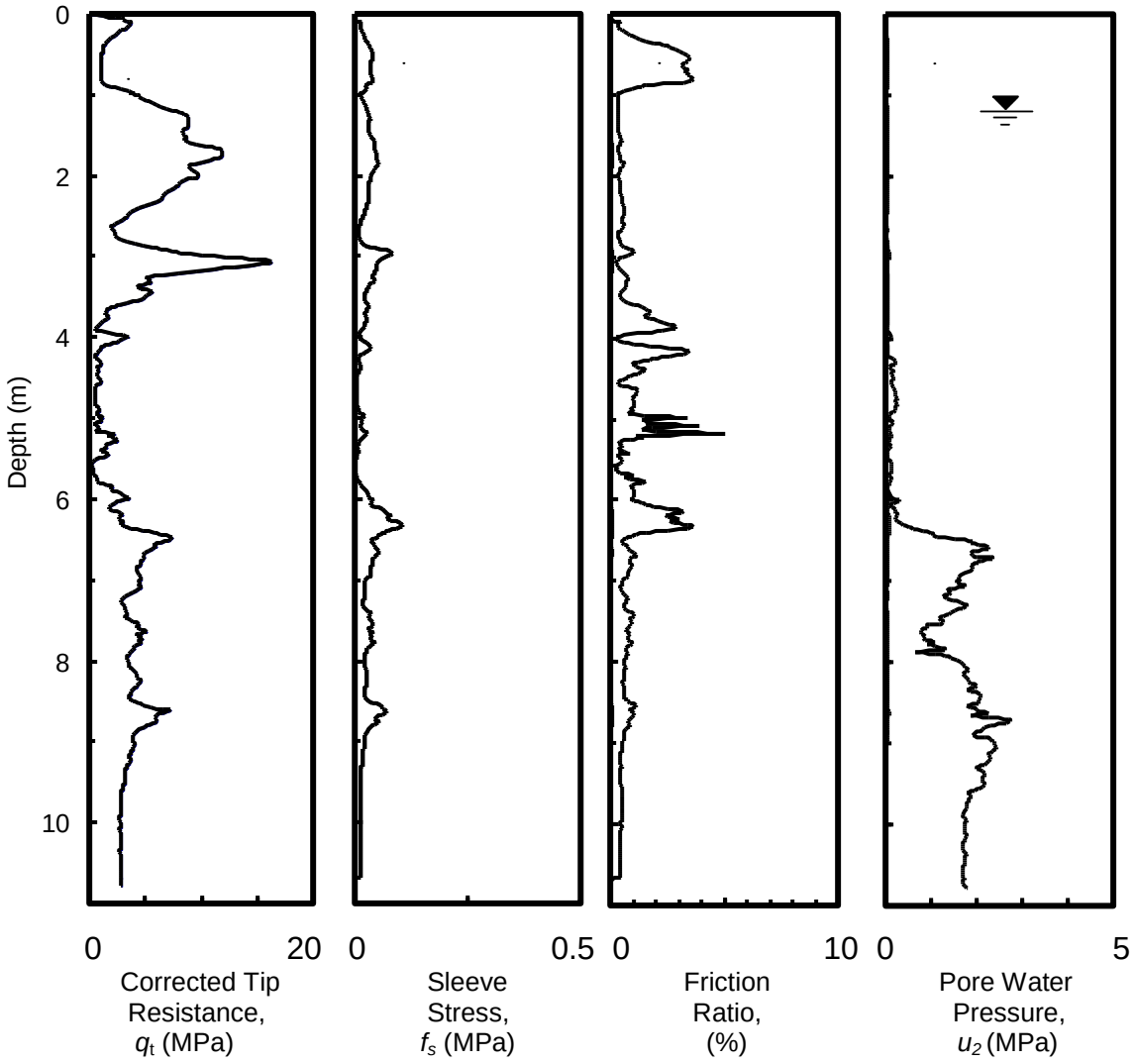

Figure A.2 Composite profile of CPT C 2 at the CREC site.

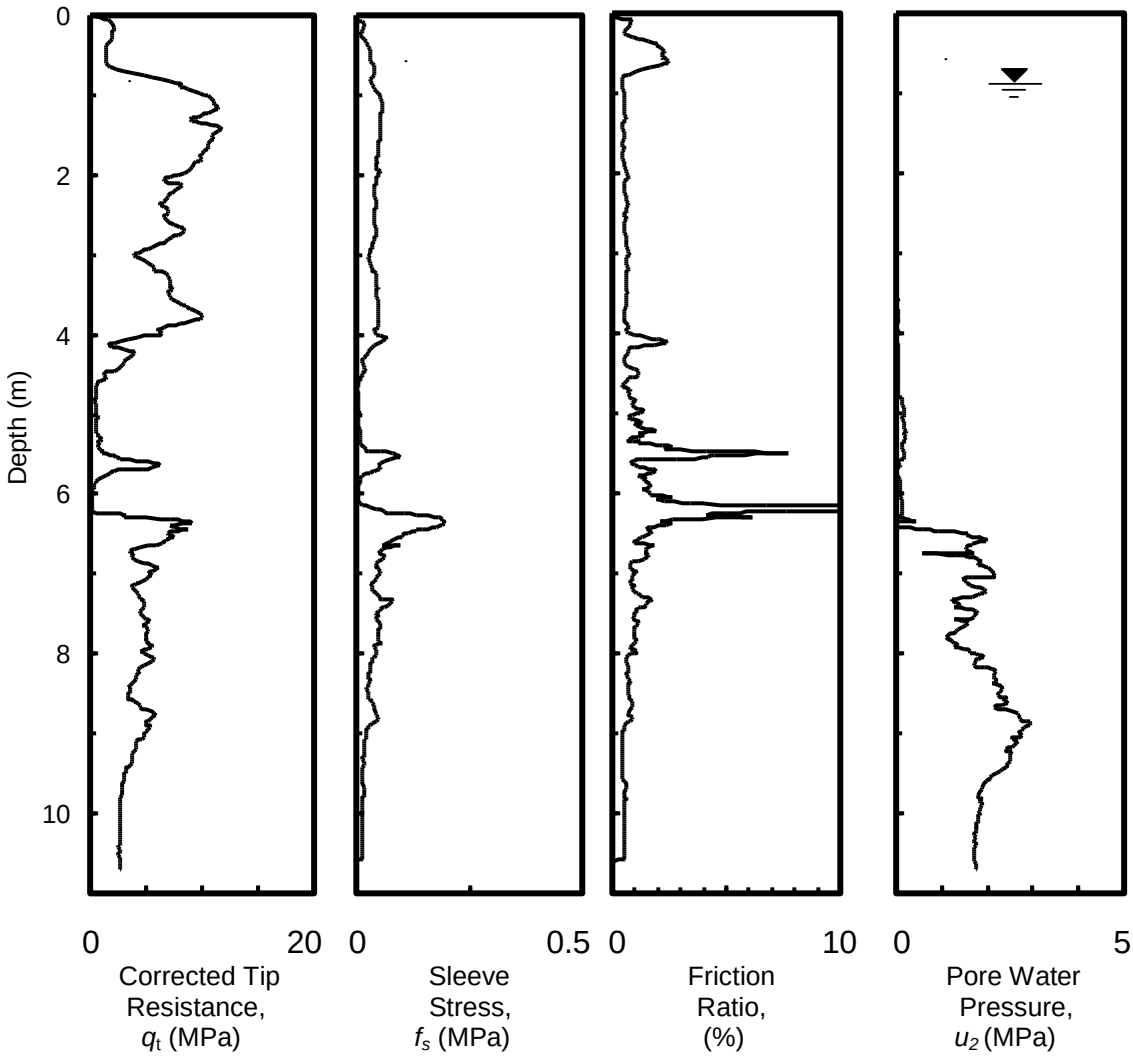

Figure A.3 Composite profile of SCPT SC 3 at the CREC site.

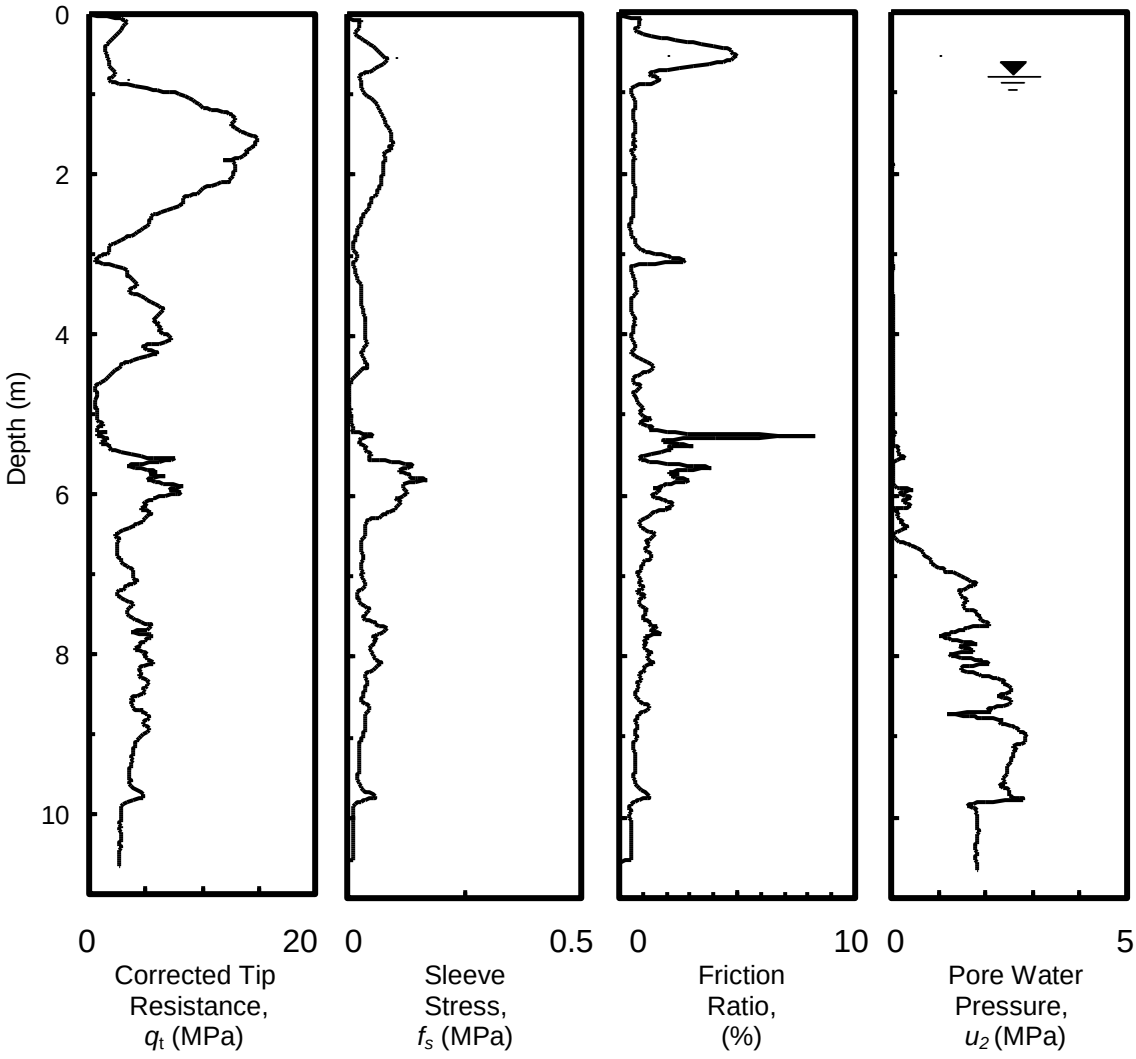

Figure A.4 Composite profile of CPT C 4 at the CREC site.

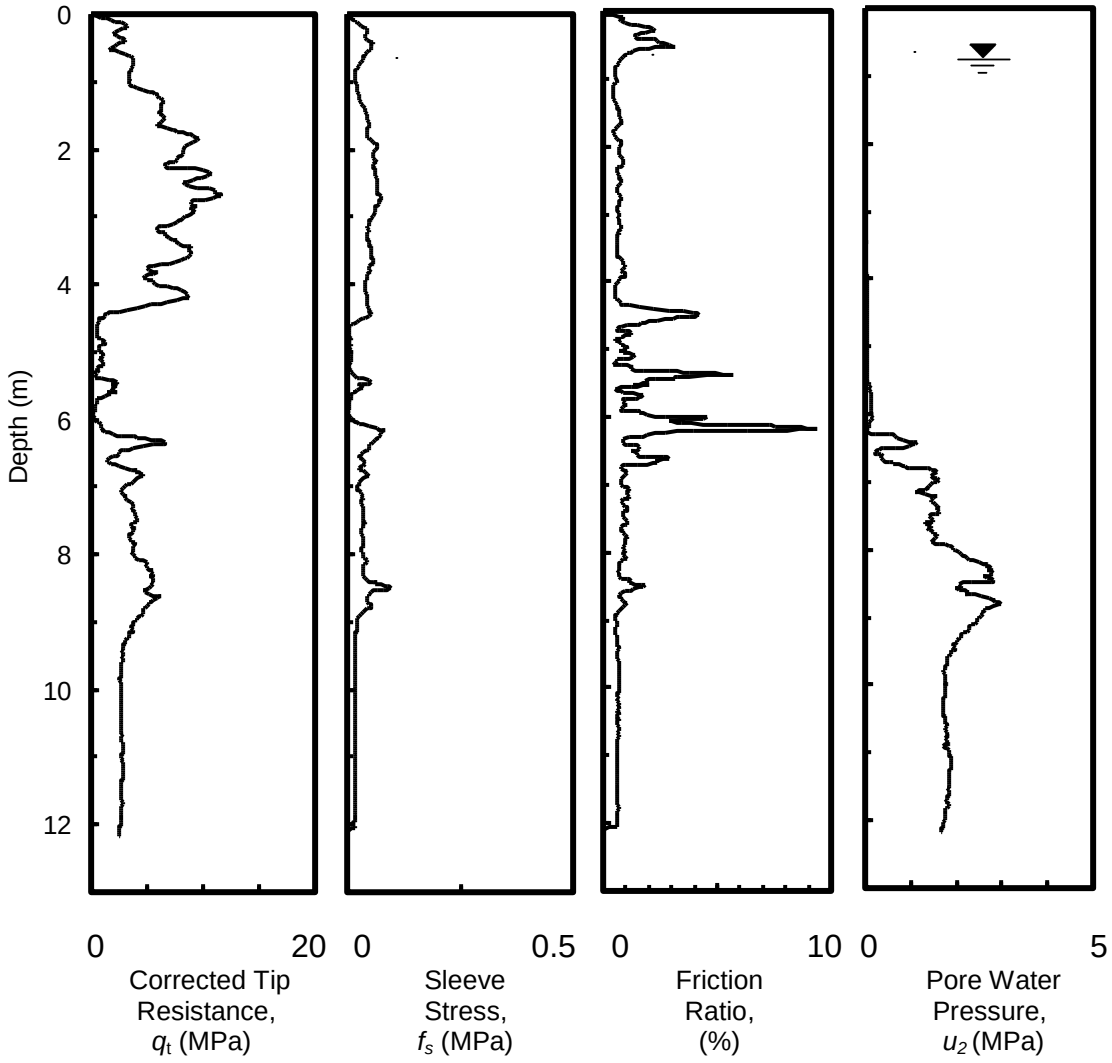

Figure A.5 Composite profile of CPT C 5 at the CREC site.

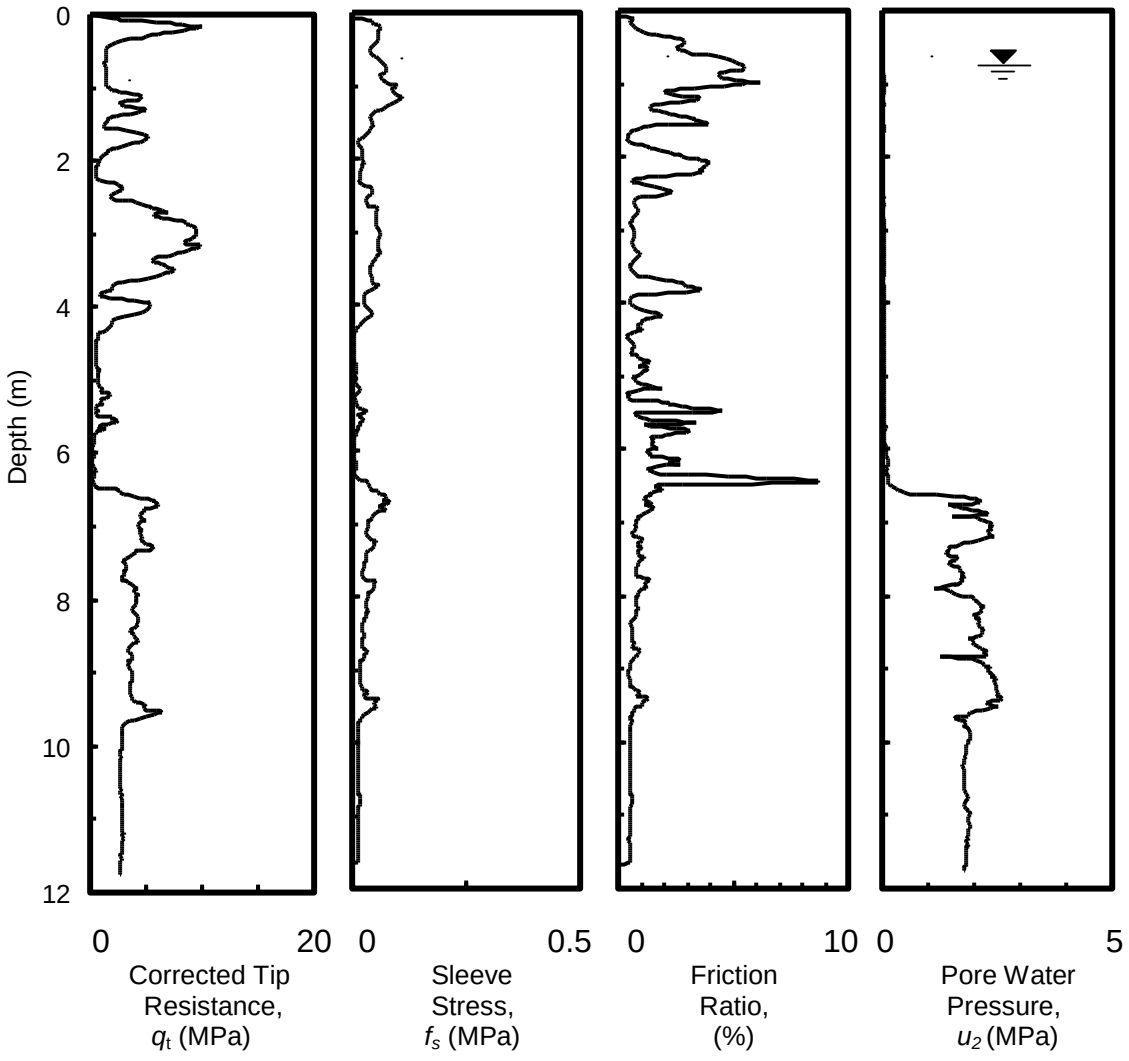

Figure A.6 Composite profile of SCPT SC 6 at the CREC site.

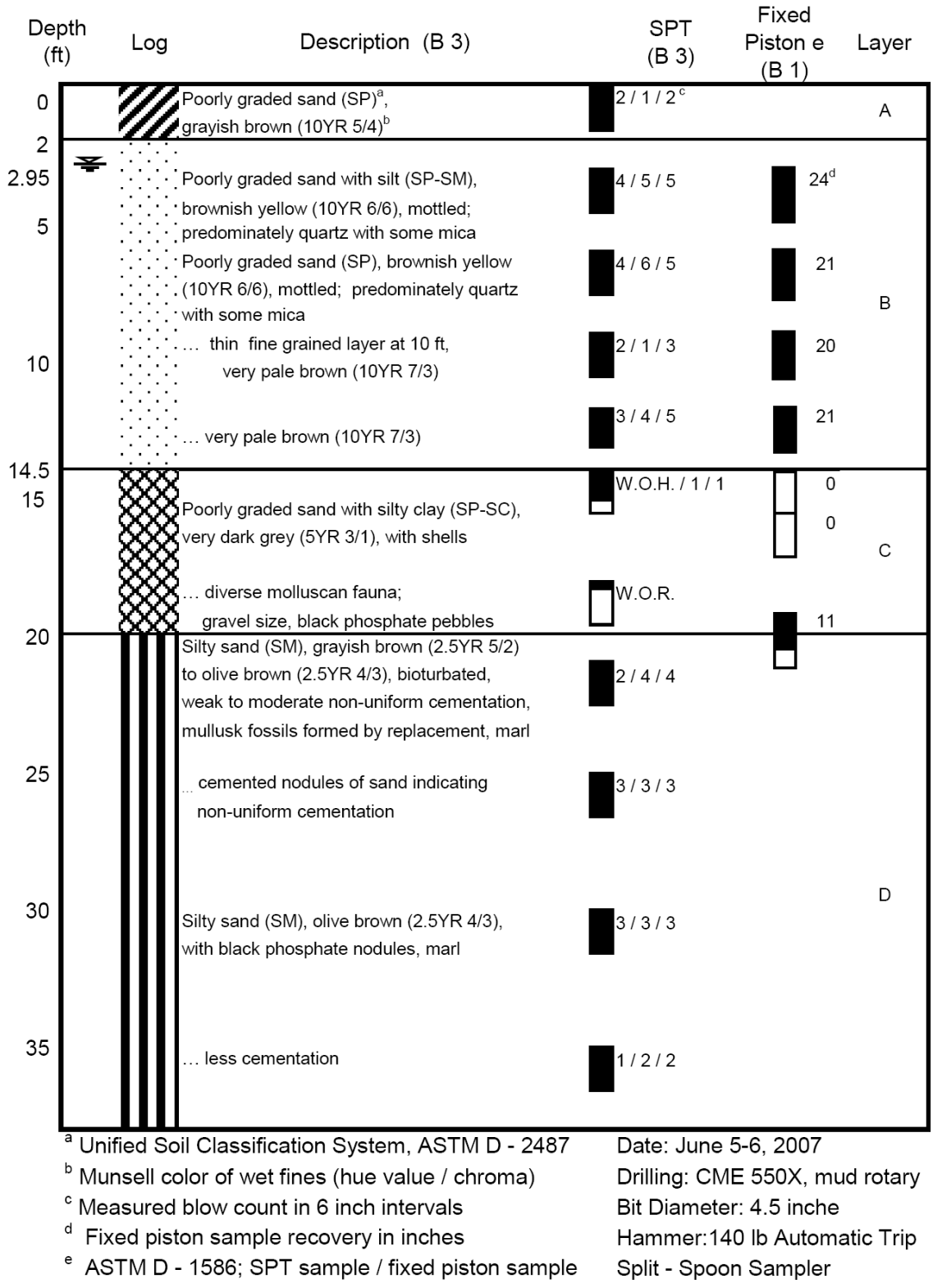

Figure A.7 Boring Log for B 3 and B 1 at the CREC site.

Table A.2 Correction of blowcounts for boring B 3 at the CREC site.

Test Depth (ft)	N_m	Range of Energy Efficiency In Last 12 in. (%)	Average Energy Efficiency (%)	C_E	C_B	C_R	C_S	N_{60}	σ'_{vo} (lb/ft^2)	C_N [b]	$(N_1)_{60}$
0 - 1.5	3	44 - 64	54	0.89	1	n/a [a]	1	3	105	1.70	5
3 - 4.5	10	72 - 88	75	1.25	1	n/a	1	12	358	1.60	20
6 - 7.5	11	73 - 87	79	1.32	1	n/a	1	14	485	1.52	22
9 - 10.5	4	74 - 78	76	1.26	1	n/a	1	5	613	1.46	7
12 - 13.5	9	35 - 43	40	0.66	1	n/a	1	6	741	1.40	8
15- 16.5	2	-	40[c]	0.66	1	n/a	1	1	869	1.35	2
18 - 19.5	1	-	40[c]	0.66	1	n/a	1	1	997	1.30	1
21 - 22.5	8	38 - 39	39	0.64	1	n/a	1	5	1124	1.25	6
25 - 26.5	6	36 - 40	39	0.64	1	n/a	1	4	1295	1.19	5
30 - 31.5	6	39 - 45	42	0.70	1	n/a	1	4	1508	1.13	5
35 -36.5	4	-	40[c]	0.66	1	n/a	1	3	1721	1.07	3

[a] No rod length correction need; energy efficiency measured at each depth.
[b] $C_N = 2.2 / (1.2 + \sigma'_{vo}/P_a)$, where P_a = 2000 lb/ft^2 (Kayen et al., 1992).
[c] Estimated average energy efficiency.
[d] Ground water table = 3.0 ft.
[e] Assumed unit weight of soil = 105 lb/ft^3.

Table A.3 Split-spoon data from boring B 3 and fixed piston data from boring B 1 at the CREC site.

Depth (ft)	Recovery in. / in.	C_u [a]	C_c [b]	D_{50} [c]	Grain Size Data – Percent Retained									Atterberg Limits LL[d] | PL[e]		*w*(%)[f]	Soil Type[g]
					Gravel		Sand					Silt	Clay				
					4.75	2.00	0.850	0.425	0.250	0.150	0.075	0.002 mm					
B 3																	
0 – 1.5	17 / 18	2.00	0.99	0.300	-	1	3	7	53	30	5	1		np		19	SP
3 – 4.5	16 / 18	2.40	1.42	0.190	-	-	1	1	8	64	19	7		np		25	SP-SM
6 – 7.5	12 / 18	2.00	1.24	0.190	-	-	-	-	6	70	21	3		np		29	SP
9 – 10.5	13 / 18	2.20	1.30	0.190	-	1	1	2	11	60	21	4		np		33	SP
12 – 13.5	12.5 / 18	1.90	1.20	0.200	-	-	-	1	15	66	15	3		np		27	SP
15 – 16.5	11 / 18	10.1	0.66	0.480	9	11	17	14	12	12	12	10	3	40	23	36	SP-SC
18 – 19.5	1 / 18	n/a	n/a	n/a	n/a									n/a		40	SP-SC
21 – 22.5	18 / 18	21.1	5.49	0.094	1	1	2	2	8	16	27	38	5	34	46	39	SM
25 – 26.5	18 / 18	18.3	3.23	0.059	1	2	2	2	9	21	24	39	3	33	41	41	SM
30 – 31.5	17.5 / 18	6.67	1.78	0.121	1	2	2	2	8	23	31	29	2	29	55	48	SM
35 – 36.5	18 / 18	5.70	2.10	0.110	1	1	2	4	4	14	46	23	5	54	np	65	SM
B 1																	
19.5 – 21	11/24	27.15	2.52	0.014	3	5	7	8	10	14	20	31	3	28	27	30	SM

[a] C_u = coefficient of uniformity.
[b] C_c = coefficient of curvature.
[c] D_{50} = Median grain size.
[d] LL = Liquid Limit water content (%) ASTM D 4318.
[e] PL = Plastic Limit water content (%) ASTM D 4318; np = non-plastic.
[f] In-situ moisture content.
[g] Soil Type based on Unified Soil Classification System ASTM D 2487.

Table A.4 Results of DMT D 1 performed at the CREC site.

Start of DMT		End of DMT		Average			Assumed Soil Unit Weight 105 (lb/ft^3)			
ΔA	ΔB	ΔA	ΔB	ΔA	ΔB	Z_m				
0.2	0.7	0.2	0.5	0.2	0.6	0				
Depth (ft)	A (bar)[a]	B (bar)	C (bar)	P_o (tsf)	P_1 (tsf)	σ_{vo}' (tsf)	I_D	K_D	K_o	E_D (bar)
1	2.95	10.00	-	2.84	9.40	105	2.31	56.44	-	228
2	2.70	6.35	-	2.76	5.75	210	1.09	27.42	-	104
3	2.45	7.75	-	2.43	7.15	315	1.95	16.08	3.32	164
4	2.65	8.50	-	2.60	7.90	420	2.04	12.92	2.36	184
5	2.90	12.00	-	2.69	11.40	494	3.26	11.29	1.40	302
6	2.55	11.00	-	2.37	10.40	536	3.46	9.04	1.02	279
7	3.45	16.40	-	3.04	15.80	579	4.30	10.71	1.02	443
8	3.05	10.80	-	2.90	10.20	622	2.61	9.40	1.25	253
9	2.35	11.00	-	2.16	10.40	664	4.07	6.36	1.17	286
10	2.55	11.80	0.05	2.33	11.20	707	4.10	6.39	0.60	308
11	2.85	12.20	0.10	2.62	11.60	749	3.70	6.77	0.50	312
12	2.65	10.20	0.10	2.51	9.60	792	3.10	6.03	0.50	246
13	1.75	8.15	0.15	1.67	7.55	835	4.15	3.54	0.45	204
14	1.80	3.25	0.20	1.97	2.65	877	0.41	4.01	-	24
15	1.90	3.10	0.65	2.08	2.50	920	0.24	4.01	0.99	15
16	3.00	4.55	1.60	3.16	3.95	962	0.28	6.12	0.99	27
17	1.55	3.90	0.35	1.67	3.30	1005	1.25	2.70	1.34	56
18	1.40	3.05	0.30	1.56	2.45	1048	0.77	2.30	0.34	31
19	1.00	2.30	0.45	1.18	1.70	1090	0.71	1.42	0.62	18
20	1.40	2.80	0.45	1.57	2.20	1133	0.57	2.04	0.37	22
21	2.50	11.80	-	2.28	11.20	1175	5.01	3.17	0.56	310
22	6.45	38.40	-	5.09	37.80	1218	7.16	7.84	0.82	1135
23	12.20	24.00	-	11.85	23.40	1261	1.02	18.72	0.80	401
24	4.90	10.60	0.10	4.86	10.00	1303	1.20	6.85	2.67	179
25	6.70	14.40	-	6.56	13.80	1346	1.22	9.22	1.44	251
26	9.05	22.60	-	8.61	22.00	1388	1.68	11.99	1.00	465
27	8.35	17.80	-	8.12	17.20	1431	1.22	10.87	1.46	315
28	9.70	17.20	0.05	9.57	16.60	1474	0.79	12.56	1.25	244
29	7.15	10.80	1.10	7.21	10.20	1516	0.46	8.92	2.12	104
30	12.40	26.20	0.20	11.95	25.60	1559	1.22	14.99	1.71	474
31	15.60	29.80	0.60	15.13	29.20	1601	0.98	18.70	2.34	488
32	15.80	22.40	5.15	15.71	21.80	1644	0.41	18.91	2.67	211
33	13.40	18.00	8.10	13.41	17.40	1687	0.32	15.55	2.69	138

[a] 1 bar = 105 P_a ≈ 2089 lb/ft^2

Table A.5 Measured shear wave velocity using pseudo interval method for SCPT SC 1 at the CREC site.

Geophone Depth (ft)	Average Depth Between Geophones (ft)	Measured V_s (ft/s)	Quality of Time Histories
4.4			
7.6	6.0	621	POOR
10.8	9.2	625	FAIR
14.0	12.4	567	POOR
17.2	15.6	617	FAIR
20.4	18.8	757	POOR
23.6	22.0	1493	FAIR
26.8	25.2	1500	FAIR
30.0	28.4	1317	FAIR
33.2	31.6	1440	FAIR
36.4	34.8	1867	FAIR
39.9	38.1	1641	FAIR
43.1	41.5	1767	FAIR
46.2	44.6	962	FAIR
49.4	47.8	879	FAIR
52.6	51.0	908	GOOD
55.8	54.2	737	GOOD
59.0	57.4	1272	GOOD
62.2	60.6	1090	GOOD
65.3	63.7	860	GOOD
68.5	66.9	1216	GOOD
71.7	70.1	992	GOOD
74.9	73.3	986	GOOD
78.0	76.4	1319	GOOD
81.5	79.7	1227	GOOD
84.6	83.0	1088	GOOD
87.8	86.2	980	GOOD
89.4	88.6	1005	GOOD

Table A.6 Measured shear wave velocity using pseudo interval method for sounding SCPT SC 3 at the CREC site.

Geophone Depth (ft)	Average Depth Between Geophones (ft)	Measured V_s (ft/s)	Quality of Time Histories
4.2			
7.5	5.8	648	POOR
10.7	9.1	512	POOR
13.9	12.3	629	FAIR
17.1	15.5	462	FAIR
20.3	18.7	1565	GOOD
23.5	21.9	1425	GOOD
26.5	25.0	1742	GOOD
30.0	28.3	2337	FAIR
33.2	31.6	1320	GOOD

Table A.7 Measured shear wave velocity using pseudo interval method for sounding SCPT SC 6 at the CREC site

Geophone Depth (ft)	Average Depth Between Geophones (ft)	Measured V_s (ft/s)	Quality of Time Histories
1.4			
4.6	3.0	751	POOR
7.8	6.2	519	POOR
11.1	9.4	632	FAIR
14.3	12.7	507	FAIR
17.5	15.9	584	FAIR
20.7	19.1	950	GOOD
23.9	22.3	2247	GOOD
27.1	25.5	2401	GOOD
30.3	28.7	1871	GOOD
33.5	31.9	1449	POOR
36.8	35.2	1389	GOOD

APPENDIX B

SUMMARY OF DATA FOR THE BORROW PIT SITE

Table B.1 Local site coordinates for the geotechnical investigation at the Borrow Pit site.

Test Sites	X (m)	Y (m)
Oak Tree at Reference 3	0	0
Oak Tree at Reference 1	25	10
Oak Tree at Reference 2	1	19
HB 1	8	19
HB 2	4	-1
HB 3	23	-4
D 1	8	17

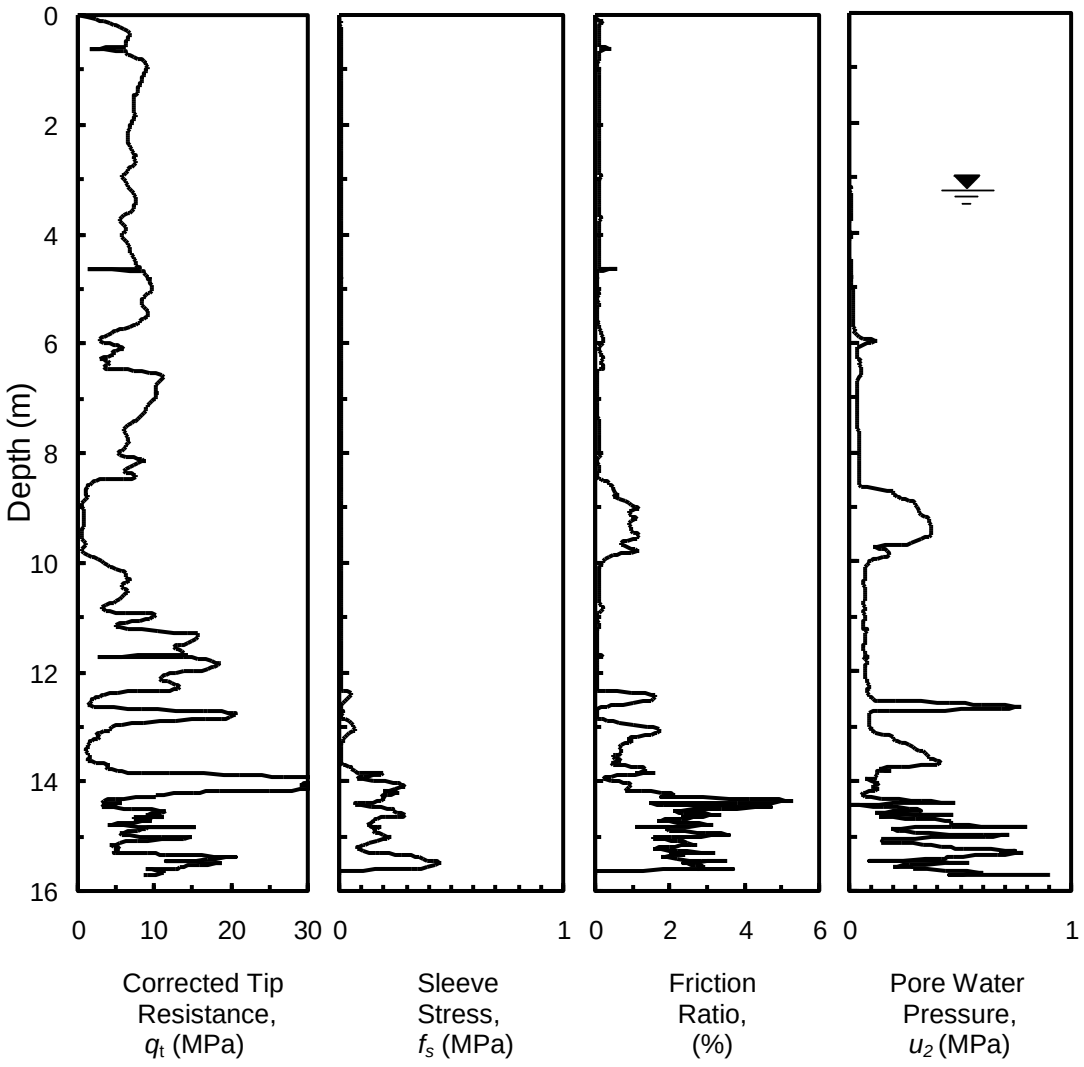

Figure B.1 Composite profile of SCPT HB 1 at the Borrow Pit site.

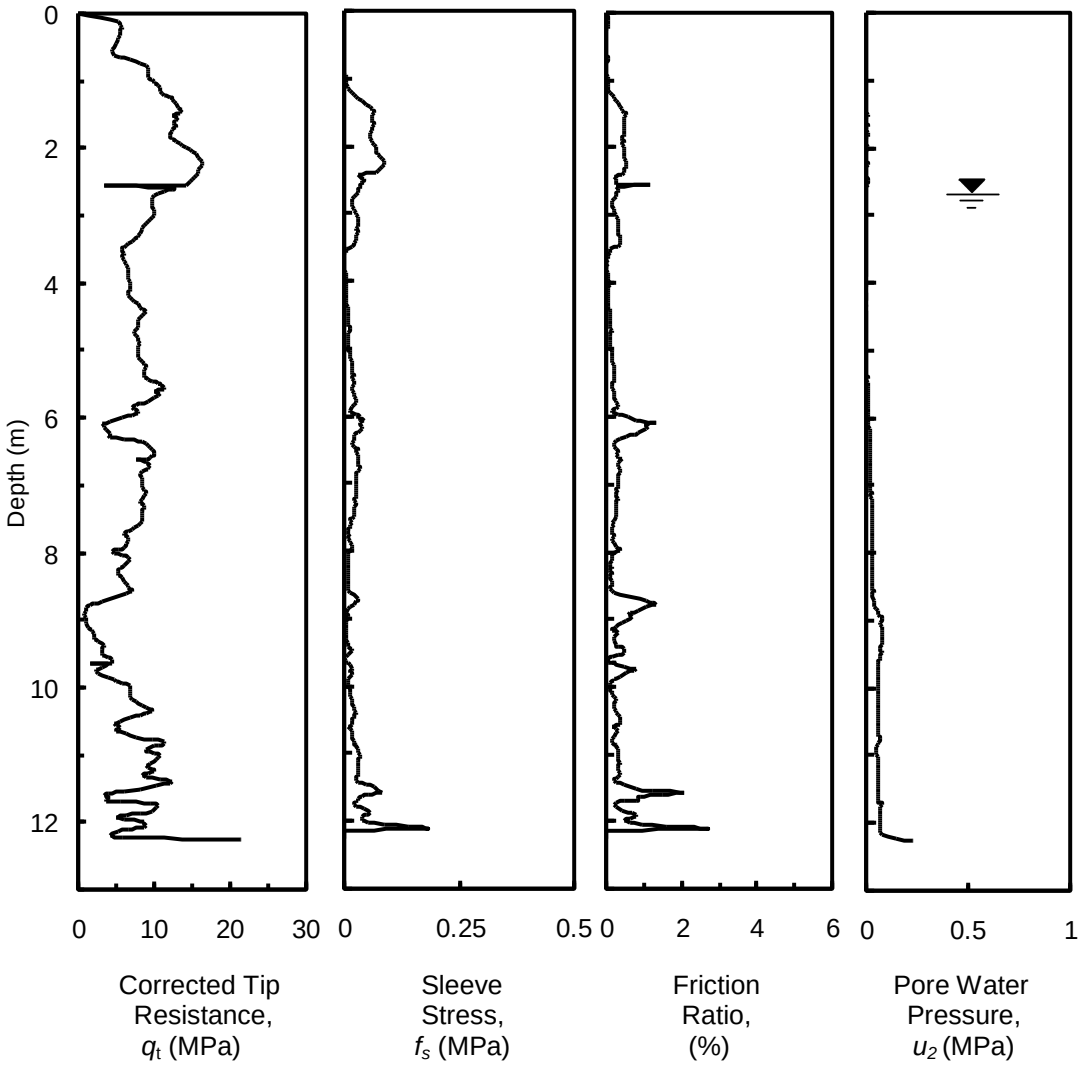

Figure B.2 Composite profile of SCPT HB 2 at the Borrow Pit site.

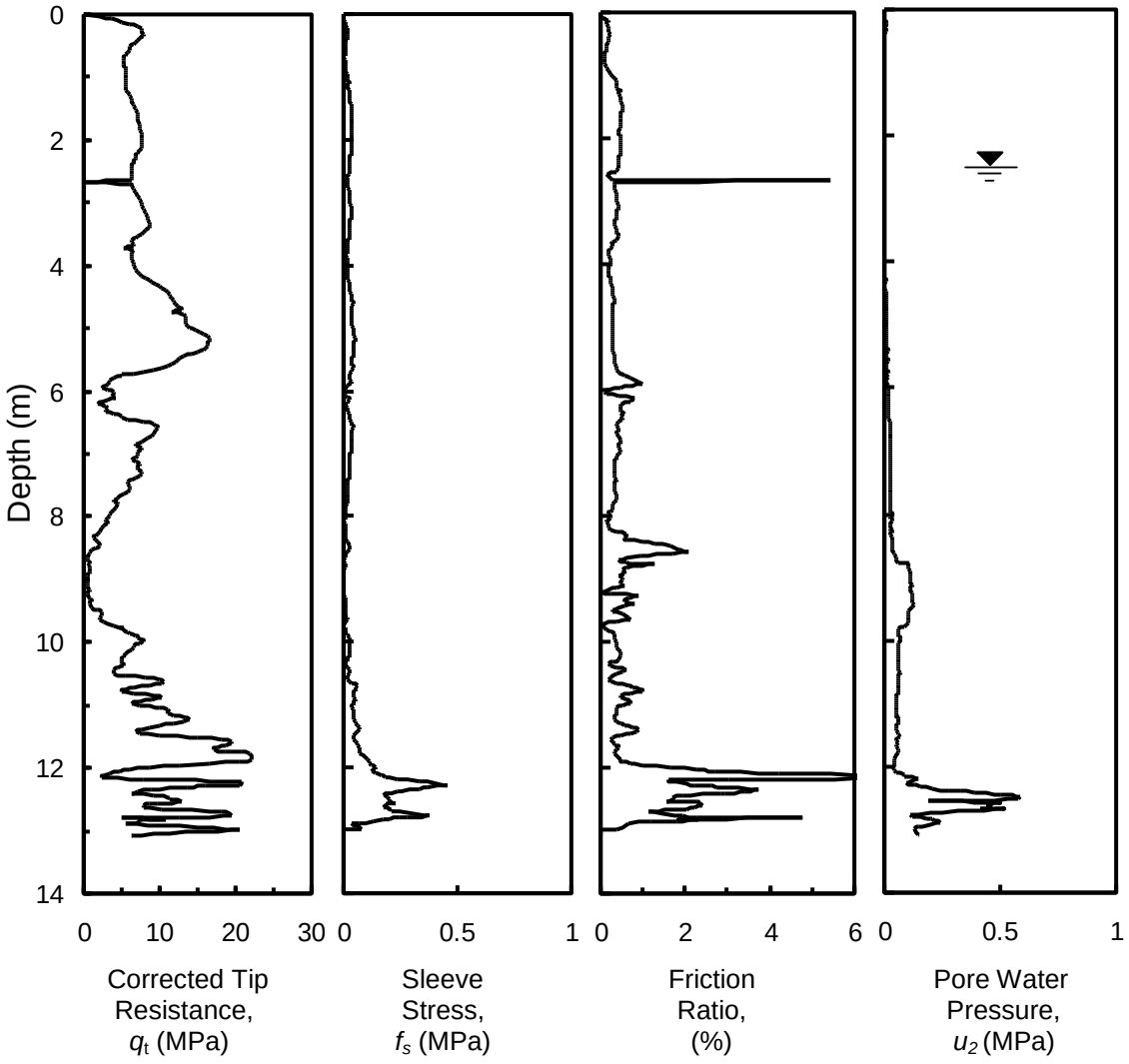

Figure B.3 Composite profile of SCPT HB 3 at the Borrow Pit site.

Table B.2 Results of DMT D 1 performed at the Borrow Pit site.

Start of DMT		End of DMT		Average			Assumed Soil Unit Weight 105 (lb/ft^3)			
ΔA	ΔB	ΔA	ΔB	ΔA	ΔB	Z_m				
0.13	0.65	0.15	0.50	0.14	0.58	0				
Depth (ft)	A (bar)[a]	B (bar)	C (bar)	P_o (tsf)	P_1 (tsf)	σ_{vo}' (tsf)	I_D	K_D	K_o	E_D (bar)
1	-	-	-	-	-	-	-	-	-	-
2	3.20	11.00	3.50	2.99	10.43	210	2.49	-	-	258
3	3.10	11.50	4.60	2.86	10.93	315	2.83	2.70	2.70	280
4	4.20	15.60	5.20	3.81	15.03	420	2.95	2.70	2.70	389
5	4.90	16.80	6.90	4.48	16.23	525	2.62	2.69	2.69	408
6	5.10	17.60	7.70	4.65	17.03	630	2.66	2.39	2.39	429
7	5.10	17.50	7.60	4.66	16.93	735	2.64	2.00	2.00	426
8	4.50	16.10	6.70	4.10	15.53	840	2.79	1.50	1.50	397
9	4.60	16.80	7.60	4.17	16.23	945	2.89	1.20	1.20	418
10	4.30	16.40	9.00	3.87	15.83	988	3.11	1.11	1.11	415
11	4.30	15.80	6.90	3.90	15.23	1030	2.95	1.02	1.02	393
12	3.40	14.00	6.80	3.05	13.43	1073	3.51	0.80	0.80	360
13	2.80	11.20	5.90	2.56	10.63	1115	3.31	0.71	0.71	280
14	2.90	13.00	6.50	2.57	12.43	1158	4.07	0.68	0.68	342
15	2.20	10.60	5.10	1.96	10.03	1201	4.54	0.56	0.56	280
16	3.30	17.00	10.20	2.79	16.43	1243	5.28	0.68	0.68	473
17	3.30	15.40	7.10	2.87	14.83	1286	4.54	0.68	0.68	415
18	4.20	17.20	4.90	3.73	16.63	1328	3.73	0.74	0.74	448
19	2.80	13.80	5.60	2.43	13.23	1371	5.08	0.56	0.56	375
20	3.40	12.80	4.60	3.11	12.23	1414	3.28	0.80	0.80	316
21	2.70	15.40	10.00	2.24	14.83	1456	6.69	0.63	0.63	437
22	6.00	25.80	14.20	5.19	25.23	1499	4.18	0.91	0.91	695
23	5.70	22.00	4.90	5.06	21.43	1541	3.52	0.85	0.85	568
24	4.90	17.20	7.80	4.46	16.63	1584	3.03	0.58	0.58	422
25	2.90	12.20	4.90	2.61	11.63	1627	4.23	0.60	0.60	313
26	2.30	9.60	4.20	2.11	9.03	1669	4.31	0.50	0.50	240
27	2.70	10.60	4.20	2.48	10.03	1712	3.88	0.56	0.56	262
28	2.60	10.80	4.60	2.37	10.23	1754	4.37	0.56	0.56	273
29	2.80	12.60	5.40	2.49	12.03	1797	5.05	0.68	0.68	331
30	4.20	5.70	4.50	4.30	5.13	1840	0.22	1.02	1.02	29
31	4.80	6.70	5.60	4.88	6.13	1882	0.29	1.11	1.11	43
32	3.50	5.40	3.20	3.58	4.83	1925	0.43	0.82	0.82	43
33	2.00	6.20	2.50	1.97	5.63	1967	2.93	0.58	0.58	127
34	3.30	7.80	3.70	3.25	7.23	2010	1.59	0.63	0.63	138

[a] 1 bar = 105 P_a ≈ 2089 lb/ft^2

Table B.3 Measured shear wave velocity using true interval method for sounding SCPT HB 1 at the Borrow Pit site.

Geophone Depth (ft)	Average Depth Between Geophones (ft)	Measured V_s (ft/s)	Quality of Time Histories
1.1			
4.4	2.7	357	FAIR
7.6	6.0	802	GOOD
10.9	9.3	602	GOOD
14.3	12.6	700	GOOD
17.5	15.8	756	GOOD
20.8	19.2	799	FAIR
24.1	22.4	747	GOOD
27.4	25.8	616	GOOD
30.8	29.2	559	GOOD
34.2	32.5	644	VERY GOOD
37.5	35.8	746	VERY GOOD
40.8	39.1	827	GOOD
44.8	42.4	641	GOOD
47.4	45.7	995	GOOD
50.7	49.1	1037	EXCELLENT

Table B.4 Measured shear wave velocity using true interval method for sounding SCPT HB 2 at the Borrow Pit site.

Geophone Depth (ft)	Average Depth Between Geophones (ft)	Measured V_s (ft/s)	Quality of Time Histories
0.7			
4.0	2.3	-	VERY POOR
7.4	5.8	683	GOOD
10.8	9.2	669	GOOD
14.1	12.5	703	VERY GOOD
17.4	15.8	797	VERY GOOD
20.7	19.1	792	VERY GOOD
24.1	22.4	555	FAIR
27.4	25.8	670	GOOD
30.7	29.0	614	VERY GOOD
34.0	32.4	801	GOOD
37.4	35.7	781	GOOD
39.4	37.7	838	GOOD

Table B.5 Measured shear wave velocity using true interval method for sounding SCPT HB 3 at the Borrow Pit site.

Geophone Depth (ft)	Average Depth Between Geophones (ft)	Measured V_s (ft/s)	Quality of Time Histories
1.3			
4.6	2.9	858	FAIR
7.8	6.2	769	FAIR
11.2	9.6	621	GOOD
14.6	12.9	718	FAIR
17.9	16.2	878	FAIR
21.2	19.5	660	GOOD
24.5	23.2	639	GOOD
27.8	26.2	502	GOOD
31.1	29.5	553	GOOD
34.4	32.8	721	GOOD
37.7	36.1	704	VERY GOOD
41.1	39.4	844	GOOD
42.1	40.4	905	GOOD

APPENDIX C

SUMMARY OF DATA FOR THE MARSH ROAD SITE

Table C.1 Local site coordinates for the geotechnical investigation at the Marsh Road site.

Test Sites	X (m)	Y (m)
Survey Marker 2	0	0
Survey Marker 1	28	23
Marsh Road Reference Point	2	26
HM 1	38	13
HM 2	22	21
HM 3	-2	6

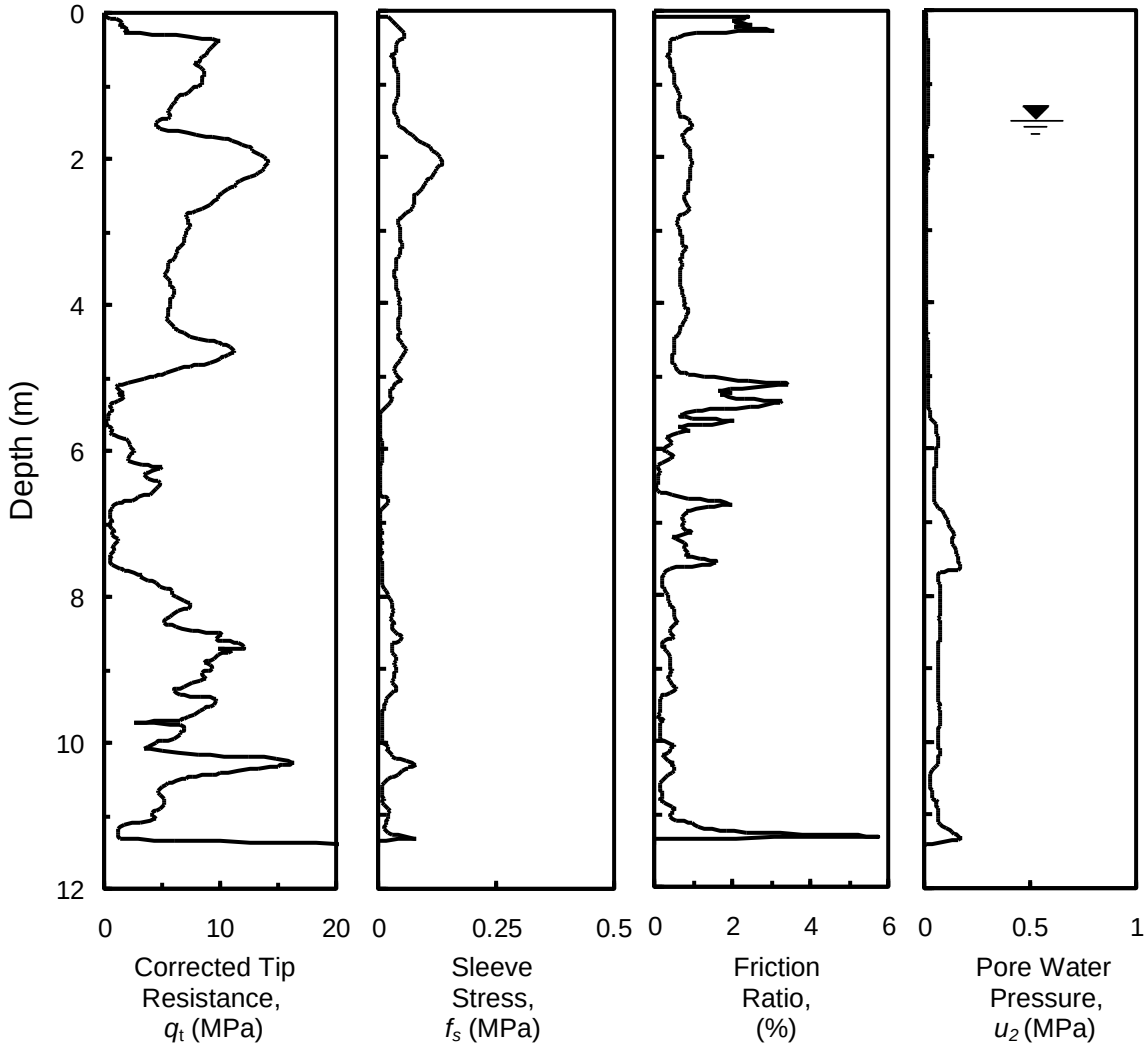

Figure C.1 Composite profile of SCPT HM 1 at the Marsh Road site.

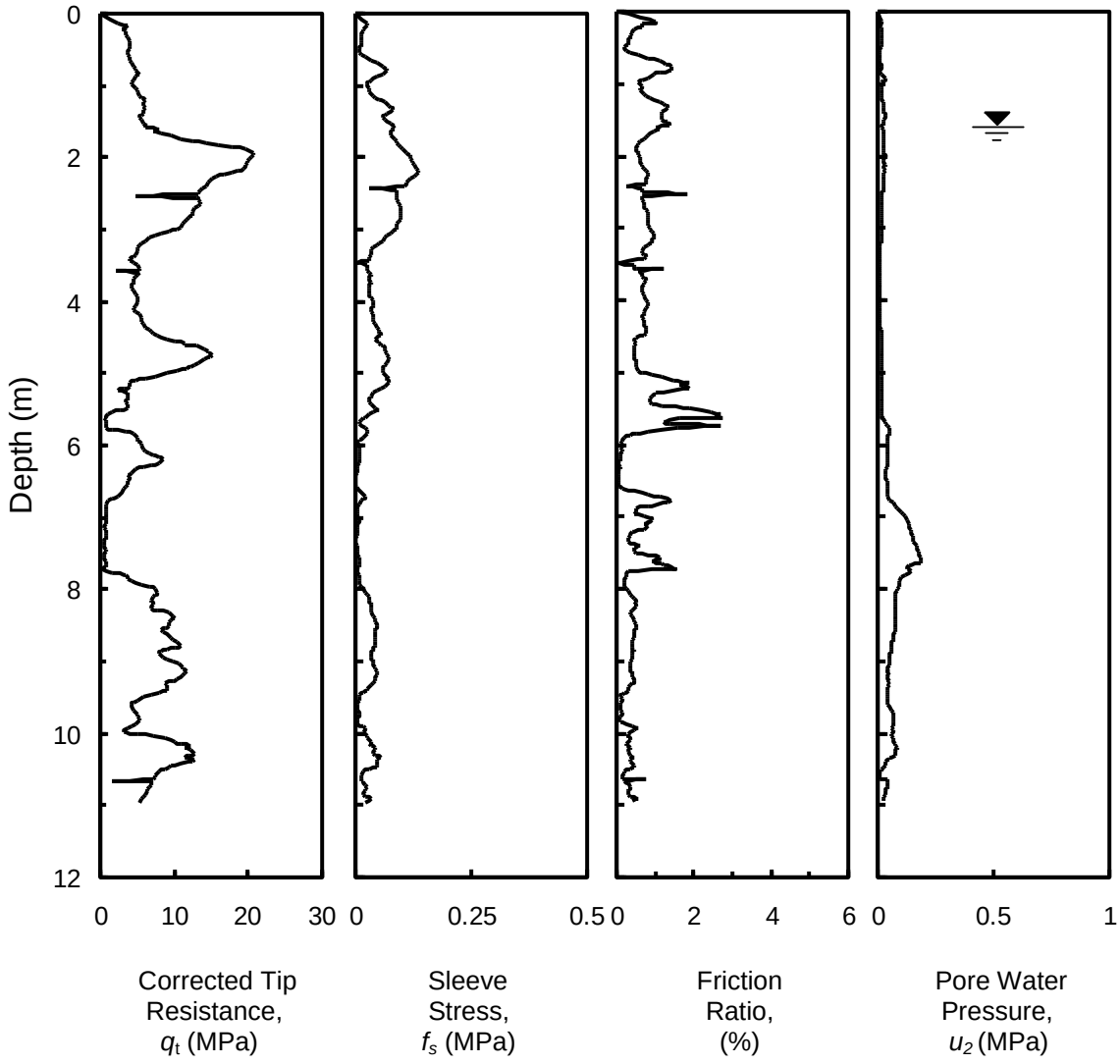

Figure C.2 Composite profile of SCPT HM 2 at the Marsh Road site.

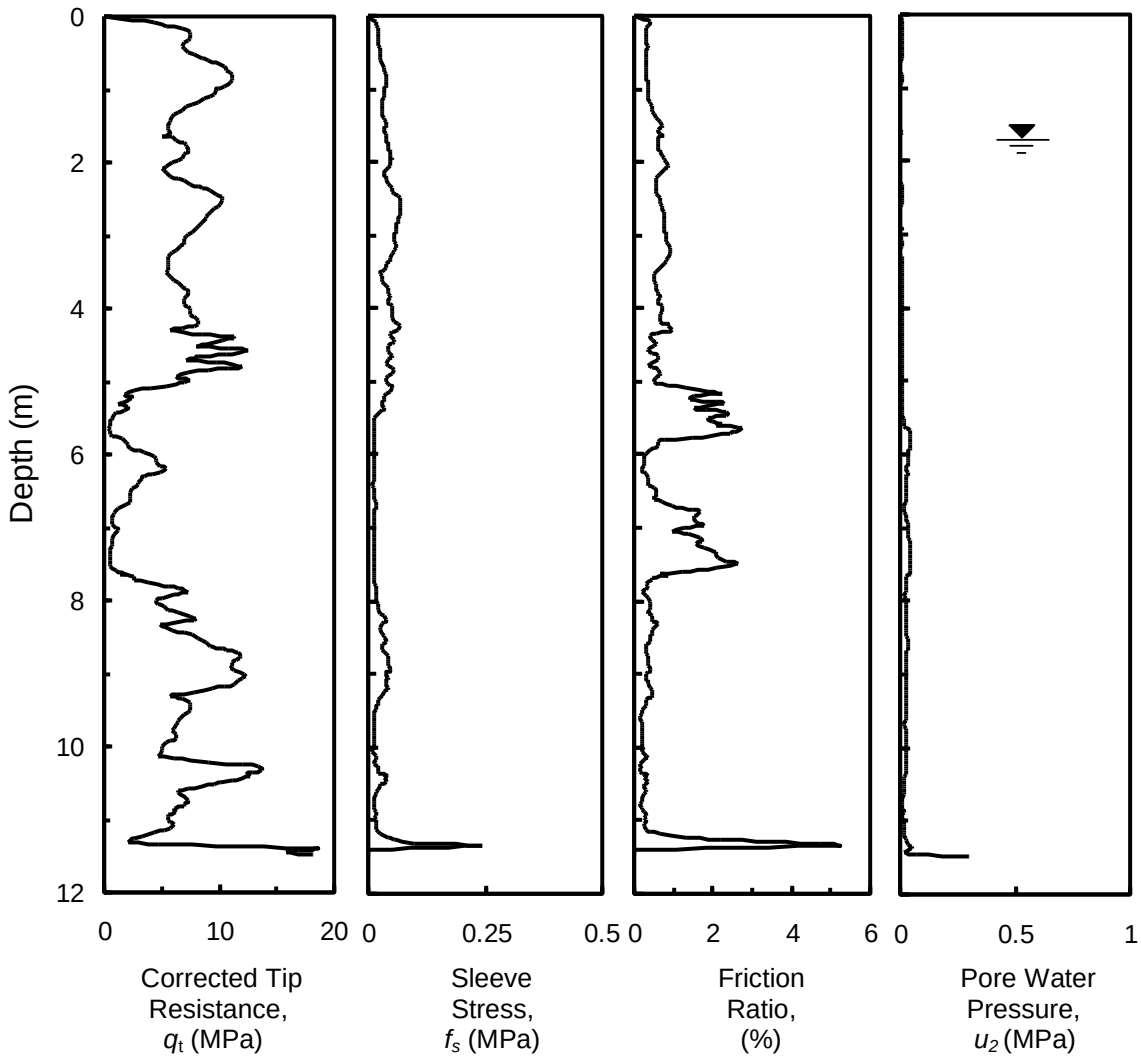

Figure C.3 Composite profile of SCPT HM 3 at the Marsh Road site.

Table C.2 Measured shear wave velocity using true interval method for sounding SCPT HM 1 at the Marsh Road site.

Geophone Depth (ft)	Average Depth Between Geophones (ft)	Measured V_s (ft/s)	Quality of Time Histories
3.9			
7.2	5.5	1265	FAIR
10.2	8.6	901	FAIR
13.7	12.0	779	GOOD
17.1	15.4	540	VERY GOOD
20.5	18.8	555	FAIR
23.9	22.3	596	VERY GOOD
27.4	25.7	736	GOOD
30.6	29.0	887	VERY GOOD
34.1	32.4	1130	GOOD
36.2	34.6	1524	GOOD

Table C.3 Measured shear wave velocity using true interval method for sounding SCPT HM 2 at the Marsh Road site.

Geophone Depth (ft)	Average Depth Between Geophones (ft)	Measured V_s (ft/s)	Quality of Time Histories
0.9			
4.2	2.6	-	VERY POOR
7.3	5.7	583	FAIR
10.8	9.1	858	FAIR
14.1	12.5	863	GOOD
17.5	15.8	627	VERY GOOD
20.8	19.2	632	GOOD
24.1	22.5	550	GOOD
27.3	25.6	658	EXCELLENT
30.6	29.0	805	GOOD
34.0	32.3	1041	GOOD
36.6	35.0	1307	GOOD

Table C.4 Measured shear wave velocity using true interval method for sounding SCPT HM 3 at the Marsh Road site.

Geophone Depth (ft)	Average Depth Between Geophones (ft)	Measured V_s (ft/s)	Quality of Time Histories
1.1			
4.4	2.7	816	GOOD
7.7	6.1	-	VERY POOR
10.9	9.2	1322	FAIR
14.2	12.6	826	EXCELLENT
17.5	15.9	512	GOOD
20.9	19.2	560	GOOD
24.1	22.5	584	GOOD
27.5	25.9	654	GOOD
30.7	29.0	838	EXCELLENT
34.0	32.4	875	GOOD
36.8	35.1	1507	GOOD

REFERENCES

American Society for Testing and Materials ASTM (2004). *Annual Book of ASTM Standards*. Vol. 4.08. Philadelphia, PA.

Andrus, R.D., Mohanan, N.D., Piratheepan, P., Ellis, B.S., and Holzer, T.L. (2007) "Predicting the shear-wave velocity from cone penetration resistance," *4th International Conference on Earthquake Geotechnical Engineering*, Greece, Paper No. 1454.

Arango, I., Lewis, M.R., and Kramer, C. (2000). "Updated liquefaction potential analysis eliminates foundation retrofitting of two critical structures," *Soil Dynamic Earthquake Engineering*, Vol. 20, pp. 17 - 25.

Baldi, G., Belloti, R., Ghionna, V., Jamiolkowski, M. and Pasqualini, E. (1986). "Interpretation of CPTs and CPTUs. Part 2: drained penetration of sands," *Proceedings, 4th International Geotechnical Seminar Field Instrumentation and In Situ Measurements*, Singapore, pp. 143 - 156.

Cetin, K.O., Seed, R.B., and Der Kiureghian, A., Tokimatsu, K., Harder, L.F., Kayen, R.E., Moss, R.E.S. (2004). "Standard penetration test-based probabilistic and deterministic assessment of seismic soil liquefaction potential," *Journal of Geotechnical and Geoenvironmental Engineering*, 130(12), pp. 1314 - 1340.

Hayati, H., and Andrus, R.D. (2008). "Liquefaction potential map of Charleston, South Carolina based on the 1886 earthquake," *Journal of Geotechnical and Geoenvironmental Engineering,* accepted for publication.

Hayati, H., Andrus, R.D., Gassman, S.L., Hasek, M., Camp. W.M., and Talwani, P. (2008). "Characterizing the liquefaction resistance of age soils," *Geotechnical Earthquake Engineering and Soil Dynamics IV*, accepted for publication.

Idriss, I.M., and Boulanger, R.W. (2004). "Semi-empirical procedures for evaluating liquefaction potential during earthquakes*," Proceeding, 11th International Conference on Soil Dynamics and Earthquake Engineering (SDEE) and 3rd International Conference on Earthquake Geotechnical Engineering (ICEGE)*, Berkley, CA, pp. 32-56.

Kayen, R. E., Mitchell, J. K., Seed, R. B., Lodge, A., Nishio, S., and Coutinho, R. (1992). ‘‘Evaluation of SPT, CPT, and shear wave-based methods for liquefaction potential assessment using Loma Prieta data,’’ *Proceedings, 4th Japan-U.S. Workshop on Earthquake Resistant Design of Lifeline Facilities and Countermeasures for Soil Liquefaction*: Buffalo, N.Y., National Center for Earthquake Research Technical Report NCEER-92-0019, Vol. 1, pp. 177 - 204.

Kulhawy, F. H., and Mayne, P. W. (1990). “Manual on estimating soil properties for foundation design,” *Final Report, 1493-6, EL-6800*, Electric Power Research Institute, Palo Alto, CA.

Lewis, M.R., Arango, I., Kimball, J.K., and Ross, T.E. (1999). “Liquefaction resistance of old sand deposits,” *11th, Pan-America Conference on Soil Mechanics and Geotechnical Engineering*, Foz do Iguassu, Brazil.

Lunne. T., Robertson, P., and Powel, J. (1997). *Cone Penetration Testing in Geotechnical Practice*. Thomson, Florence, KY.

Martin, J.R., and Clough, G.W. (1990). "Implications from a geotechnical investigation of liquefaction phenomena associated with seismic events in the Charleston, SC area," *USGS Report, No. 14-08-00 1-G-1348*.

Moss, R. S., Seed, B .R., Kayen, R. E., Stewart, J. P., Kiureghian, A., Cetin, O. K. (2006). “CPT-based probabilistic and deterministic assessment of in situ seismic soil liquefaction potential,” *Journal of Geotechnical and Geoenvironmental Engineering*, Vol. 132, pp. 1032 - 1051.

Marchetti, S. (1980). "In-situ tests by flat dilatometer," Journal Geotechnical Engineering 106 (GT3) Proc. Paper 15290, pp. 299 - 321.

May, J.P., (1978). “Quaternary geology of hobcaw barony Georgetown, South Carolina,” *Geological Research Project*, The Belle W. Baruch Forest Science Institute, Georgetown, South Carolina.

McCartan, L., Lemon, E.M. Jr., and Weems, R.E. (1984). “Geologic map of the area between Charleston and Orangeburg,“ scale 1:250,000, U.S. Geological Survey, Reston, VA.

Robertson, P.K., (1990). “Soil classification using the cone penetration test,” *Canadian Geotechnical Journal,* 27(1), pp. 151-158.

Robertson, P.K., and Wride, C.E. (1998). "Evaluating cyclic liquefaction potential using the cone penetration test," *Canadian Geotechnical Journal,* 35(3), pp. 442 - 459.

Seed, H.B., (1979). "Soil liquefaction and cyclic mobility evaluation for level ground during earthquakes," *Journal of Geotechnical Engineering* Division, 105(2) pp. 201 - 255.

Seed, H.B., Tokimatsu, K., Harder, L.F., and Chung, R.M. (1984). "The influence of the SPT procedures in soil liquefaction resistance evaluation," University of California at Berkeley, *Report No. UCB/EERC-84/15*, October.

Siple, G. E., (1957). *Guidebook for the South Carolina Coastal Plain Field Trip*. U.S. Geological Survey, Columbia, SC, pp. 3 - 5.

Troncoso, J., Ishihara, K., and Verdugo, (1988). "Aging effects on cyclic shear strength of tailing materials," Proceedings, 11th, *Pan-American Conference on Soil Mechanics and Geotechnical Engineering*, New York, NY.

Weems, R. E., and Lemon, E. M. Jr., (1993). "Geology of the Cainhoy, Charleston, Fort Moultrie, and North Charleston Quadrangles, Charleston and Berkley Counties, South Carolina," USGS Misc. Investigation Map I-1935, scale 1:24,000, Department of the Interior, U.S. Geological Survey, Reston, VA.

Youd, T.L., and Perkins, D.M. (1978). "Mapping of liquefaction-induced ground failure potential," *Journal of Geotechnical Engineering Division, ASCE*, 104(3), pp. 433 - 466.